

Thesis

Particle Balance and Solids Distribution in Circulating Fluidized Beds (CFB)

Thesis for the Degree of Doctor of Technical Science under the supervision of

Ao. Univ. Prof. Dr. techn. Dipl.-Ing. A. Werner

Institut für Technische Wärmelehre
(Institute of Thermal Engineering)


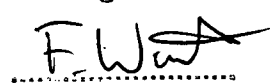
Submitted at the Technische Universität Wien
Fakultät für Maschinenbau
(Vienna University of Technology
Faculty of Mechanical Engineering)

by

Dipl.-Ing. Bedri Dragusha
Matrikelnummer 9726263
Erlachgasse 70/30
1100 Wien Austria

Vienna, June 2003

Diese Dissertation haben begutachtet:

Acknowledgements

I would like to express my appreciation to the Ao.Univ.Prof. Dipl.-Ing. Dr.techn. Andreas Werner, for his indefatigable helpfulness, for excellence supervision and support all areas.

For the acceptance of the lecture I would like to thank Ao.Univ.Prof. Dipl.-Ing. Dr.techn. Franz Winter.

Special thank I would like to express the head of the Institute o.Univ.Prof. Dipl.-Ing. Dr.techn. Wladimir Linzer for making this work possible.

Further I would like to thank the members of the institute (ITW) Ao.Univ.Prof. Dipl.-Ing. Dr.techn. Karl Ponweiser, Dipl.-Ing. Dr.techn Friedrich Frasz, Dipl.-Ing. Dr.techn Heimo Walter and secretaries Frau Jutta Amon and Frau Sabine Traxler for the friendly atmosphere at the institute.

Special thanks owe to my parents, Mehmet and Nafije, who showed me the right way of life and for their moral and material help. My brothers, Nazmi and Basri, and sisters, Kimete, Elfete and Drita I would like to thank for moral and material support during my study. Especial I would like to thank Nazmi for his material support.

Mr. Astrit Ademaj, Nysret Musliu and Yll Haxhimusa helped me with their good tips and their firm friendship during my study, thank you.

Generally I would like to thank all those, who facilitated by their assistance the creation of this work.

Danksagung

Für die Themenstellung, seine unermüdliche Hilfsbereitschaft, für die hervorragende Betreuung und Unterstützung in allen Bereichen danke ich Ao.Univ.Prof. Dipl.-Ing. Dr.techn. Andreas Werner.

Herrn Ao.Univ.Prof. Dipl.-Ing. Dr.techn. Franz Winter danke ich für die Übernahme des Koreferates und die wertvollen Hinweise.

Dem Institutsvorstand Herrn o.Univ.Prof. Dipl.-Ing. Dr.techn. Wladimir Linzer danke ich für das Ermöglichen dieser Arbeit.

Weiterhin werde ich die Mitarbeiter des Institutes, Ao.Univ.Prof. Dipl.-Ing. Dr.techn. Karl Ponweiser, Dipl.-Ing. Dr.techn. Friedrich Frasz, Dipl.-Ing. Dr.techn. Heimo Walter und die Sekretärinnen Frau Jutta Amon und Frau Sabine Traxler durch das freundliche Klima, das sie im Institut schufen, in guter Erinnerung behalten.

Dank schulde ich besonders meinen Eltern, Mehmet und Nafije, dafür, dass sie mir den richtigen Weg ins Leben wiesen. Für ihre finanzielle und moralische Unterstützung danke ich meinen Geschwistern Nazmi, Kimete, Basri, Elfete und Drita. Besonders gilt dies für meinen Bruder Nazmi.

Herr Astrit Ademaj, Nysret Musliu und Yll Haxhimusa halfen mir durch gute Tipps und ihre feste Freundschaft während meines Studiums, danke.

Allgemein möchte ich all jenen danken, die mir durch ihre Hilfe die Erstellung dieser Arbeit erleichterten.

Falenderim

Për këshillime dhe punë të palodhshëme, përkrahje në çdo aspekt gjatë studimeve dhe punës sime si bashkpunëtorë shkencorë në institutin e termoteknikës në Vjenë (ITW) falenderoj zotëri Ao.Univ.Prof. Dipl.-Ing. Dr.techn. Andreas Werner.

Zotin Ao.Univ.Prof. Dipl.-Ing. Dr.techn. Franz Winter falenderoj për pranim të kooreferatit dhe këshilla të plotfrytshme rreth punimit.

Shefin e insitutit të termoteknikës (ITW) o.Univ.Prof. Dipl.-Ing. Dr.techn. Wladimir Linzer falenderoj që më mundësoj këtë punim.

Më tutje dëshiroj t'i falenderoj te gjithë bashkpunëtorët e Instutit, Ao.Univ.Prof. Dipl.-Ing. Dr.techn. Karl Ponweiser, Dipl.-Ing. Dr.techn Friedrich Frasz, Dipl.-Ing. Dr.techn Heimo Walter si dhe znj. Jutta Amon dhe znj. Sabine Traxler për klimë të ngroht pune që krijuan në insitut.

Prindërit e mi, Mehmet dhe Nafije, dëshiroj t'i falënderoj për përkrahje morale dhe material gjatë gjithë kohës së studimeve si dhe për rrugën drejt të jetës që më mësuam. Vllëzërit, Nazmiun dhe Basriun, si dhe motrat, Kimeten, Elfeten dhe Dritën, falënderoj për perkrhaje morale dhe materiale gjatë gjithë kohës së sdudimeve. Posaqërisht do vequr Nazmiun për përkrahje të pakursyer materiale.

Astrit Ademajn, Nysret Musliun dhe Yll Haxhimusen falenderoj për këshillime rreth punimit si dhe për shoqëri gjatë kohës së studimeve në Vjenë.

Falenderoj të gjithë ata, të cilët në çfarëdo mënyre ndihmuan në përfundimin e këtij punimi.

Abstract

In the course of this work the solid flow program (SOLDIST) and the main simulation program for circulating fluidized bed boilers (CFBB) have been extended, partially reprogrammed and tested. The solids flow program has been designed as a "Stand-Alone-Version" and has been extended to a "multi-air injection model".

In the solids flow program, the common blocks structure (feature of the programming language Fortran 77) has been exchanged against parameter-list based variables transfer. Furthermore, the functionality of the program is checked. The current version of the simulation program allows to inject additional air to each cell of the combustion chamber. Examples where an additional mass flow of secondary air ($\dot{m}_{Air,add} = 5 \text{ kg/s}$) is injected to certain cells are discussed.

Three plants are tested with the simulation flow program and the results are compared to each other. The data of plant are: plant A has a height of 19.925 m, side length 4.2 m x 2.3 m at the bottom and 4.2 m x 4.2 m over the conical part and plant C has a height of 29.95 m, the diameter of the distributor plate was 3.9 m and the diameter of the furnace over the conical part was 7.3 m. Data for plant B are given below.

Furthermore the results calculated with the overall simulation program are discussed and compared to measured experimental data. The plant (B) for which the results are given has a height of 37.2 m with a squared cross section (side length 4.2 m x 7.48 m at the bottom and 7.48 m x 7.48 m above the conical part). Experiments and calculations are made for full load conditions. The performance test was done for a steam rate of 250 t/h, 540°C and 125 bar. Air is injected to the furnace as primary, secondary and tertiary air. It is shown that the results obtained with overall simulation program are comparative to the experimental results.

Kurzfassung

Im Rahmen dieser Arbeit wurde das Feststoffverteilungsprogramm (SOLDIST) und ein Gesamtsimulationsprogramm für zirkulierende Wirbelschichten erweitert, teilweise umprogrammiert und getestet. Das Feststoffverteilungsprogramm wurde als „Stand-Alone-Version“ konzipiert und um das „Multi air injection model“ erweitert.

Im Feststoffverteilungsprogramm wurde die COMMON-Block Struktur (ein Element der Programmiersprache Fortran 77) aufgelöst und durch eine parameterlistenbasierte Variablenübergabe ersetzt. Danach wird eine detaillierte Beschreibung des Feststoffverteilungsprogrammes gegeben.

Die aktuelle Version des Simulationsprogramms erlaubt es, Sekundärluft in jede gewünschte Zelle des Feuerraumes einzudüsen. Es folgt der Vergleich einer Berechnung, bei der kein Sekundärluftmassenstrom zusätzlich zugeführt wird, mit einer solchen, bei der dies in jeweils einzelnen Zellen ($\dot{m}_{Air,add} = 5 \text{ kg/s}$) Sekundärluft zugeführt wird.

Drei verschiedene Anlagen werden mit dem Feststoffverteilungsprogramm getestet, um die Ergebnisse miteinander zu vergleichen. Die Höhe des Steigrohres der Anlage A beträgt 19.925 m, die Seitenlänge am Düsenboden mißt 4.2 m x 2.3 m und über dem konischen Teil 4.2 m x 4.2 m. Die Daten für die Anlage B werden unten gegeben. Die Höhe des Steigrohres der Anlage C beträgt 29.95 m, der Durchmesser am Düsenboden ist 3.9 m und über dem konischen Teil 7.3 m.

Weiters werden die Ergebnisse der Berechnungen des Gesamtsimulationsprogramms mit den Messungen aus den Experimenten verglichen. Die Höhe des Steigrohres der Anlage (B) beträgt 37.2 m, die Seitenlängen am Düsenboden ist 4.2 m x 7.48 m und über dem konischen Teil 7.48 m x 7.48 m. Experimente und Berechnungen wurden für Vollast der Anlage gemacht. Die Experimente wurden bei einem Frischdampfmassenstrom von 250 t/h und Dampfparametern von 540°C und 125 bar durchgeführt. Luft wird als Primär-, Sekundär- und Tertiärluft zugeführt. Es wird gezeigt, dass die Ergebnisse des Gesamtsimulationsprogramms in etwa mit den Messungen aus den Experimenten übereinstimmen.

Abstrakt (in Albanian language)

Në këtë punim programi simulues „solid flow“ (SOLDIST) dhe programi kryesorë simulues për llogaritje të kaldajave të avullit „circulating fluidized bed boilers“ (CFBB) (të zhvilluar në institutin e termoteknikës në Vjenë (ITW)) janë zgjëruar, pjesërisht riprogramuar dhe testuar. Programi SOLDIST është koncipuar të punoj si version i pavarur „Stand-Alone-Version“ nga programi kryesor dhe i zgjeruar të funksionoj si model „multi-air injection“.

Në programin „solid flow“ (SOLDIST) janë fshirë „COMMON“ bloqet (veti e gjuhës programuese FORTRAN 77) dhe variablat e definuara në këto blloqe janë bartë në listat e parametrave. Funksionaliteti i programit është vertetuar përmes një shembulli ku si shtesë e ajrit sekondar të injektuar (fatur) në kaldajë është marrë sasia e ajrit prej $\dot{m}_{Air,add} = 5 \text{ kg/s}$.

Pastaj janë bërë llogaritjet për tri kaldaja me gjeometri të ndryshme dhe rezultatet e fituara i kemi krahasuar njëra me tjetrën (ndërmjet veti). Parametrat e kaldajës A janë: Lartësia 19.925 m, në pjesën fundore gjerësi/gjatësi 4.2 m x 2.3 m dhe mbi pjesën konike gjerësi/gjatësi 4.2 m x 4.2 m. Parametrat e kaldajës B janë dhëne me poshtë. Ndërsa të dhënat e kaldajës C janë: lartësia 29.95 m, diametri në pjesën fundore është 3.9 m ndërsa mbi pjesën konike 7.3 m.

Me ndihmen e programit kryesor simulues janë bërë llogaritje të reja dhe rezultatet e fituara i kemi krahasuar me rezultatet eksperimentale të fituar për të njëjten kaldajë avulli për të cilën janë bërë eksperimentet laboratorike. Lartësia e kaldajës është 37.2 m, në pjesën e fundore ka gjerësinë/gjatësinë 4.2 m x 7.48 m dhe mbi pjesën konike me gjerësi/gjatësi 7.48 m x 7.48 m. Llogaritja dhe testi eksperimental janë bërë nën ngarkesën e plotë të kaldajës dhe nën kushte atmosferike. Sasia e avullit të prodhuar është 250 t/h, me temperaturë 540°C dhe shtypje 125 bar. Ajri është fatur (injektuar) në kaldajë si ajër primarë, sekondarë dhe terciarë. Resultatet e fituara përmes llogaritjeve janë në përputhshmeri të mirë me rezultatet e fituara eksperimentalish (siq janë sqaruar në kapitujt përkatës).

Dedicated to my parents, brothers and sisters,
which survive the war in Kosova (1998-99)

Gewidmet meinen Eltern und Geschwistern,
die den Krieg im Kosova (1998-99) überlebt haben.

Dedikur prinderve, vllëzerve dhe motrave
te cilët mbijetun luftën e Kosovës (1998-99).

1	INTRODUCTION.....	1
2	EXTENTION OF THE SOLIDS DISTRIBUTION PROGRAM SOLDIST.....	4
2.1	Program SOLDIST_MAIN.....	5
2.2	Subroutine SDMREADMAI.....	6
2.3	Subroutine SOLDIST.....	6
2.4	Subroutine SOLDIST1.....	11
2.5	Subroutine AUSGABE.....	13
2.6	Subroutine FRACTIONSTERN.....	14
2.7	Real Function LEVA.....	15
2.8	Subroutine INFINIT.....	15
2.9	The functions RTBIS.....	16
2.10	Real Function Masse.....	16
2.11	Subroutine EUNDW.....	17
2.12	Function BLASE.....	18
2.12.1	Real Function WIRTH1.....	19
2.12.2	Real function GL427.....	20
2.13	Real Function VT.....	21
2.14	Real Function EUN.....	22
2.15	Real Function ONLY.....	23
2.16	Real Function FUNC1.....	23
2.17	Subroutine BUBPOR.....	27
2.18	Real Function VOLUME.....	27
2.19	Subroutine SUMME.....	28
2.20	Real Function YANG.....	30
2.21	Real Function FUNCEPS.....	30
2.22	Real Function FUNC2LOS.....	31
2.23	Subroutine ZWEILOS.....	31
2.24	Real Function JOHNS.....	33
2.25	Real Function EPSA.....	34
2.26	Real Function VSRAND.....	34
3	CHECKING THE FUNCTIONALITY OF THE PROGRAM.....	35
3.1	Generally Remarks About the Program.....	35
3.2	Upwards and Downwards Solid Mass Flux.....	36
3.3	Ratio of Core to Total Area.....	38
3.4	Solids Concentration.....	39
3.5	Gas Velocity.....	40

4	OVERVIEW ABOUT A MODEL FOR THE DESCRIPTION OF THE BUBBLE-FORMING ZONE.....	43
4.1	<i>General Aspects.....</i>	43
4.2	<i>Pressure Drop Across Distributors.....</i>	45
4.3	<i>Time for Bubble Formation.....</i>	45
4.4	<i>Determination of the Bubble Size.....</i>	46
4.5	<i>Estimation of the Bubble Velocity.....</i>	50
5	TEST CALCULATIONS WITH THE FLOW PROGRAM FOR THREE PLANTS.....	52
5.1	<i>Geometrical Data and the Input Parameters.....</i>	52
5.2	<i>Simulation Results.....</i>	56
6	CALCULATION AND COMPARISON WITH OVERALL SIMULATION PROGRAM CFBB.....	62
6.1	<i>Estimation of Pressure Profiles over the Furnace Height.....</i>	62
6.2	<i>Determination of Temperature Profile over Furnace Height.....</i>	65
6.3	<i>Boiler Efficiency.....</i>	67
6.4	<i>Size distribution of bed and circulating material.....</i>	69
6.5	<i>Solids Mass Flow through Ash Classifier and Filter.....</i>	71
7	OVERVIEW ABOUT GRAIN SIZE REDUCTION MECHANISMS IN FLUIDIZED BED BOILERS.....	74
7.1	<i>General Remarks about Attrition and Fragmentation.....</i>	74
7.1.1	<i>Fragmentation.....</i>	74
7.1.1.1	<i>Fuel Fragmentation.....</i>	74
7.1.1.2	<i>Sorbent Fragmentation.....</i>	75
7.1.2	<i>Attrition.....</i>	76
7.1.2.1	<i>Char Attrition.....</i>	78
7.1.2.2	<i>Catalyst Attrition.....</i>	78
7.2	<i>Coal Ash Attrition.....</i>	81
8	Summary.....	83
9	References.....	85

NOTATION

Symbol	Units	Physical dimension
a	$[m^{-1}]$	Decay constant in the splash zone
a	$[-]$	Coefficient used in Equation 7.2.3
A	$[\%]$	Extent of attrition Equation 7.2.2
A_c	$[m^2]$	Core cross section
A_{db}	$[m^2]$	Cross section of the distributor plate 4.4.4
A_D	$[m^2]$	Cross-section area of distributor plate per number of orifices (4)
A_{FR}	$[m^2]$	Cross-section area of combustion chamber
A_{lokal}	$[m^2]$	Furnace cross section
Ar	$[-]$	Archimedes number
a_{VSTR}	$[-]$	Variable for calculation of radiation loss (DIN 1942)
A_{ZYKL}	$[m^2]$	Corresponding equivalent cross-section of the inlet orifice from riser to cyclone
b	$[-]$	Coefficient in equation 7.2.3
b_{VSTR}	$[-]$	Variable for calculation of radiation loss (DIN 1942)
B_{ZYKL}	$[m]$	Equivalent diameter of the cyclone's outlet
C_0	$[-]$	Virtual mass coefficient
$c_{p,a}$	$[J/kg\ K]$	Specific heat capacity of ash
$c_{pf,Abg}$	$[J/kg\ K]$	Specific heat capacity of the flue gas
$c_{p,S}$	$[J/kg\ K]$	Specific heat of total solid matter
$d_{Av(i)}$	$[m]$	Average particle diameter of size fraction
$D_{AE(i)}$	$[m]$	Equivalent diameter at respective height of the furnace
d_{b0}	$[m]$	Initial bubble size
d_b	$[m]$	Bubble diameter
d_{bmax}	$[m]$	Maximum bubble diameter
D, D_0	$[m]$	Bed diameter Eq. 4.2.2 and Eq. 2.14.1
D_c	$[m]$	Local core diameter
D_{DB}	$[m]$	Diameter of distributor plate

DEL, TE	[-]	The number of partitionings in the riser
$DELTA$	[-]	Parameter to calculate each layer ($= 1/TE$)
d_{eq}	[m]	Equivalent bubble diameter
D_{HO}	[m]	Equivalent diameter at current layer Eq. 2.10.4
D_{FR}	[m]	Diameter of furnace
D_{lokal}	[m]	Local diameter of the combustion chamber
d_{ps}	[m]	Average (Sauter's) diameter of solid inventory material
d_{psBed}	[m]	Sauter diameter of bed material
d_{psCirc}	[m]	Sauter diameter of circulating material
D_{STP}	[m]	Diameter of return leg
D_{ZYKL}	[m]	Equivalent diameter of immersion tube of the cyclone
E	[kg/m ² s]	Upwards mass flux of solid matter
F	[-]	Parameter according to [7] used in equations 2.13.3
Fr_p	[-]	Particle Froude number
Fr_{pwf}	[-]	Particle Froude number with descending velocity
Fr_{pumf}	[-]	Particle Froude number with minimum fluidization velocity
F_{STR}	[s/m]	Parameter used in equation 2.13.3 [7]
$F_{urcellNumo}$	[-]	Number of balance cells in furnace
g	[m/s ²]	Acceleration of gravity
G_{sges}	[kg/m ² s]	Mass flow of circulating solid matter for each fraction
G_s, G_{s2}	[kg/m ² s]	Mass flow of circulating solid matter per cross section
G_{sINF}	[kg/m ² s]	Mass flow rate of the circulating solid matter at height H_{GES1}
G_{slokal}	[kg/m ² s]	Mass flux of circulating solid matter per local cross-section

h	[m]	Height of the furnace Eq. 4.4.3 and 5.2.8
H_{AM}	[m]	Height of refractory in furnace
H_{AS}	[m]	Height of secondary air injection
H_{AT}	[m]	Height of tertiary air injection
$\Delta \tilde{H}_{CO,CO}$	[J/kmol]	Molar reaction enthalpy due to the combustion of CO to CO ₂
H_{DEN}	[m]	Height of the dense bed
H_{GES1}	[m]	Height of the furnace up to the centreline of the cyclone's outlet
H_{FUELL}	[m]	Filling height of solids in furnace at minimum fluidization velocity
H_{FR}	[m]	Height of the furnace without refractory
$H_{GAS(i)}$	[m]	Height at which air will be injected in furnace
H_{GES}	[m]	Total height of the furnace
H_{HAUBE}	[m]	Height of the cover in the furnace
H_K	[m]	Height of cone in furnace
H_{mf}	[m]	Height of solids bed at minimum fluidization velocity
H_O	[m]	Lower level of layer in loop
H_{O1}	[m]	Upper level of layer in loop
$H_{STERN}, H, BALAN$	[m]	Height of transition zone measured from the top
H_u	[J/kg]	Net calorific value of fuel
H_{uK}	[J/kg]	Calorific value of unburned carbon
$H_{ZELL(JM)}$	[m]	Height of each cell
H_1	[m]	Height at the distributor plate
H_2	[m]	Height at which the secondary air is injected
k_a	[min ⁻¹]	The coefficient used in equations 2.4.2 and 5.2.9
k_a	[min ⁻¹]	Constant of attrition rate used in Equation 7.1.2.1.1
k	[min ⁻¹]	Constant which is a function of the initial particle size, Eq. 7.1.2.2.1
k_1, k_2	[-]	Coefficients to determinate ε_a
K	[1/s]	Attrition rate constant, Equation 7.2.4

K	[-]	Constant used in equation 4.5.1
K	[m/s]	Difference of local velocities, Eq. 2.24.2 (as auxiliary parameter)
K_{ab}	[-]	Coefficient used in Eq. 2.16.12
k_{BV}	[-]	Correction factor for external fuel preheating
k_{GDS}	[kg/kg]	Specific mass of flue gas
k_L	[kg/kg]	Specific air request at air excess
k_{LV}	[-]	Correction factor for external air preheating
k_{sBed}	[-]	Particle size distribution of bed material (mass fraction of size fraction)
k_{sCirc}	[-]	particle size distribution of circulating material (mass fraction of size fraction)
k_s	[kg/m ² s ⁻¹ Pa ⁻¹]	Surface reaction rate coefficient 7.1.2.1.2
$k_{S/K}$	[-]	Correction factor for calcination and sulfation
$LAST$	[-]	Load factor for HeatFlowSteaNet (1 corresponds to 100% load)
LLV	[m]	Horizontal length of return leg
LP	[m]	Inclined length
$m_{s,LAY}$	[kg]	Mass of solid matter within the respective layer 2.10.2
m	[-]	Exponent used in Equation. 7.1.2.2.1
\dot{m}_{BR}	[kg/s]	Feed mass flow
\dot{m}_{BR0}	[kg/s]	Feed mass flow of fuel
M_{CO}	[kg/mol]	Molar mass of the carbon
$\dot{m}_{CaS,Q}$	[kg/s]	Mass flow of sorbent
M_{DEN}	[kg]	Mass of solid matter in the dense zone
\dot{m}_{FA}	[kg/s]	Mass flow of fine ash
$\dot{m}_{FA,K}$	[kg/s]	C_{fix} mass flow at fine ash
\dot{m}_{GA}	[kg/s]	Mass flow of bottom (coarse) ash
$\dot{m}_{GA,K}$	[kg/s]	C_{fix} mass flow at coarse ash

\dot{m}_{gas}	[kg/s]	Gas mass flow
\dot{m}_{GASP}	[kg/s]	Primary mass flow injected air
\dot{m}_{GASS}	[kg/s]	Secondary mass flow injected air
\dot{m}_{GAST}	[kg/s]	Tertiary mass flow injected air
\dot{m}_I	[kg/s]	Mass flow of inert material
\dot{m}_{I_FA}	[kg/s]	Mass flow of inert material through filter
\dot{m}_{K_FA}	[kg/s]	Mass flow of char through filter
\dot{m}_{L_FA}	[kg/s]	Mass flow of sorbent through filter
$\dot{m}_S, \dot{m}_{zirk}$	[kg/s]	Mass flow of circulating material
M_{sFR}	[kg]	Mass of solid matter in the furnace
$\dot{m}_{FGASGES}$	[kg/s]	Total mass flow of injected air
$\dot{m}_{FGASSUM}$		
$\dot{m}_{FGAS}(i)$	[kg/s]	Mass flow of injected air at each cell
M_s	[kg]	Mass of solid matter in the transition zone
M_{sB}	[kg]	Mass in the vertical section of return leg
M_{sBULK}	[kg]	Mass of solid matter at that part of the furnace without refractory
M_{sGES}	[kg]	Mass of inventory material in the system, cyclone and return leg included
$M_{s,FuncCalc}$	[kg]	Calculated mass of solid in the furnace
M_{sSYF}	[kg]	Mass of solids in siphon
M_{sZY}	[kg]	Mass of solids in cyclone
M_{TRANS}	[kg]	Mass of solid contained in one cell
\dot{m}_{Verb}	[kg/s]	Mass flow of burned char
n_b	[s ⁻¹]	Frequency of bubble formation
$NMATRIX$	[-]	The dimension of output matrix, which is equal to the number of calculated layers.
N_{or}	[-]	Number of orifice
n_s	[-]	Richardson-Zaki exponent
N_{ZYKL}	[-]	Number of cyclones
p_{O2}	[Pa]	Partial pressure of oxygen
Δp	[Pa]	Pressure loss in Eq. 2.12.1.1 and pressure loss of the layer due to solid matter Eq. 2.10.5

Δp_{acc}	[Pa]	Pressure loss due to friction and acceleration
Δp_B	[Pa]	Pressure drop of the dense bed
Δp_{DB}	[Pa]	Pressure drop across the air distributor
Δp_{FR}	[Pa]	Pressure loss in the furnace
Δp_{TRAN}	[Pa]	Pressure loss in the transition zone
Δp_{vent}	[Pa]	Pressure loss in L-valve or siphon
Δp_{zykl}	[Pa]	Pressure loss in the cyclone
\dot{Q}	[m ³ /s]	Volumetric flow through the jet nozzles
\dot{Q}_{ND}	[W]	Available heat flow of steam
r_b	[m]	Radius of bubble Eq. 4.4.6
R	[J/mol K]	Gas constant (8,314)
R	[min ⁻¹]	Attrition rate Equation 7.2.1
R_{∞}	[min ⁻¹]	Attrition rate at steady-state
Re_b	[-]	Bubbles Reynolds number
Re_{umf}	[-]	Reynolds number for minimum fluidization velocity
Re_t, Re_p	[-]	Reynolds number
S_1	[m]	Length of furnace at level H1
S_2	[m]	Width of furnace at level H1
S_3	[m]	Length of furnace at level H2
S_4	[m]	Width of furnace at level H2
S_{1A}	[m]	Local length dependent on current height A
S_{2A}	[m]	Local width dependent on current height A
S_{1B}	[m]	Local length dependent on current height B
S_{2B}	[m]	Local width dependent on current height B
S_{1DB}	[m]	Length of air distributor plate
S_{1FR}	[m]	Length of furnace at the upper part (above the cone)
S_{2DB}	[m]	Width of air distributor plate
S_{2FR}	[m]	Width of furnace at the upper part (above the cone)

$S_{1A(i)}$	[m]	Length of the furnace wall at the level of secondary/tertiary air injection
$S_{2A(i)}$	[m]	Width of the furnace wall at the level of secondary/tertiary air injection
S_{1HO}	[m]	Length of furnace wall at height of H_0
S_{2HO}	[m]	Width of furnace wall at height of H_0
S_{UM}	[-]	Volume fraction of bubbles in the riser
SUM	[m ³]	Volume of the actual layer of the riser
S	[m ²]	Surface area of char, Equation 7.1.2.1.2
t_{a1}	[K]	Air temperature before the air preheater
t_{Abg}	[K]	Temperature of flue gas
t	[min]	Time, Eq. 7.1.2.1.1
t_b	[s]	Time for bubble formation
T_S	[K]	Temperature of char surface
$t_{S,GA}$	[K]	Temperature of raw ash
$t_{S,FA}$	[K]	Temperature of fine ash
$u_{0AB(i)}$	[m/s]	Superficial gas velocity closely below the tertiary air injection level
$u_{0BE(i)}$	[m/s]	Superficial gas velocity closely below the secondary air injection level
u_{0FR}	[m/s]	Superficial velocity in furnace
u_{0db}	[m/s]	Superficial velocity above the air distributor
u_0	[m/s]	Superficial velocity
$u_{g,c}$	[m/s]	Gas velocity in the core of the riser
u_b	[m/s]	Bubble rise velocity
$u_{b\infty}$	[m/s]	Bubble rise velocity of an isolated bubble
u_f	[m/s]	Gas velocity in dilute phase region, u_0/ε
u_{mf}	[m/s]	Minimum fluidization velocity
u_{mb}	[m/s]	Minimum bubbling velocity
u_{0AO}	[m/s]	Superficial velocity closely above the secondary air injection

u_{0AU}	[m/s]	Superficial velocity closely below the secondary air injection
u_{0AO}	[m/s]	Superficial velocity at the current layer
u_{STOK}	[m/s]	Terminal velocity according to Cheremisinoff [4-8]
V_{ABGV}	[-]	Losses due to the waste (exhaust) gas
v_a	[m/s]	Particle velocity in annulus
V_b	[m ³]	Bubble volume
V_{CO}	[-]	Combustion loss due to the CO content
V_{FA}	[-]	Losses due to unburned material in fly ash
V_w	[m ³]	Wake volume
V_G	[m/s]	Gas velocity
V_{GA}	[-]	Losses due to unburned in bottom ash
V_{INZY}	[m/s]	Inlet velocity in the cyclone
V_t, V_{t1}, V_{t2}	[m/s]	Terminal velocity
V_{FR}	[m ³]	Total volume of furnace
V_{FR1}	[m ³]	Volume of the part of the furnace without refractory
V_{FRV}	[-]	Combustion loss
$V_{Section}$	[m ³]	Volume of the current section
V_s	[m/s]	Solid velocity, Eq.. 2.12.1.4
V_{srand}	[m/s]	Velocity of the particles falling downward in the annulus
V_{srob}	[m/s]	Velocity of particles falling down in the annulus at the upper part of the riser
V_{srunt}	[m/s]	Velocity of particle falling down in the annulus at the lower part of the riser or above the dense zone
V_{STRV}	[-]	Radiation loss
V_{WAV}	[-]	Losses due to the sensible heat in ash
W	[kg]	Mass of coal or char
w	[m/s]	Cluster velocity, Eq. 2.12.1.2

W, W_{s2}, W_{LOW}	[kg/m ² s]	Downward solid mass flux
W_0	[kg]	Initial mass of coal or char
$x_{CO,abg}$	[kg/kg]	CO weight fraction in the flue gas

Greek Symbols

Symbol	Units	Physical dimension
α	[-]	Ratio of core cross-section to total furnace cross-section
α_{ex}	[-]	Ratio of core to total area at the outlet height of the furnace
α_{INF}	[-]	Ratio of core to total area at the infinite height
α_1	[-]	Empirical constant Eq. 4.4.3
δ_b	[-]	Volume fraction of bubbles in furnace
ε	[-]	Porosity at the respective height (output parameter)
ε_a	[-]	Annulus porosity
ε_{av}	[-]	Average porosity of solids in annulus
ε_{AU}	[-]	Average porosity closely below/above secondary air injection
ε_b	[-]	Voidage of bubbles
ε_{BU1}	[-]	Average porosity between air distribution and H_{AS} height of secondary air injection
ε_{BU2}	[-]	Average porosity between secondary air injection and tertiary air injection
ε_{BU3}	[-]	Average porosity between H_{AT} and H_K
ε_{BU4}	[-]	Average porosity between H_K and transition zone H_{GES1} - H_{STERN}
ε_c	[-]	Core porosity
ε_{CAU}	[-]	Average porosity closely below/above tertiary air injection
ε_{cex}	[-]	Porosity of core area at the level of the outlet
ε_{cINF}	[-]	Core porosity at infinite height
ε_{db}	[-]	Porosity closely above the air distributor
ε_{DEN}	[-]	Porosity at the dense zone
ε_{ex}	[-]	Porosity at the level of the furnace outlet
ε_{mf}	[-]	Porosity at minimal fluidization velocity
ε_p	[-]	Average porosity at emulsion phase
ε_{fm}	[-]	Average porosity of total furnace

ε_{fm1}	[-]	Average porosity of range without refractory
ε_{l1}	[-]	Porosity at the level H_0
ε_{l2}	[-]	Porosity at the end of the layer, starts at transition zone
ε_K	[-]	Porosity at the end of conical part
ε_{LI}	[-]	Average porosity at the layer
$\varepsilon^*, \varepsilon_\infty$	[-]	Porosity at theoretical infinite furnace height
ε_0	[-]	Porosity at height h_0
λ	[-]	Parameter calculated in Eq. 2.14.1
λ	[-]	Solid friction factor, Eq. 2.20.1
η_{ex}	[-]	Separation efficiency for solids at furnace outlet
η_{DE}	[-]	Boilers efficiency
$\eta_{F,s}$	[-]	Separation efficiency of solids in cyclone
$\eta_{Z,s}$	[-]	Separation efficiency of solids in filter
θ_w	[deg]	Wake angle
ρ_s	[kg/m ³]	Density of solids
ρ_f	[kg/m ³]	Density of gas
ρ_{bulk}	[kg/m ³]	Mean bulk density in the furnace
ρ_{bul1}	[kg/m ³]	Average density above dense bed
μ, μ_a	[kg/ms]	Dynamic viscosity
μ	[-]	Solid loading of the gas flow Eq. 2.12.1.2
ν	[m ² /s]	Kinematic viscosity of flue gas at furnace temperature
Φ	[-]	Relative free cross-section of tube

Index	Meaning
<i>a</i>	Annulus
<i>ab</i>	Separation
<i>Abg</i>	Flue gas
<i>acc</i>	Acceleration
<i>av</i>	Average
<i>b, bub</i>	bubbling
<i>B</i>	bed
<i>BR</i>	fuel
<i>bulk,BU</i>	bulk
<i>c</i>	core
<i>CaO</i>	calcium carbonate (kalk)
<i>CO</i>	carbon monoxide
<i>DB,db</i>	distributor plate (Düsen Boden)
<i>DEN</i>	dense
<i>eq</i>	equivalent
<i>ex</i>	exit
<i>f</i>	fluid
<i>FA</i>	fly ash
<i>FR</i>	Combustion chamber (Feuerraum)
<i>FUELL</i>	fill
<i>G, g</i>	gas
<i>GA</i>	bottom ash
<i>GES,GES1,ges</i>	Total (Gesamt)
<i>HAUBE</i>	cover
<i>I</i>	inert
<i>INF</i>	infinite
<i>K</i>	cone, sorbent
<i>L</i>	limestone
<i>lokal</i>	local
<i>max</i>	maximum
<i>mb</i>	minimum bubbling
<i>mf</i>	Minimum fluidization
<i>O₂</i>	oxygen
<i>p</i>	particle
<i>P</i>	Primary
<i>rand</i>	annulus
<i>rob</i>	upper
<i>runt</i>	lower
<i>s</i>	solid (Feststoff)
<i>S</i>	Secondary, sulfur, Solid, surface
<i>STERN</i>	star (infinite height)
<i>STR</i>	radiation
<i>t,t1,t2</i>	terminal
<i>T</i>	Tertiary
<i>TRAN</i>	transition
<i>V</i>	loss
<i>vent</i>	valve
<i>w</i>	wake

XXIII

ZELL zirk ZYKL, ZY	Cell (Zelle) Circulating Cyclone (Zyklon)
0	initial (anfänglich)

List of figures

1	Chart flow of main simulation program of CFBB.....	3
2	Chart flow of solid distribution program.....	5
3	Calculated upward mass flux of solids.....	38
4	Calculated downwards mass flux of solids.....	38
5	Calculated ratio of core to total cross-section area.....	39
6	Vertical profiles of solids concentration.....	41
7	Geometrical dates of the plant.....	43
8	Examples of distributor configurations.....	44
9	Behavior of bubbles just above the distributor.....	48
10	Proposed modes of bubble formation.....	48
11	Basic form of a bubble.....	49
12	Bubble parameters as a function of Re_b	51
13	Particle distribution of inventory material for plant B and C.....	55
14	Particle distribution of inventory material for plant A.....	55
15	Upwards mass flux of solids for plant A, B and C.....	58
16	Downwards mass flux of solids for plant A, B and C.....	58
17	Ration of core to total cross-section area for plant A, B and C.....	59
18	Porosity in annulus for plant A, B and C.....	60
19	Average porosity for plant A, B and C.....	60
20	Pressure profile over furnace height.....	63
21	Pressure measuring points.....	64
22	Comparison of calculated and measured temperature values along furnace height	66
23	Temperature measuring points.....	67
24	Particle size distribution of bed material.....	70
25	Particle size distribution of circulating material.....	71
26	Overall mass balance for solid matter.....	71
27	Particle size of combustion ash before milling.....	72
28	Particle size of combustion ash after milling.....	73
29	Some variables affecting attrition.....	76
30	Paths for the size reduction of particles.....	76
31	Types for test attrition.....	77
32	Apparatus for the determination of attrition (from Forsythe and Hertwig).....	79
33	Modification of attrition apparatus by Gwyn.....	80
34	Size reduction mechanisms.....	81

1 Introduction

With the development of CFB-Technology the requirement for simulation programs increased continuously. Numerous simulation programs have been developed for the description of different fields of application e.g. power plants, process technology, multiphase flow etc. The most simulation programs for fluidized beds concern the one-dimensional gas/solids systems. Three groups of models can be distinguished according to the following enumeration:

- 1-dimensional models:

They concern usually empirical models, whose qualitative and quantitative force of expression is limited due to one dimensionality. A comparison of 1-dimensional models for solids distributions given from Glatzer [50].

- 1.5-dimensional models:

This group presents the models from Hirayama *et al.* [41], from Laux *et al.* [47], from Berruti *et al.* [38], from Wong *et al.* [31], from Senior *et al.* [35], from Manno *et al.* [29] and from Ishii *et al.* [28].

Remark: Two-dimensional models are unusual in the field of simulation of CFBBs because instead of them 1.5 dimensional models were used.

- 3-dimensional models:

Only a few works have been done in the field of 3-dimensional models. Some works are published from Knoebig *et al.* [42], from Hyppänen *et al.* [26], from Leithner *et al.* [27], from O'Brien *et al.* [57] and from Fischer [58].

Three-dimensional modeling of CFBC systems are not very common because of complicated decomposition processes, inhomogeneities and missing input data from corresponding experiments.

At the Institute of Thermal Engineering (ITE) the following simulation programs are in use:

- The solid flow program (SOLDIST) (calculation of the solid circulation, the vertical porosity profile and the resulting pressure loss over furnace height for different conditions and plant geometry) and
- The main program for simulation of CFBB's (calculates the heat transfer, coal combustion and pollutant release, temperature profile, etc.)

Determination of the particle distribution in a circulating fluidized bed boiler without determining the whole combustion process and the temperature distribution is made with the solid flow program "SOLDIST". The solid flow program is part of the main program for the simulation of Circulating Fluidized Bed Boilers (CFBB).

The developed simulation program at the Institute of Thermal Engineering (ITE) is based on a 1,5-dimensional model. Two reasons led to selection of a 1,5-dimensional model.

- Experiments showed, that the porosity over the cross section is almost constant except near to the wall of the riser. Therefore it was not necessary to use a full 2- respectively 3-dimensional model.
- The main simulation program of the circulating fluidized bed boiler (CFBB) was developed to calculate heat transfer, coal combustion and pollutant release etc. For that purposes 1-dimensional models are not precise enough.

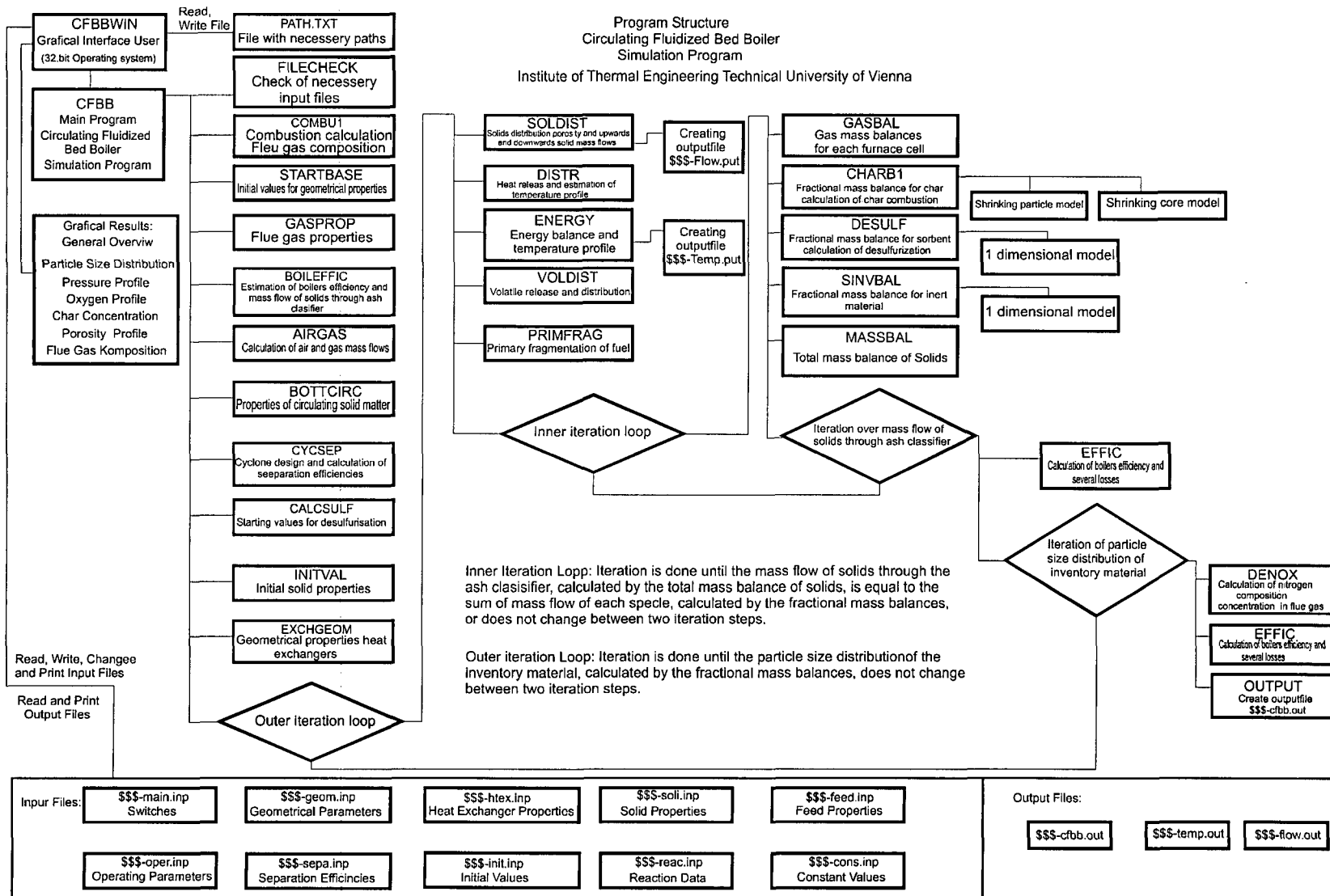
The calculation is an iterative procedure including several parts of the main program. The subroutines for calculating initial values are excluded.

In the program two main iteration loops exist:

The first iteration loop is done over the total mass balance of solids: the solids mass flow through the ash classifier and the sum of concentrations of solid species in the inventory material are the iteration criterions. This iteration loop is done over the fractional mass balances for each solid component. In course of the change of the particle size distribution of inventory material due to attrition, reaction, combustion and mass extraction a second iteration loop is necessary. This second loop starts with the recalculation of the solids distribution and temperature profile and is followed by the calculation of the fractional mass balances. The second iteration criterion is the particle size distribution of the inventory material.

More about this simulation program (CFBB) can be found at the works from Rosza [52], Glatzer [5], Haider [53], Krause [51], Werner [59] and Eder [30].

Fig. 1.1 Chart flow of main simulation program of CFBB



2 Extension of the solids distribution program SOLDIST

In the present chapter are documented and described the subroutines and functions of the simulation flow program SOLDIST, where the following main improvements and extensions were done:

- Implementation of the multi-air injection model (allows to inject additional air to each balance cell of the riser)

The above model is used, to allow a secondary air injection over the all furnace height. This enhanced flexibility allows to model (simulate) of staged combustion and the injection of after burning air.

- Reorganization of the whole program, which means that:

This modification are made in order that, the future users can work with a well structured and clear program.

- a) the "COMMON-BLOCK" based concept of variable's declaration was exchanged to a parameter list based handling of variables,
and
- b) each function and subroutine was written to an own file, whereby each module was documented and described.

The new version of the program was tested and compared to experimental results in chapter 3 and 5.

In the following a description of the current version of the program SOLDIST is given.

The determination of the particle distribution in a circulating fluidized bed boiler without taking into consideration the whole combustion process is done by use of SOLDIST.

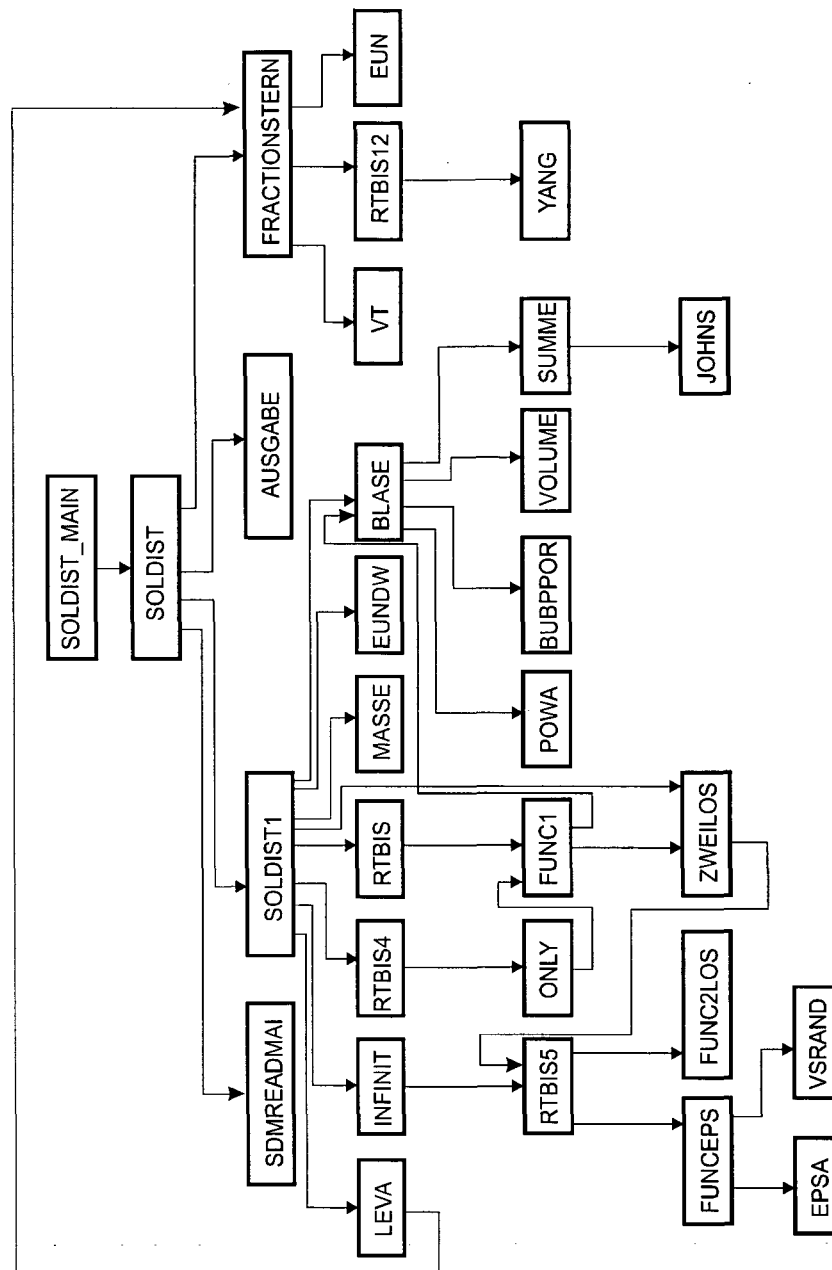


Fig. 2.1 Flow chart of the program

2.1 Program SOLDIST_MAIN

I. Purpose:

The program 'SDMAIN' is a driver program to use the program unit 'SOLDIST' as a Stand-Alone-Version. Normally, SOLDIST is a subroutine of the main program CFBMAIN, which is a "simulation and design tool" for Circulating Fluidized Bed Boilers.

II. Description:

The main steps of SOLDIST_MAIN are:

1. Check whether input files exist (File path.txt with the necessary path and plant identifier).
2. Reading the name of plant
3. Reading the data from the input file
4. Call of Subroutine SOLDIST

The subroutine ends with different messages in case if:
any key-word is not found or if the input file itself was not found.

2.2 Subroutine SDMREADMAI

I. Purpose:

The Subroutine SDMREADMAI reads necessary parameters from input files and transfers them to the subroutine 'SOLDIST'.

The subroutine ends with checking errors when the parameters in the input files are read.

2.3 Subroutine SOLDIST

I. Purpose:

With help of subroutine SOLDIST the solids distribution in a circulating fluidized bed is calculated. The number of fractions can be selected before starting the calculation.

Secondary and tertiary air has to be added in the conical part of the riser.

The height of the riser is subdivided into a certain number of layers whereby for each height of the riser (the number depends on the number of partitioning units "DEL" which can be related in the input file) the program computes the corresponding values for porosity ε , downwards mass flux of solids W , upwards mass flux of solids E , α (ratio of core area to total area of the riser) and the complying mass of solids for each layer. Furthermore, the average density of suspension and the pressure difference (relative to the riser's outlet) are

determined, which are given in separate matrices. The same parameters are calculated for the JM balance cells of the riser, therefore a recalculation of average values for the large balance cells compared to the small (level) original layers is necessary.

II. Description:

1. *Calling subroutine SDMreadmai:*

In subroutine SDMreadmai all input parameters from the input files are read.

2. *Estimation of the height of furnace without refractory:*

$$H_{FR} = H_{GES} - H_{AM} \quad 2.3.1$$

where H_{GES} is the total height of the riser, H_{AM} is the height of refractory in the riser.

3. *Checking of input parameters:*

In this part of the program are "verified" the parameters written below, whether they are available in the used input files:

ε_{mf} - porosity at minimum fluidization velocity,

ε^* - porosity at infinite furnace height,

η_{ex} - separation efficiency of solids at furnace outlet

$S_{1DB}, S_{1FR}, S_{2DB}, S_{2FR}$ - geometrical parameters (length and width of furnace wall at the height of the air distributor plate and in the upper (perpendicular) part of the riser),

$\dot{m}_{GASP}, \dot{m}_{GASS}, \dot{m}_{GAST}$ - primary, secondary and tertiary mass flow of gas

$NMATRIX$ - the dimension of the output matrix, which is equal to the number of calculated layers,

N_{ZYKL} - number of cyclones,

$H_{ZELL(JM)}$ - height of the cell.

4. **Estimation of the geometrical data of the cyclone:**

The geometrical data of the cyclone are determined according to an empirical design equation of a boiler producer:

B_{ZYKL} -Equivalent diameter of the orifice of the outlet:

$$B_{ZYKL} = \sqrt{\frac{0.32 \cdot \left(\frac{\dot{m}_{FGASGES}}{LAST} \right)}{N_{ZYKL} (0.8 \cdot 20 \cdot \rho_f)}} \quad 2.3.2$$

A_{ZYKL} - Corresponding equivalent cross-section of the inlet orifice from riser to a cyclone:

$$A_{ZYKL} = \frac{B_{ZYKL} \cdot 0.8}{0.32} \quad 2.3.3$$

D_{EZYKL} - Equivalent diameter of the vortex finder of the cyclone:

$$D_{EZYKL} = 1.40625 \cdot B_{ZYKL} \quad 2.3.4$$

5. **Height of centerline of the furnace outlet:**

Calculation of the height of the centerline of the furnace outlet above the air distributor plate H_{GES1} :

$$H_{GES1} = H_{GES} - H_{HAUBE} - \frac{B_{ZYKL}}{2} \quad 2.3.5$$

6. **Checking of the assigned values of height:**

Verification whether the assigned values of heights are set to a logical order. The entire calculation of the program SOLDIST is performed for the case that the heights of secondary and tertiary air injection points are lower than the height of cone in furnace. If H_{AT} and H_{AS} don't fulfill this condition invalid values occur during the calculation.

7. Calculation of the diameter of furnace:

The geometrical data of the plant in the input file are given only for rectangular form.

For the further calculations the rectangular area section of the combustion chamber is transformed to circular shape. The same is done for the distribution plate.

$$D_{FR} = \sqrt{\frac{4 \cdot S_{1FR} \cdot S_{2FR}}{\pi}}, \quad D_{DB} = \sqrt{\frac{4 \cdot S_{1DB} \cdot S_{2DB}}{\pi}} \quad 2.3.6$$

8. Length and width of the furnace:

Determination of the length and width of the furnace at secondary and tertiary air injection:

$$S_{1A}(i) = S_{1DB} + \frac{(S_{1FR} - S_{1DB}) \cdot H_{GAS}(i)}{H_K} \quad 2.3.7$$

$$S_{2A}(i) = S_{2DB} + \frac{(S_{2FR} - S_{2DB}) \cdot H_{GAS}(i)}{H_K} \quad 2.3.8$$

9. Determination of an equivalent diameter:

$$D_{AE}(i) = \sqrt{\frac{4 \cdot S_{1A}(i) \cdot S_{2A}(i)}{\pi}} \quad 2.3.9$$

10. Superficial gas velocity (u_{0BE}):

Calculation of superficial gas velocity closely below the secondary air injection (u_{0BE}):

$$u_{0BE}(i) = \frac{4 \cdot \dot{m}_{FGASSUM}}{\rho_f \cdot \pi \cdot D_{AE}^2(i)} \quad 2.3.10$$

11. Superficial gas velocity (u_{0AB}):

Calculation of superficial gas velocity closely below the tertiary air injection (u_{0AB}):

$$u_{0AB}(i) = \frac{4 \cdot (\dot{m}_{FGASSUM} + \dot{m}_{FGAS}(i))}{\rho_f \cdot \pi \cdot D_{AE}^2(i)} \quad 2.3.11$$

This procedure was selected (velocities at point 10 and 11), in order to keep the gas velocity in the conical part constant, because in flow program no combustion procedures are modeled.

12. Superficial gas velocity in the furnace, if entirety of air is injected in conical part of the riser:

$$u_{0FR} = \frac{4 \cdot (\dot{m}_{FGASSUM} + \dot{m}_{FGAS}(F_{urnCellNumo}))}{\rho_f \cdot \pi \cdot D_{FR}^2} \quad 2.3.12$$

13. Total mass of solid matter in combustion chamber:

The total mass of solid matter in the combustion chamber either is given as an input parameter (MassSoliTotal) in the input file or it is calculated. In this case the filling height of solid matter the riser (HeigSoliFurn) has to be given as an input parameter.

14. Calling of subroutine FRACTIONSTERN.

In subroutine FRACTIONSTERN are calculated the following parameters:

- ε^* - Porosity above TDH (transport disengaging height)
- G_s - Mass flow rate of circulating solid matter
- d_{ps} - Average Sauter's diameter of solid inventory material

15. Calling subroutine SOLDIST1.

In the input file the switch (SoliDist) is defined which defines the way of calculation of solids distribution. When switch *SoliDist*=0 the calculation of particle distribution is done with Sauter's diameter and the Subroutine SOLDIST1 is called only once. If the switch *SoliDist*=1 the calculation of the height dependent particle distribution is made for each size fraction of the inventory material.

Generally SOLDIST1 calculates the following parameters; a more detailed description follows in chapter 2.4.

- Upwards mass flux of solids E
- Downwards mass flux of solid W
- Mass flow rate of circulating solid matter G_s
- Pressure loss of cyclone Δp_{ZYKL}
- Pressure loss of furnace Δp_{FR}
- Pressure loss due acceleration Δp_{acc}
- Porosity of the annulus ε_a
- Ratio of core to total cross section area α
- Downwards velocity of the particle in the annulus v_t
- Porosity of the core area ε_c
- Estimation of the bulk density ρ_{bulk}

16. Call of Subroutine AUSGABE and creation of the Output Files.

2.4 Subroutine SOLDIST1

I. Purpose:

This subroutine serves to determine the distribution of porosity and pressure loss in the circulating fluidized bed with optional secondary and tertiary air injection.

II. Description:

1. Geometrical data of cyclone.

More explanation is given above in section 2.3 under point 4.

2. Calling the Subroutine FRACTIONSTERN.

More explanation is given above in section 2.3 under point 15.

3. Calculation of Archimedes number:

$$Ar = \frac{gd_{ps}^3}{v^2} \frac{\rho_s - \rho_f}{\rho_f}$$

2.4.1

4. Calculation of the coefficient k_a for the exponent a Wein, [4]:

$$k_a = 1 + 0.5 Ar^{\frac{1}{3}} \quad 2.4.2$$

5. Function LEVA returns the value of the minimum fluidization velocity to the variable u_{mf} .

6. Calling subroutine INFINIT

Calculation of the below parameters at height H_{GES1} (Height of center line of cyclone's outlet):

- Mass flow rate of circulating solid matter G_s
- Ratio of core to total cross section area α
- Porosity of the core area ε_c
- Porosity above TDH (transport disengaging height) ε^*

7. Mass flow rate of the circulating matter:

Calculation of the mass flow rate of the circulating matter at height H_{GES1} (height of the median line at the outlet to the cyclone):

$$G_{INF} = G_s \cdot \frac{S_{1A} \cdot S_{2A}}{S_{1FR} \cdot S_{2FR}} \quad 2.4.3$$

8. Setting initial values for the porosities:

The below porosities are used for the iteration process in function FUNC1. The meaning of these parameters is given in the notation.

$$\varepsilon_{DEN} = \varepsilon_{BU1} = \varepsilon_{BU2} = \varepsilon_{BU3} = \varepsilon_{BU4} = 0.8$$

9. Checking of the filling height of the riser (H_{FUELL}):

If the filling height (H_{FUELL}) of the riser is greater than $H_{GES1}/3$ the program stops with message:

Verify the assigned value of the height; H_{FUELL} (filling height), H_{GES} (total height of the riser) and H_{HAUBE} (Height of the cover in the furnace).

10. Calculation of the height of the dense zone:

$$H_{DEN} = H_{GES} - BALAN$$

where BALAN is the height of the transition zone (measured from the top of the riser).

11. Calling subroutine EUNDW:

A more detailed description of Subroutine EUNDW is given in the following.

12. Check of the logical parameter LEIDER.

2.5 Subroutine AUSGABE

I. Purpose:

This subprogram writes the results of the flow program SOLDIST to the output file \$\$\$-flow.out. Most computed values are plotted versus the height, for instance porosity against height at each level. The values are for JM = NZell (number of cells) levels displayed.

II. Description:

1. Comparison of the number of cells (NZELL):

If the number of cells given in the input files is not equal to the number of cells given in "include-file" INDMENSION the program stops with the error message "Verify values of JM and NZELL".

2. Geometrical data of cyclone.

More explanation is given above in section 2.3 under point 4.

3. Preparation of output parameters:

With help of the matrix POROS(JZELLE, KOUNT) the output parameters which depend on the height of the furnace are prepared for writing. Also the output parameters which are not dependent on the height of the furnace are prepared for being written (writing) to the output file.

4. Determination of an average bulk-density in the furnace:

$$\rho_{bulk} = \frac{M_{sFR} + (V_{FR} - \frac{M_{sFR}}{\rho_s}) \cdot \rho_f}{V_{FR}} \quad 2.5.1$$

5. Determination of the average bulk-density in the region above refractory (H_{AM} to H_{ZELL} (JM)):

$$\rho_{bul1} = \frac{M_{sBULK} + (V_{FR1} - \frac{M_{sBULK}}{\rho_s}) \cdot \rho_f}{V_{FR1}} \quad 2.5.2$$

6. Determination of the average porosity of total furnace:

$$\varepsilon_{fm} = 1 - \frac{M_{sFR}}{\rho_s \cdot V_{FR}} \quad 2.5.3$$

7. Determination of the average porosity in the region above refractory (H_{AM} to H_{ZELL} (JM)):

$$\varepsilon_{fm1} = 1 - \frac{M_{sBULK}}{\rho_s \cdot V_{FR1}} \quad 2.5.4$$

8. Output of the results of the flow program:

Preparation of the output parameters to be written to the output file.

2.6 Subroutine FRACTIONSTERN

I. Purpose:

Determination of the porosity ε^* above TDH (transport disengaging height above the transition zone) and G_s (circulating mass flow of solids per furnace cross-section). In the current version ε^* is calculated according to the correlation of Yang, [13].

II. Description:

1. Determination of circulating mass flux of solid matter:

The circulating mass flux of solid matter at infinite height of the furnace is determined according to the correlation of Geldart, [14] and [25].

$$G_s = \rho_f \cdot u_0 \cdot 23.7 \exp\left(-5.3 \frac{v_t}{u_0}\right) \quad 2.6.1$$

2. Determination of the porosity ε^* above TDH according to Geldart, [25]:

$$\varepsilon^* = 1 - \frac{G_{sges}}{\rho_s \cdot (u_0 - v_t)} \quad 2.6.2$$

2.7 Real Function LEVA

I. Purpose:

Function LEVA calculates the minimum fluidization velocity (Cheremisinoff, [8]).

II. Description:

1. Determination of Archimedes number (Ar):

More about Ar see section 2.4 (Subroutine SOLDIST1).

2. Determination of the Reynolds (Re) number at u_{mf} :

$$\text{Re}_{u_{mf}} = \sqrt{(27.2)^2 + 0.048 \text{Ar}} - 27.2 \quad 2.7.1$$

3. Determination of the minimum fluidization velocity u_{mf} :

$$u_{mf} = \frac{\text{Re}_{u_{mf}} \cdot \nu}{d_{ps}} \quad 2.7.2$$

2.8 Subroutine INFINIT

I. Purpose:

The subroutine IFINIT calculates the average porosity (ε^*), the core porosity (ε_c), the ratio of core to total area of cross-section (α) and the mass flux of solid matter G_s at the level of H_{GES1} (centreline of cyclone outlet).

II. Description:

1. **Calling subroutine FRACTIONSTERN (described in section 2.6).**

2. **New mass flux of circulating solid matter:**

$$G_{sINF} = \left(\frac{u_0}{\varepsilon_{cINF} \cdot \alpha_{INF}^2} - v_t \right) \cdot (1 - \varepsilon_{cINF}) \cdot \rho_s \cdot \alpha_{INF}^2 - v_{strand} \cdot (1 - \varepsilon_a) \cdot \rho_s \cdot (1 - \alpha_{INF}^2) \quad 2.8.1$$

3. **The subroutine ends with the reassignment of the below parameters:**

$\varepsilon^* = \varepsilon_{INF}$ average porosity,

$\varepsilon_c = \varepsilon_{cINF}$ core porosity,

$\alpha = \alpha_{INF}$ ratio of core to total area of cross section in the riser.

2.9 Use of RTBISx for zero points determination:

The functions RTBIS, RTBIS1, RTBIS12, RTBIS2, RTBIS4, RTBIS5 are used for the determination of the zero points of different functions within the iteration process.

2.10 Real Function MASSE

I. Purpose:

The function MASSE calculates the mass and pressure loss of each layer. The calculation is made for each layer, whereby $\Delta = 1/TE$ expresses the height of the layer per meter in the cone section.

II. Description:

1. Determination of the constant (a):

The constant (a) describes the increase of porosity along the transition zone in the CFB-reactor respectively, respectively the decrease of density and solid concentration decrease.

$$a = \frac{k_a}{u_0} \quad 2.10.1$$

2. Calculation of the porosity at the end of each layer:

This vary of calculating the porosity is valid for the transition zone of the riser.

$$\varepsilon_{I2} = \varepsilon^* - (\varepsilon^* - \varepsilon_{I1}) \cdot e^{-a \cdot DELTA} \quad 2.10.2$$

3. Average porosity:

Calculation of an average porosity for each layer.

4. Determination of the mass in each layer:

$$m_{s,LAY} = \rho_s (1 - \varepsilon_{ILL}) \cdot DELTA \cdot \frac{\pi \cdot D_{HO}^2}{4} \quad 2.10.3$$

5. Determination of the pressure loss in each layer:

$$\Delta p = \frac{4 \cdot m_{s,LAY} \cdot g}{\pi \cdot D_{HO}^2} \quad 2.10.4$$

where D_{HO} is the equivalent furnace diameter at current height.

2.11 Subroutine EUNDW

I. Purpose:

This subroutine calculates the parameters of the matrix EPS(NMATRIX,8) such as:

E (upwards mass flux of solids, EPS(1,3)),

W (downwards mass flux of solids, EPS(1,4)),

M_s (mass of solid matter, EPS(1,5)),

α (ratio of core area to total cross section of the riser tube, EPS(1,6)),

ε_a (porosity of solid matter in the annulus, EPS(1,7)),

v_{sand} (velocity of the particles falling downwards in the annulus, EPS(1,8))

II. Description:

1. Determination of diameter and superficial velocity:

In this part of the simulation program calculations are made to determine the diameter of the furnace and the superficial velocity at the current height of the riser. Calculation is made for each layer, where DEL is a factor which determines the number of layers in the furnace.

2. Reassignment of EPS:

In the second step the values of matrix EPS are reassigned.

2.12 Function BLASE

I. Purpose:

Function BLASE calculates the average porosity of the dense zone and the local average porosity at the end of the dense zone.

II. Description:

1. Porosity in the emulsion phase, see Geldart, [25]:

$$\varepsilon_p = 1 - (1 - \varepsilon_{mf}) \cdot \frac{d_{ps}^{0.1} (g \cdot (\rho_s - \rho_f))^{0.118} (H_{GES1} - H_{STERN})^{0.043}}{2.54 \cdot \rho_f^{0.082} v^{0.066}} \quad 2.12.1$$

2. Minimum bubbling velocity:

The minimum bubbling velocity is calculated according to Hetsroni, [1]. At this velocity the formation of bubbles starts and depends on the type of particles.

$$u_{mb} = 33 \cdot d_{ps} \cdot v^{-0.1} \quad 2.12.2$$

3. **Maximum bubble diameter:**

The maximum bubble diameter is calculated according to Hetsroni, [1]:

$$d_{b\max} = \frac{2 \cdot v_t^2}{g} \quad 2.12.3$$

4. **Call of subroutine SUMME.**

Now subroutine SUMME is called, where Function JOHNS with parameter DENSE is calculating the (average) porosity in the bubbling zone (ε_{bub}). The furnace height here is subdivided into three parts:

- Range below the level of secondary air injection
- Range between the level of secondary air injection and the height of cone (H_K),
- Range between the height of cone (H_K) and the height of the centreline of the outlet to the cyclone (H_{GES1}).

5. **Calling subroutine BUBPOR:**

By using subroutine BUBPOR the following parameters are determined:

BLASE, the mean porosity of the total dense zone,

DENSE, the local porosity at the end of the dense zone.

2.12.1 Real Function WIRTH1:

I. **Purpose:**

The real function WIRTH1 calculates:

- pressure loss,
- cluster velocity,
- gas velocity,
- solids velocity and
- Froude number (Fr)

The calculations are made according to Wirth, [3].

II. Description:

1. Calculation of pressure loss:

Determination of the pressure loss according to clusters and strands in the transition zone:

$$\Delta p = (1 - \Phi) \cdot (\rho_s - \rho_f) \cdot (1 - \varepsilon_{mf}) \cdot g \cdot H_{GES1} \quad 2.12.1.1$$

2. Calculation of cluster velocity:

$$w = \frac{u_{0FR} \cdot \mu \cdot \rho_f}{\rho_s \cdot (1 - \Phi) \cdot (1 - \varepsilon_{mf})} \quad 2.12.1.2$$

where μ [-] is the loading of the gas flow and Φ [-] the relative free cross section of the tube.

3. Calculation of gas velocity:

$$v_G = \frac{u_{0FR}}{\Phi} \left(1 - \varepsilon_{mf} \frac{w}{u_{0FR}} \cdot (1 - \Phi) - (1 - \Phi)^2 \frac{u_{mf}}{u_{0FR}} \right) \quad 2.12.1.3$$

4. Calculation of solids velocity (clusters and strands):

$$v_s = v_G - w \quad 2.12.1.4$$

5. Calculation of Fr, see Wirth, [3]:

$$Fr_p = \frac{u_{0FR}^2}{(\rho_s - \rho_f) \cdot d_{ps} \cdot g} - \frac{(1 - \varepsilon_{mf}) \cdot \Phi \cdot (1 - \Phi)}{0.0053 \cdot \frac{v_G}{u_{0FR}} \cdot \left(\frac{v_s}{u_{0FR}} - \frac{w}{u_{0FR}} \right)} \quad 2.12.1.5$$

2.12.2 Real Function GL427

I. Purpose:

Real function GL427 calculates:

- Particle Froude number,
- particle Froude number at the terminal velocity of single particles,
- particle Froude number at minimum fluidization velocity according to Wirth, [3].

II. Description:

1. Particle Froude number Fr_p :

Calculation of the particle Froude number at superficial velocity:

$$Fr_p = \frac{u_{0FR}}{\sqrt{\frac{(\rho_s - \rho_f)}{\rho_f} \cdot d_{ps} \cdot g}} \quad 2.12.2.1$$

2. Particle Froude number at terminal velocity:

Calculation of the particle Froude number at terminal velocity of single particles:

$$Fr_{p_{wf}} = \frac{v_t}{\sqrt{\frac{(\rho_s - \rho_f)}{\rho_f} \cdot d_{ps} \cdot g}} \quad 2.12.2.2$$

3. Particle Froude number:

Calculation of the particle Froude number at minimum fluidization velocity:

$$Fr_{p_{unf}} = \frac{u_{mf}}{\sqrt{\frac{(\rho_s - \rho_f)}{\rho_f} \cdot d_{ps} \cdot g}} \quad 2.12.2.3$$

4. Dimensionless pressure loss:

The dimensionless pressure loss is calculated according to Wirth, [3] as given in Eq. 4.27, see Wirth, [3].

2.13 Real Function VT

I. Purpose:

This subprogram calculates the terminal velocity of a single particle taking into account the sphericity (included in the factors F and F_{STR} of equation 2.13.2) of the particle, according to Haider and Levenspiel, [7]:

II. Description:

1. Terminal velocity:

Determination of the terminal velocity according to Cheremisinoff, [8]:

$$u_{STOK} = \frac{(\rho_s - \rho_f) \cdot g \cdot d_{ps}^2}{18 \cdot \rho_f \cdot \nu} \quad 2.13.1$$

2. Reassignment of the terminal velocity u_{STOK} :

$$v_{t1} = u_{STOK}$$

3. The determination of Ar is done according to chapter 2.4.

4. Determination of the new terminal velocity v_{t2} :

Determination of a new particle terminal velocity according to Haider and Levenspiel, [7]:

$$v_{t2} = v_{t1} - \frac{F}{F_{STR}} \quad 2.13.2$$

5. Checking of the iteration loop.

If v_{t2} is not calculated correctly, the program stops the calculation with the message that the iteration loop has not been finished successfully.

2.14 Real Function EUN

I. Purpose:

The function EUN calculates the porosity (ε) at infinite furnace height (h_{∞}) according to Geldart, [25]:

II. Description:

1. Determination of parameter λ , see Geldart, [25]:

$$\lambda = \frac{5.17 \cdot (D_0 \cdot d_{ps})^2}{\rho_s \cdot v^{2.5}} \left((u_0 - v_t) \cdot \frac{d_{ps}}{v} \right)^{-1.5} \quad \text{if } (u_0 - v_t) \cdot \frac{d_{ps}}{v} \leq \frac{2.38}{D_0} \quad 2.14.1$$

$$\lambda = \frac{12.3 \cdot (D_0 \cdot d_{ps})^2}{\rho_s \cdot v^{2.5} \cdot \left((u_0 - v_t) \cdot \frac{d_{ps}}{v} \right)^{2.5}} \quad \text{if } (u_0 - v_t) \cdot \frac{d_{ps}}{v} > \frac{2.38}{D_0} \quad 2.14.2$$

2. Porosity at infinite height of the riser:

Determination of the porosity at (theoretical) infinite height of the riser, see Geldart, [25]:

$$\varepsilon_{\infty} = \left(1 + \frac{\lambda \cdot (u_0 - v_t)^2}{2 \cdot g \cdot D_0} \right)^{-\frac{1}{4.7}} \quad 2.14.3$$

2.15 Real Function ONLY:

I. Purpose:

In this case the transition zone exists along the total height of the furnace. So there is no dense bed above the air distributor plate (mass and pressure balance cannot be closed). FUNC1 is called from ONLY. In this case ONLY varies the initial value of ε_{db} (EPSDB) (porosity closely above distributor plate) until mass- and pressure balance are closed.

Function ONLY distinguishes whether an extended dense zone exists above the air distributor plate or not. Usually ONLY tries to close the pressure loop along the

CFB-loop, which means to split the solid matter between riser and return leg. If it is not possible to close the pressure loop function ONLY varies the initial value of ε_{db} (EPSDB) (porosity closely above the air distribution plate) until mass- and pressure balance are closed instead of varying the height H (height of the transition zone).

2.16 Real Function FUNC1:

I. Purpose:

The function FUNC1 calculates the pressure balance at a definite height H of the transition zone. Furthermore H_{STERN} is determined by varying the height H and an average profile of porosity is determined depending on the case whether a dense bed exists or not.

II. Description:

1. Determination of H_{DEN} :

$$H_{\text{DEN}} = H_{\text{GES1}} - H \quad 2.16.1$$

In this case H is the height of the transition zone in the furnace.

2. Checking the number of the air injection points:

Air has to be injected to the conical part of the furnace. Therefore it is checked, whether all the air is really injected in the conical part of the riser.

3. Checking the porosity over furnace height:

By using function BLASE the porosity over the furnace height is checked. The calculation is divided into two parts:

First from the bottom zone to the end of the conical part of the riser (H_K) the profile of porosity is checked and in the second step the zone from the end of the conical part of the riser to the centreline of the outlet to the cyclone (H_{GES1}) is checked. For the first case function BLASE (determination of average porosity of the dense zone) is set to the porosity at the dense bed ε_{db} (EPSDB) and for the second case function BLASE is set to ε_{11} (ε_{11} is the average porosity at the transition zone):

Furthermore the following parameters are determined:

- the mass of solid matter for each height of the riser,
- the pressure (difference) of each layer,
- the volume of each layer.

4. Porosity at the end of the transition zone:

$$\varepsilon_{ex} = \varepsilon^* - (\varepsilon^* - \varepsilon_K) \cdot e^{-a(H_{GEN} - H_K)} \quad 2.16.2$$

where ε_K is the porosity at height H_K (conical height of the riser).

5. Determination of the porosity of the core area at the outlet of the riser:

$$\varepsilon_{cex} = \frac{\varepsilon_{ex} - \varepsilon_a}{\alpha_{ex}^2} + \varepsilon_a \quad 2.16.3$$

6. Mass flux rate of circulating solid matter:

$$G_{s2} = \left(\frac{u_{0FR}}{\varepsilon_{cex} \alpha_{ex}^2} - v_{srand} \right) \cdot (1 - \varepsilon_{cex}) \cdot \rho_s \cdot \alpha_{ex}^2 - (1 - \alpha_{ex}^2) \cdot \rho_s \cdot (1 - \varepsilon_a) \cdot v_{srand} \quad 2.16.4$$

7. Downwards-mass flux rate of solid matter:

$$W_{s2} = (1 - \alpha_{ex}^2) \cdot \rho_s \cdot (1 - \varepsilon_a) \cdot v_{srand} \quad 2.16.5$$

8. Mass in the siphon:

In the case that a siphon is installed the mass inside is calculated:

$$M_{sSYF} = \frac{(2 \cdot D_{STP} \cdot \pi \cdot D_{STP}^2)}{4} \rho_s (1 - \varepsilon_{mf}) \quad 2.16.6$$

9. Mass in the vertical section of the return leg:

$$\begin{aligned}
M_{sB} = & M_{sGES} - M_{sZY} N_{ZYKL} - M_{DEN} - M_{TRANS} - \\
& \frac{1}{3} N_{ZYKL} \cdot LLV \cdot \rho_s \cdot (1 - \varepsilon_{mf}) \cdot \frac{\pi \cdot D_{STP}^2}{4} - \\
& (H_{GES} - H_{GES1}) \cdot \rho_s \cdot (1 - \varepsilon_{ex}) \cdot \frac{\pi \cdot D_{FR}^2}{4}
\end{aligned} \quad 2.16.7$$

10. Mass in each cyclone:

If there are more return legs/cyclones installed, then M_{sB} for one return leg/cyclone is calculated:

$$M_{sB} = \frac{M_{sB}}{N_{ZYKL}} \quad 2.16.8$$

11. Determination of the inclined length of siphon:

$$LP = \frac{4 \cdot M_{sB}}{\rho_s \cdot (1 - \varepsilon_{mf}) \cdot \pi \cdot D_{STP}^2} \quad 2.16.9$$

After the estimation of the inclined length (LP) a security check is made to find out whether the cyclone is overfilled with solid matter. In that case the program stops the calculation with the message:

"Return leg is overcrowded with solid matter, please check the data in input file".

12. Pressure loss in the L-valve:

Calculation of the pressure loss in the L-valve:

$$\begin{aligned}
\Delta p_{vent} = & \left(\rho_s \cdot (1 - \varepsilon_{mf}) \cdot \left(\frac{G_s}{N_{ZYKL} \cdot \rho_s \cdot (1 - \varepsilon_{mf}) \cdot D_{STP}^2} \right)^{0.45} \left(\frac{d_{ps}}{D_{STP}} \right)^{0.25} \right) \cdot \\
& (4.266 \cdot g \cdot LLV + 13.8)
\end{aligned} \quad 2.16.10$$

13. Calculation of the pressure loss in cyclone:

In the first step the inlet velocity of the flue-gas to the cyclone is calculated:

$$v_{INZY} = \frac{\dot{m}_{FGASGES}}{N_{ZYKL} (A_{ZYKL} \cdot B_{ZYKL} \cdot \rho_f)} \quad 2.16.11$$

Then the pressure loss of the cyclone is determined:

$$\Delta p_{ZYKL} = K_{ab} \cdot \left(\frac{A_{ZYKL} \cdot B_{ZYKL}}{D_{ZYKL}^2} \right) \frac{\rho_f \cdot v_{INZY}^2}{2} \quad 2.16.12$$

14. Pressure loss due to acceleration and friction:

$$\Delta p_{acc} = \frac{\rho_s (1 - \varepsilon_{db}) \cdot (1 - \varepsilon_{ex}) (u_{0db} - v_t)^2}{2} \quad 2.16.13$$

15. Determination of pressure loss in the furnace:

$$\Delta p_{FR} = \Delta p_{acc} + \Delta p_{TRAN} + (1 - \varepsilon_{DEN}) \cdot g \cdot \rho_s \cdot (H_{GES1} - H) + (H_{GES} - H_{GES1}) \cdot \rho_s \cdot (1 - \varepsilon_{ex}) \cdot g \quad 2.16.14$$

16. Determination of solid mass in the furnace:

$$M_{s,FurnCalc} = M_{DEN} + M_{TRANS} + (H_{GES} - H_{GES1}) \cdot \rho_s \cdot (1 - \varepsilon_{ex}) \frac{\pi \cdot D_{FR}^2}{4} \quad 2.16.15$$

2.17 Subroutine BUBPOR

I. Purpose:

Based on the fraction of bubbles ε_b this subroutine calculates the porosity of the cross-section.

II. Description:

1. Average porosity:

Determination of the average porosity of the cross-section:

$$\varepsilon_{av} = (1 - \varepsilon_b) \varepsilon_p + \varepsilon_b \quad 2.17.1$$

2.18 Real Function VOLUME

I. Purpose:

The function VOLUME calculates the volume of the conical part of the riser in the range between height H_1 and H_2 . Here $H_1=0$ m is height at the distributor plate and H_2 is the height where the secondary air is injected.

II. Description:

1. Calculation of the length of the sidewall at level H_1 :

$$S_1 = S_{1DB} + (S_{1FR} - S_{1DB}) \cdot \frac{H_1}{H_K} \quad 2.18.1$$

2. Calculation of the width of the wall at level H_1 :

$$S_2 = S_{2DB} + (S_{2FR} - S_{2DB}) \cdot \frac{H_1}{H_K} \quad 2.18.2$$

3. Calculation of the length of the wall at level H_2 :

$$S_3 = S_{1DB} + (S_{1FR} - S_{1DB}) \cdot \frac{H_2}{H_K} \quad 2.18.3$$

4. Calculation of the width of wall at level H_2 :

$$S_4 = S_{2DB} + (S_{2FR} - S_{2DB}) \cdot \frac{H_2}{H_K} \quad 2.18.4$$

5. Calculation of the volume at the current section:

$$V_{Section} = \frac{(S_1 \cdot S_2 + (S_1 + S_3) \cdot (S_2 + S_4) + S_3 \cdot S_4) \cdot (H_2 - H_1)}{6} \quad 2.18.5$$

2.19 Subroutine SUMME

I. Purpose:

The subroutine SUMME calculates the average part of bubbles of the local reference segment (range from height level A to level B). The range starts at the distributor and reaches up to the end of the conical height of the riser (H_K). It is important to denote that the bubbles are formed only at the lower part of the riser.

The calculation is performed for a number of TE cylindrical layers, referenced to height section between level A and B .

II. Description:

1. Length and width of the furnace:

Determination of the local length and width of the furnace wall at height A :

$$S_{1A} = S_{1DB} + (S_{1FR} - S_{1DB}) \cdot \frac{A}{H_K} \quad 2.19.1$$

$$S_{2A} = S_{2DB} + (S_{2FR} - S_{2DB}) \cdot \frac{A}{H_K} \quad 2.19.2$$

2. Local length and width of the furnace:

Determination of the local length and width of the furnace wall at height B :

$$S_{1B} = S_{1DB} + (S_{1FR} - S_{1DB}) \cdot \frac{B}{H_K} \quad 2.19.3$$

$$S_{2B} = S_{2DB} + (S_{2FR} - S_{2DB}) \cdot \frac{B}{H_K} \quad 2.19.4$$

For a number of TE layers per reference segment ($B-A$) the current length and width of the furnace wall are determined to calculate the local volume fraction of bubbles.

3. Length and width of the furnace wall.

Calculation of the length and width of the furnace wall at the current height for each layer:

$$S_{1HO} = S_{1DB} + (S_{1FR} - S_{1DB}) \cdot \frac{H_O}{H_K} \quad 2.19.5$$

$$S_{2HO} = S_{2DB} + (S_{2FR} - S_{2DB}) \cdot \frac{H_O}{H_K} \quad 2.19.6$$

4. **Average volume fraction of the bubbles:**

Calculation of an average volume fraction of bubbles for the local reference element:

SUM, an auxiliary parameter, is the volume of the actual layer of the riser:

$$SUM = FUNC(H_O) \cdot S_{1HO} \cdot S_{2HO} \cdot (H_{O1} - H_O) \quad 2.19.7$$

$$S_{UM} = \frac{6 \cdot SUM}{(B - A) \cdot (S_{1A} \cdot S_{1B} + (S_{1A} + S_{1B}) \cdot (S_{2A} + S_{2B}) + S_{1B} \cdot S_{2B})} \quad 2.19.8$$

where the S_{UM} is the volume fraction of bubbles in the riser.

2.20 Real Function YANG

I. **Purpose:**

Calculation of the porosity (ε^*) at infinite height depending on the respective friction factor according to a correlation of Yang, [13]. First a zero points search is performed because the porosity ε is not known explicitly.

II. **Description:**

1. **Determination of the solid friction factor λ according to Yang, [13]:**

$$\lambda = 0.041 \cdot \left((1 - \varepsilon) \cdot \frac{Re_t}{Re_p} \right)^{-1.021} \cdot \frac{1 - \varepsilon}{\varepsilon^3} \quad 2.20.1$$

where Re_t is the Reynolds number determined according to: $Re_t = \frac{d_{ps} v_t}{\nu}$

and Re_p : $Re_p = \frac{d_{ps} \cdot (u_f - u_p)}{\nu}$

2. Porosity at infinite height:

Calculation of the porosity at (theoretically) infinite height of the riser ε^* according to Yang, [13]:

$$\varepsilon^* = \varepsilon - \left(1 + \lambda \cdot \frac{\left(\frac{U_{0FR}}{\varepsilon} - v_t \right)^2}{2 \cdot g \cdot D_{FR}} \right)^{-\frac{1}{4.7}} \quad 2.20.2$$

2.21 Real Function FUNCEPS

I. Purpose:

The function FUNCEPS determines a new α considering the separation efficiency at the upper end of the furnace. Thus, not the total upwards-mass flux of solid matter is leaving the furnace at the outlet to the cyclone, there is a certain amount of back flow of solids to the annulus. Consequently α and ε^* (referring to infinite furnace height) are decreasing.

II. Description:

1. Determination of (α_{ex}):

Determination of α_{ex} (ratio of core area to total cross section area of the furnace) considering the separation efficiency (η_{ex}) of the furnace exit:

$$\alpha_{ex}^2 = \frac{(1 - \varepsilon_c) \cdot \eta_{ex} \cdot \frac{u_0}{\varepsilon_c} - (1 - \varepsilon_a) \cdot v_{sand}}{(1 - \varepsilon_c) \cdot \eta_{ex} \cdot v_t - (1 - \varepsilon_a) \cdot v_{sand}} \quad 2.21.1$$

2. *Calculation of new α considering the separation efficiency:*

FUNCEPS is the calculated new α (ratio of core to total cross section of the furnace at infinite height):

$$FUNCEPS = \alpha_{ex}^2 - \frac{(\varepsilon - \varepsilon_a)}{\varepsilon_c - \varepsilon_a} \quad 2.21.2$$

2.22 Real Function FUNC2LOS

I. Purpose:

Function FUNC2LOS calculates the new core porosity (ε_c), the ratio of core area to total cross section area of the furnace (α), the upwards mass flux (E) and the circulating mass flux of solid matter (G_s).

2.23 Subroutine ZWEILOS

I. Purpose:

Calculation of the average porosity and superficial velocity due to injected air closely above secondary or tertiary air injection.

II. Description:

1. *Mass flux of circulating solid matter:*

Determination of the local mass flux of the circulating solid matter per local cross-section:

$$G_{stokal} = G_s \cdot \frac{S_{1A} \cdot S_{2A}}{S_1 \cdot S_2} \quad 2.23.1$$

where S_1 , S_2 are the length/width of the furnace at the respective heights H_1 and H_2 and S_{1A} , S_{2A} are the local length/width of the furnace wall at height A.

2. **Ratio of core to total cross section area:**

Calculation of the ratio of core area to total cross section area of the riser:

$$\alpha^2 = \frac{\varepsilon_{AU} - \varepsilon_a}{\varepsilon_{cAU} - \varepsilon_a} \quad 2.23.2$$

After the calculation is checked whether the condition $\alpha < 1$ is fulfilled.

3. **Downwards mass flux of solid matter:**

$$W_{LOW} = (1 - \alpha^2) \cdot \rho_s \cdot v_{strand} \cdot (1 - \varepsilon_a) \quad 2.23.3$$

4. **Average porosity:**

Calculation of the average porosity closely above secondary air injection:

$$\varepsilon_{AO} = 1 - (1 - \varepsilon_{AU}) \cdot \frac{u_{0AU}}{u_{0AO}} \quad 2.23.4$$

where ε_{AU} is the average porosity closely below ,

u_{0AU} is the superficial velocity closely below and

u_{0AO} is the superficial velocity closely above secondary air injection.

2.24 Real Function JOHNS

I. **Purpose:**

Determination of the amount of bubbles at current height according to Johnsson, [2]:

II. **Description:**

1. **Calculation of the superficial velocity:**

$$u_0 = \frac{4 \cdot \dot{m}_{gas}}{\pi \cdot D_{FR}^2 \cdot \rho_f} \quad 2.24.1$$

2. Local difference velocity K .

This parameter is used only as an auxiliary parameter:

$$K = \frac{\dot{m}_{gas}}{A_{FR} \cdot \rho_f} - \frac{\pi \cdot D_{FR}^2 \cdot G_s}{4 \cdot A_{FR} \cdot \rho_f} - u_{mf} \quad 2.24.2$$

3. Calculation of the auxiliary parameter "Johns":

$$Johns = 0.24 \cdot (1.1 + 2.9^{-3.3 \cdot d_p \cdot 10^3}) \cdot (0.15 + K)^{-0.33} \quad 2.24.3$$

4. Calculation of the volume fraction of bubbles:

$$\delta_b = \frac{1}{1 + 1.3 \cdot \frac{K^{-0.8}}{Johns}} \quad 2.24.4$$

The above parameters " K " and " $Johns$ " are used in the simulation program only as auxiliary parameters (they are used only for the calculation procedure).

2.25 Real Function EPSA

I. Purpose:

Function EPSA calculates the porosity of the annulus according to a modified approach of Goedicke, [9]:

$$\varepsilon_a = 15 \cdot (1 - \varepsilon_{mf})^6 \quad 2.25.1$$

$$\varepsilon_a = \varepsilon_a \varepsilon_{mf} + (1 - \varepsilon_a) \cdot \varepsilon + 15 \cdot (\varepsilon - \varepsilon_{mf})^7 \quad 2.25.2$$

2.26 Real Function VSRAND

I. Purpose:

The function VSRAND calculates the downwards velocity of the falling particles in the annulus.

II. Description:

Calculation and security check of diameter of the air distributor plate (D_{DB}), diameter of the riser at height of the secondary air injection (D_{AS}) and diameter of the riser at the height of the tertiary air injection.

Calculation of the velocity of the particles falling downwards in the annulus:

$$v_{srand} = v_{srob} - (v_{srob} - v_{srunt}) \cdot e^{-a \cdot H} \quad 2.26.1$$

where v_{srob} is the velocity of particles falling down in the annulus in the upper part of the riser, v_{srunt} is the velocity of particles falling down in the annulus in the lower part of the riser.

3 Checking the functionality of the program

In chapter 2 the solids distribution program which was written at the Institute of Thermal Engineering (ITW), Vienna University Technology was described. This chapter checks the functionality of the program and therefore an industrial CFB-boiler (plant A, see Fig. 3.5.2) was simulated.

3.1 General remarks about the program

The current version of the simulation program allows to inject secondary air to each cell of the combustion chamber. In the following examples an additional mass flow of secondary air ($\dot{m}_{Air,add} = 5 \text{ kg/s}$) is injected to a certain cell, whereby the cell (location of injection) was varied from case to case. The results are compared for six cases. The first case is the reference case (without additionally air injection) and is defined in the diagram as "without add" air. The next calculations are made with additionally air for each cell.

The height of air injection in the combustion chamber is given in table below.

Height of air injection [m]	Mass flow injected air [kg/s]
0.0	15.287
2.2	7.643
3.2	2.5478
6.8	0
9.5	0
11.0	0
14.7	0
16.92	0

Tab. 3.1.1 Height of the air injection

3.2 Upward and downward mass flux of solids

The procedure to calculate the upward and downward directed mass fluxes is described in chapter two. The table below gives the results for different situations of air injection in the riser. The model is so developed that injection air in the different height of the riser have no influence to the upward and downward solid mass flux.

Height of air Injection [m]	Without Additional air [kg/s]	Additional air [kg/s] at height 6.8 [m]	Additional air [kg/s] at height 9.5 [m]	Additional air [kg/s] at height 11 [m]	Additional air [kg/s] at height 14.7 [m]	Additional air [kg/s] at height 16.9 [m]
0	34.17	36.96	36.75	36.38	35.30	32.57
2.2	20.54	21.91	21.60	21.42	21.01	18.15
3.2	17.72	18.65	18.32	18.20	18.01	15.02
6.8	17.44	18.25	17.91	17.81	17.69	14.55
9.5	17.25	18.12	17.67	17.59	17.50	14.32
11	17.23	18.12	17.66	17.55	17.47	14.27
14.7	17.22	18.12	17.66	17.55	17.47	14.26
16.9	17.22	18.12	17.66	17.55	17.47	14.26

Tab. 3.2.1 Results of the upward mass flux of solids (E [kg/m²s])

Height of air Injection [m]	Without Additional air [kg/s]	Additional air [kg/s] at height 6.8 [m]	Additional air [kg/s] at height 9.5 [m]	Additional air [kg/s] at height 11 [m]	Additional air [kg/s] at height 14.7 [m]	Additional air [kg/s] at height 16.9 [m]
0	19.53	21.57	21.76	21.48	20.47	21.61
2.2	5.90	6.52	6.61	6.52	6.18	7.19
3.2	3.08	3.26	3.33	3.30	3.19	4.06
6.8	2.80	2.85	2.91	2.91	2.87	3.59
9.5	2.61	2.72	2.68	2.69	2.67	3.36
11	2.59	2.72	2.67	2.65	2.65	3.31
14.7	2.58	2.72	2.67	2.65	2.64	3.30
16.9	2.58	2.72	2.67	2.65	2.64	3.30

Tab. 3.2.2 Results of the downward mass flux of solids (W [kg/m²s])

Figures 3.2.1 and 3.2.2 show the calculated ratio of the upward and downward solid mass flux versus the height of the riser. As can be seen from the diagram the injection of air at the different heights of the riser has no significant influence on the upward and downward mass flux of solid.

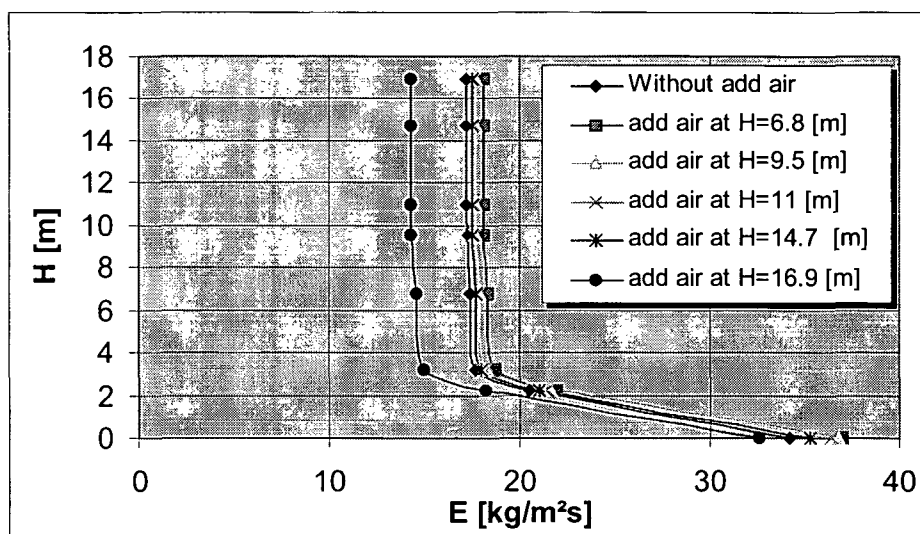


Fig. 3.2.1 Calculated upward mass flux of solids E [kg/m²s]

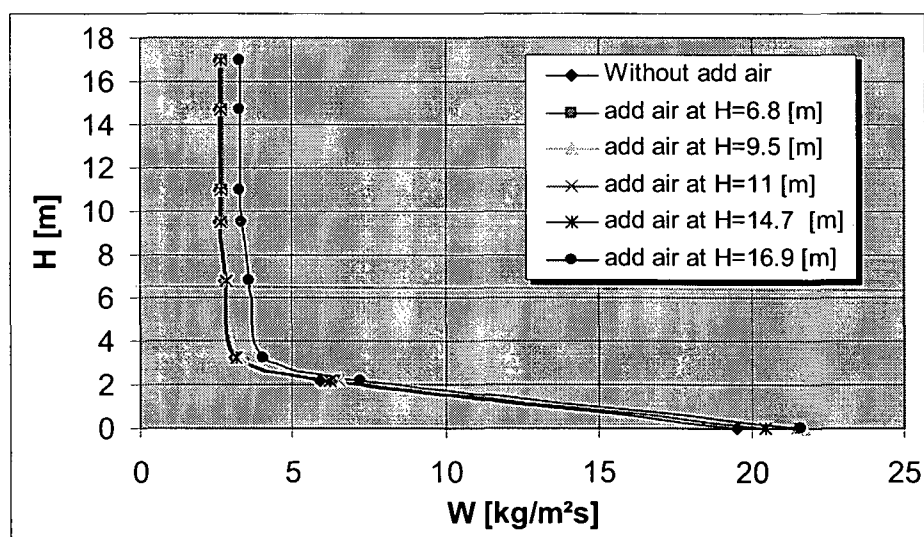


Fig. 3.2.2 Calculated downward mass flux of solids W [kg/m²s]

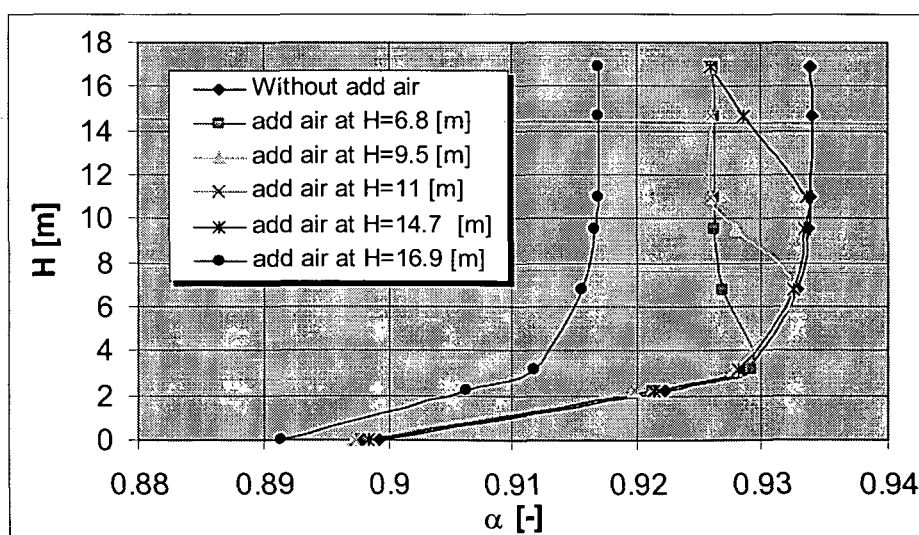
3.3 Ratio of core to total area

The ratio of core to total area is defined as ratio of the local core cross section to the cross section of the combustion chamber. The simulation program converts the rectangular to a circular cross section. Below is given the table with the results for different calculations. To the circular plant the ratio of area is equal to the square of the diameter ratio.

$$\alpha^2 = \left(\frac{D_c}{D_{\text{lokal}}} \right)^2$$

3.3.1

Height of air injection	Without Additional air	Additional air at cell 4	Additional air at cell 5	Additional air at cell 6	Additional air at cell 7	Additional air at cell 8
0	0.899	0.897	0.897	0.897	0.898	0.891
2.2	0.922	0.921	0.919	0.919	0.921	0.906
3.2	0.928	0.929	0.927	0.927	0.928	0.911
6.8	0.932	0.926	0.932	0.932	0.932	0.915
9.5	0.933	0.926	0.927	0.931	0.933	0.916
11	0.933	0.926	0.926	0.925	0.933	0.916
14.7	0.933	0.926	0.926	0.925	0.928	0.916
16.9	0.933	0.926	0.925	0.925	0.925	0.916

Table 3.3.1 Ratio of core to total area α [-]Fig. 3.3.1 Calculated ratio of core to total area of cross-section α [-]

From the Fig. 3.3.1 the influence of the additionally injected gas at certain heights of the riser can be seen.

3.4 Solids concentration

The solids concentration in a circulating fluidized bed (CFB) depends strongly on the height of the riser. The gas-solids mixture moves upwards in the core of the riser at relatively low concentration of solids, while the gas-solids flow near the wall is moving downwards at higher concentration of solids. The solids concentration at the wall and the core region are proportional to the corresponding average concentrations. Figure 3.4.1 shows the solids concentration versus height of the riser. As can be seen the additional gas injection at each cell height has a slight influence on the solids concentration.

Height of air injection	Without Additional air	Additional air at cell 4	Additional air at cell 5	Additional air at cell 6	Additional air at cell 7	Additional air at cell 8
0	0.0077	0.0085	0.0085	0.008	0.0081	0.0083
2.2	0.0033	0.0035	0.0035	0.0035	0.0034	0.0036
3.2	0.0027	0.0028	0.0028	0.0028	0.0028	0.0029
6.8	0.0026	0.0025	0.0027	0.0027	0.0027	0.0027
9.5	0.0026	0.0024	0.0025	0.0026	0.0026	0.0027
11	0.0026	0.0024	0.0024	0.0024	0.0026	0.0027
14.7	0.0026	0.0024	0.0024	0.0024	0.0024	0.0027
16.9	0.0015	0.0015	0.0015	0.0014	0.0014	0.0018

Tab. 3.4.1 Solids concentration $1-\varepsilon$ [-]

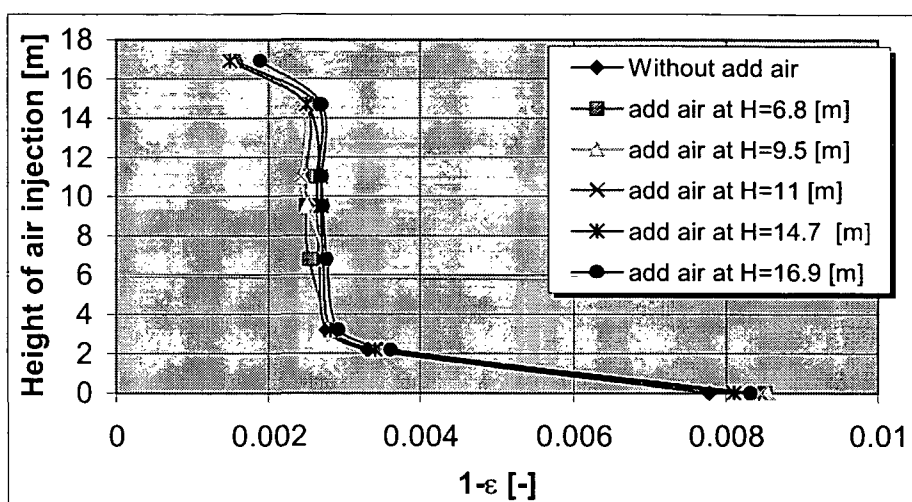


Fig. 3.4.1 Vertical profiles of the solids concentration

3.5 Gas velocity

In the table 3.5.1 the results calculated with the simulation program are given. It can be seen from table 3.5.1 that gas velocity is greater compared to the case without additional air. Additional air is injected at different heights of the riser.

Height of air Injection [m]	Without Additional air [m/s]	Additional air at cell 4 [m/s]	Additional air at cell 5 [m/s]	Additional air at cell 6 [m/s]	Additional air at cell 7 [m/s]	Additional air at cell 8 [m/s]
0	4.69	5.61	5.61	5.61	5.61	5.61
2.2	4.67	5.59	5.59	5.59	5.59	5.59
3.2	4.67	5.58	5.58	5.58	5.58	5.59
6.8	4.67	5.58	5.58	5.58	5.58	5.58
9.5	4.67	5.58	5.58	5.58	5.58	5.58
11	4.67	5.58	5.58	5.58	5.58	5.58
14.7	4.67	5.58	5.58	5.58	5.58	5.58
16.9	4.66	5.58	5.58	5.58	5.58	5.58

Tab. 3.5.1 Calculated results for gas velocity v_g [m/s]

Geometrical data of the plant are given in figure 3.5.2.

HGES –Total height of the furnace, which is defined as the distance between air distributor plate and cover,

HGES1 – Height of the furnace up to the centreline of the cyclone's outlet,

HK –Height of cone in the furnace,

HAT –Level (measured from air distributor plate) where secondary air is injected,

HAS –Level (measured from air distributor plate) where secondary air is injected,

HHAUBE –Height of cover in furnace,

DFR – Diameter of furnace at the upper part (above the cone),

DDB –Diameter of the distributor plate,

DAS –Diameter of the furnace at the secondary air injection,

DAT –Diameter of the furnace at the tertiary air injection,

LLV –Horizontal length of return leg,

HSY – Level of siphon above inlet of the return leg,

HSB –Height of return leg (standpipe),

HCONE –Height of cone beyond the storage vessel in the return leg,

DSTP –Diameter of return leg and valve (only one diameter can be defined),

DSB –Diameter of storage vessel in return leg (only of interest at laboratory test rigs where such vessels are used),

HOCH –Total height of cyclone,

HOCHO - Height of cylindrical part of cyclone,

RA –Outer radius of cyclone,

LengDleg –Length of vortex finder,

RI –Radius of vortex finder.

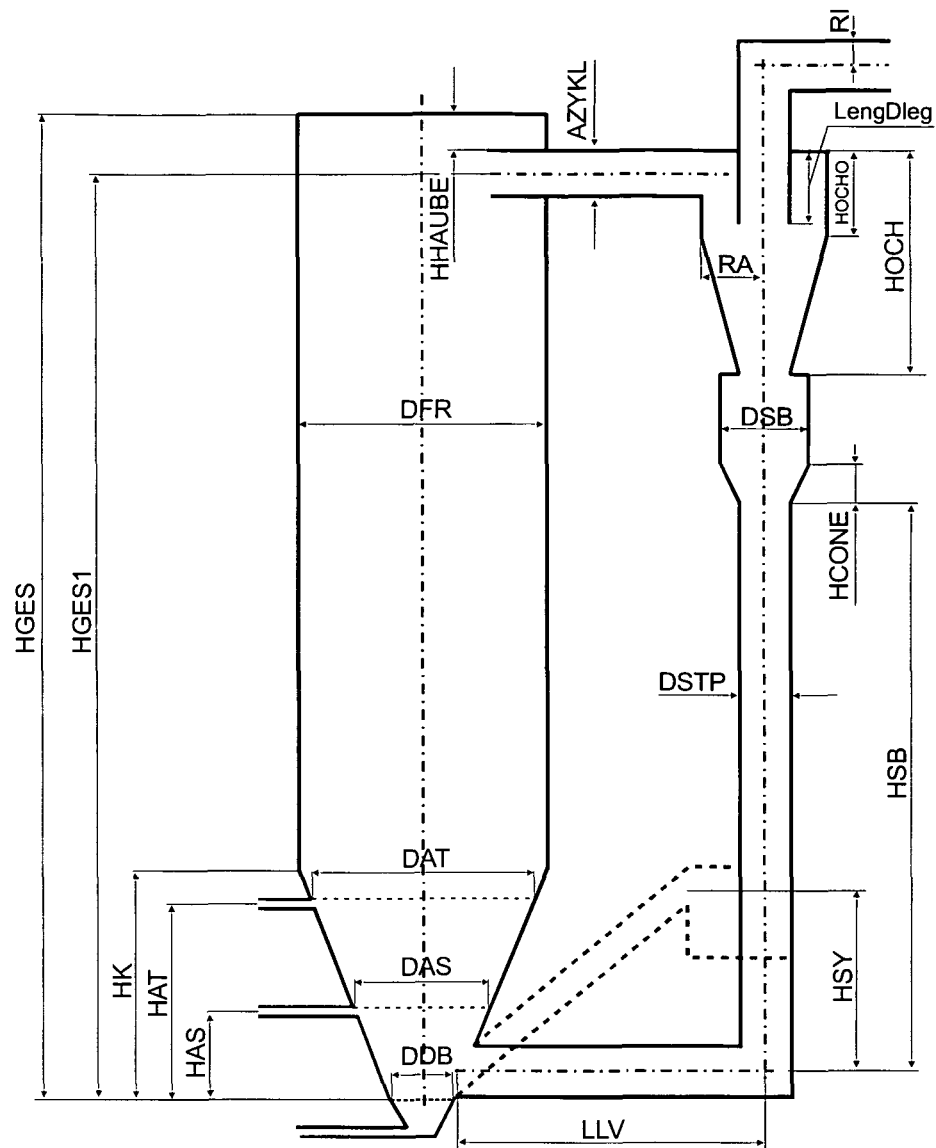


Fig. 3.5.2 Geometrical data of the plant A

4 Overview about models for the description of the bubbling zone

4.1 General aspects

Introducing the gas at minimum fluidization velocity u_{mf} through a suitable distributor plate the solids in the tube starts to move up. Normally the gas is introduced through a grid or distributor located at the bottom of the riser. According to Cheremisinoff [8], Kunii *et al.* [15] and Hetsroni [1] in Fig. 4.1.1 some types of distributor configurations are given.

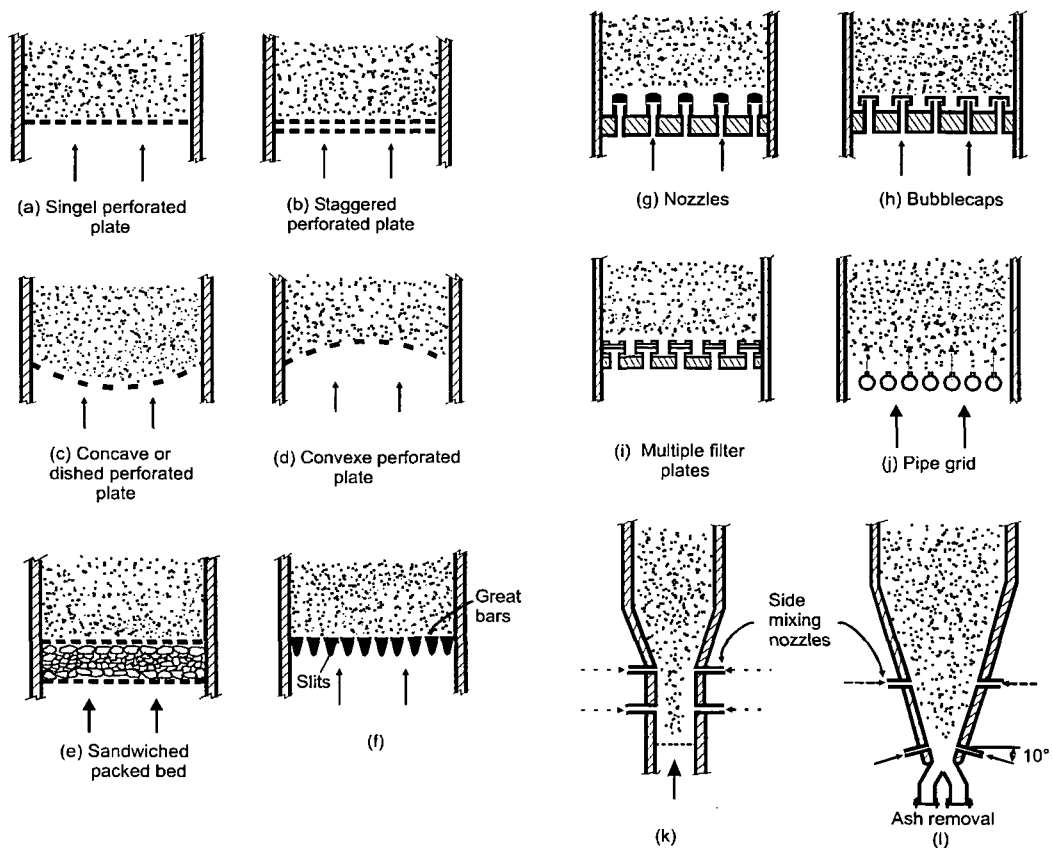


Fig. 4.1.1 Examples of distributor configurations.

The above figure illustrates:

- (a) – the flat perforated plate
- (b) – the staggered perforated plate
- (c) and (d) – curved plate distributors
- (e) - sandwiched packed-bed distributor
- (f) – an arrangement of slits between grate bars

- (g) and (h) – nozzles and bubble caps
- (i) – multiple filter plates
- (j) – pipe grid arrangements
- (k) – the gas is injected through nozzles arranged along the sidewalls.
- (l) – the gas is introduced through side-mixing nozzles.

By increasing the gas velocity beyond the value u_{mf} the bed of solids expands homogeneously and the bed height increases almost linearly with the superficial gas velocity. This regime is called the homogenous or particulate fluidization for a gas-solid system. The velocity onset of bubbling is called u_{mb} (minimum bubbling velocity).

It is generally assumed that the performance of gas-solid (G-S) fluidized beds is a function of the scale of operation and that the riser diameter and the bed height have a profound influence on the bubble hold up, interphase mass transfer and backmixing [12]. Ellenberger and Krishna [10] tried out to develop a unified approach for the scale-up of gas-solid (G-S) fluidized bed and gas-liquid (G-L) bubble column reactors. The experiments carried out from the authors Ellenberger *et al.* [10] show that based on hydrodynamic analogies in the behavior of these two systems a unified approach is possible. It is necessary to denote that the bubbles in a fluidized bed are not directly analogous to gas bubbles in liquid. Bubbles in a liquid have a clearly defined boundary separating the two phases.

Werther, [12], has used in his experiments fine catalyst particles of Geldart's group A and sand fluidized beds (Geldart's group B) in two risers with different inner diameter for estimation of the local bubble size distribution, local average bubble rise velocities and local average bubble shapes. Werther concluded that attrition and loss of fines from the system have no influence on the bubbling characteristics of the fluidized system.

Bubble characteristics are:

- size,
- shape,
- rise velocity
- number of bubbles per unit volume of bed per unit time.

4.2 Pressure drop of air distributors

Hartge and Werther [23] analyzed the performance of gas distributors in circulating fluidized bed boilers (CFBB). The problems with air distributors can be classified into the following three categories:

- a) backflow through the nozzles into the windbox of the fluidized bed
- b) erosion of the nozzles and
- c) ash sticking on the nozzles

If the pressure drop in the gas distributor is too low, the result is poor fluidization; i.e. some parts of the bed will be fluidized more vigorously and other parts may partly defluidize Hartge *et al.* [23]. The pressure drop Δp_D across the distributor should be at least 10 to 30% of the pressure drop Δp_B of the fluidized bed.

$$\frac{\Delta p_{DB}}{\Delta p_B} \geq 0.1 \dots 0.3 \quad N/m^2 \quad 4.2.1$$

The pressure drop is a function of the height at minimum fluidization H_{mf} velocity and bed diameter D .

$$\frac{\Delta p_{DB}}{\Delta p_B} \geq 0.01 + 0.2 \cdot \left[1 - \exp\left(\frac{-D}{2 \cdot H_{mf}}\right) \right] \quad 4.2.2$$

Hartge *et al.* [23] showed that the pressure drop has a strong influence on the flow structure in the bottom zone of the circulating fluidized bed.

4.3 Time for bubble formation

The formation of gas bubbles is one of the most characteristic phenomena of fluidized beds and has been recorded by Yang during several test series, where the development of bubbles dependent on time was observed. Mass and heat transfer processes are seriously affected by the mechanism of bubble formation. The corresponding time for bubble formation t_b is calculated using a correlation given from Yang *et al.* [21]:

$$t_b = \frac{1}{2 \cdot u_{mf}} \left[\frac{\dot{Q}}{\sqrt{2 \cdot \pi \cdot \dot{Q} \cdot u_{mf}}} \ln \cdot \left(\frac{2 \cdot \dot{Q} + d_b \sqrt{2 \cdot \pi \cdot \dot{Q} \cdot u_{mf}}}{2 \cdot \dot{Q} - d_b \sqrt{2 \cdot \pi \cdot \dot{Q} \cdot u_{mf}}} \right) - d_b \right] \quad 4.3.1$$

where \dot{Q} is the gas flow rate through orifice, m³/s

The gas flow rate through the orifice is estimated by use of equation $\dot{Q} = u_0 \cdot A_{FR}$

where A_{FR} is the cross section of the furnace.

Kuipers, [16] give another correlation for the estimation of the time of bubble formation:

$$t_b = \frac{1}{2 \cdot u_{mf}} \left(d_{b \max} \ln \cdot \left(\frac{d_{b \max} + d_b(h)}{d_{b \max} - d_b(h)} \right) - d_b(h) \right) \quad 4.3.2$$

Another important parameter for the bubble formation is the bubble formation frequency, which is estimated using an empirical correlation; according to Nicklin [20] and Kuipers *et al.* [16] the following relation was formed to determine the frequency of bubble formation:

$$n_b = 0.53 \cdot \frac{\dot{Q}}{V_b} \quad 4.3.3$$

where V_b is the bubble volume,

For a volumetric flow rate of gas, $\dot{Q} = 200 - 2000 \cdot \text{cm}^3/\text{s}$, Kunii and Levenspiel, [15], found a formation rate for bubbles of $n_b = 19 - 12 \text{ s}^{-1}$.

4.4 Determination of the bubble size

Most of research work about bubbles in fluidized beds, has been focused on the development of semi-empirical models to estimate parameters like bubble rise velocity and bubble diameter.

The formed bubbles have various shapes: small bubbles are close to spherical shape, large bubbles are spherical cap-shaped and largest bubbles are flattened and distorted.

Experiments show that bubble size in fluidized beds increases with gas velocity and with height above the distributor, and varies widely from system to system.

The bubbles grow in size after they have left the air distributor due to the coalescence with the neighboring bubbles.

The behavior of bubbles just above the distributor is given in Fig. 4.4.1. according to Kunii and Levenspiel [15].

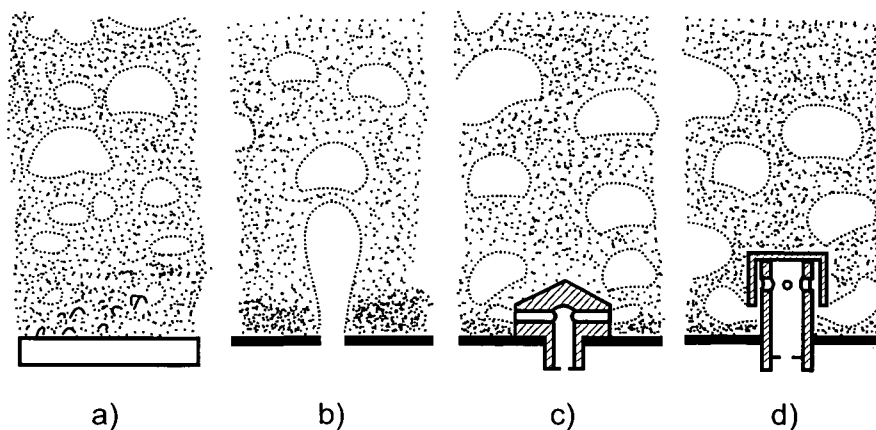


Fig.4.4.1 Behavior of bubbles just above the distributor: a) porous plate; b) perforated plate; c) nozzle-type tuyere; d) bubble cap tuyere.

Two types of bubble formation above a single orifice are given in fig. 4.4.2.

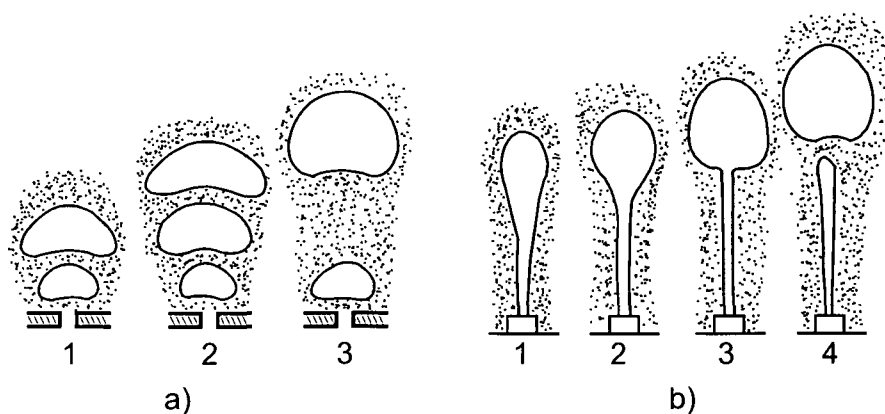


Fig. 4.4.2 Proposed modes of bubble formation (Kunii and Levenspiel [15])
a) for relatively low gas velocity, b) for high orifice velocity

It is important to denote that the bubbles reach a maximum bubble size, which is obtained using Equation 2.12.3 in chapter 2.

A number of different equations have been proposed to calculate the initial bubble size generated at an upward-facing orifice, see Miwa *et al.* [19] and

Darton *et al.* [11]:

$$d_{b0} = \frac{1.38}{g^{0.2}} \cdot \left(\frac{A_{FR} \cdot (u_0 - u_{mf})}{N_{or}} \right)^{0.4} \quad 4.4.1$$

for a porous plate distributor the same authors suggest

$$d_{b0} = 0.37 \cdot (u_0 - u_{mf})^2 \quad 4.4.2$$

Equation 4.4.2 is invalid for $u_0 - u_{mf} > 0.2 \text{ m/s}$. In fluidized bed combustors, the gas is rapidly heated when it enters the bed a fact, which is not considered in the formulas above.

To calculate the bubble size many authors take the Darton *et al.* [11] model as a basis. Considering the volume increase of bubbles and the burst of bubbles with the ascension of bubbles, the bubble diameter dependent on height can be calculated. According to Geldart [14] the bubble diameter is calculated as follows:

$$d_b(h) = \frac{\alpha_1 \cdot \left(u_0 - \frac{\dot{m}_{zirk}}{\rho_s A_{FR}} - u_{mb} \right)^{0.4} (h + 4\sqrt{A_{DB}})^{0.8}}{g^{0.2}} \quad 4.4.3$$

where α_1 is an empirical constant. The parameter α_1 is equal 0.54 estimated by Darton *et al.* [11]. The mentioned equation 4.4.3 has a wide applicability for the calculation of the bubble size.

In the equation 4.4.3 A_{DB} is the cross-section area of the distributor plate per number of orifices according to:

$$A_{DB} = \frac{A_{db}}{N_{or}} \quad 4.4.4$$

Kuipers *et al.* [16] have studied theoretically the bubble formation at a single orifice in a two-dimensional bed. The theoretically predicted bubble sizes, formation times and shapes have been compared to experimental data obtained from triggered photographs. According to Kuipers *et al.*, [16], the Davidson and Schüler model for the calculation of the bubble volume and the corresponding time of bubble formation was explained.

The bubble volume V_b is calculated with equation below (4.4.5):

$$V_b = 1.725 \cdot (C_0)^{0.6} \left(\frac{\dot{Q}^{1.2}}{g^{0.6}} \right) \quad 4.4.5$$

where C_0 represents the virtual mass coefficient (explained in Kuipers *et al.* [16]) of a sphere and depends on geometry.

Hetsroni, [1], gives another correlation to calculate the bubble volume. This equation gives the relationship between volume, radius and wake angel θ_w :

$$V_b = \frac{\pi}{3} r_b^3 (h) \cdot (2 - 3 \cos \theta_w + \cos^3 \theta_w) \quad 4.4.6$$

The wake angel θ_w in degrees has been correlated empirically according to Clift *et al.* [18] refer to Fig. 4.4.3.

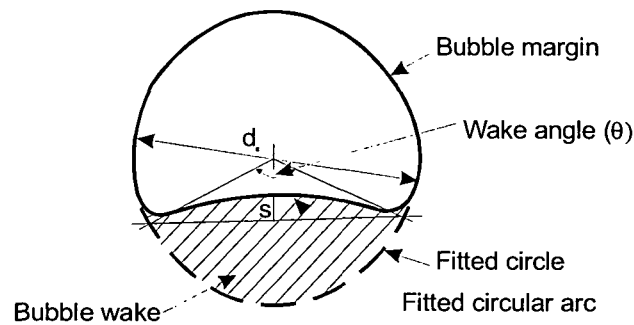


Fig. 4.4.3 Basic form of a bubble

$$\theta_w = 50 + 190 \exp(-0.62 \text{Re}_b^{0.4}) \quad 4.4.7$$

where Re is calculated according to:

$$\text{Re}_b = \rho_s \cdot (1 - \varepsilon_{mf}) \frac{d_{eq} \cdot u_b}{\mu_a} \quad 4.4.8$$

which μ_a an apparent dynamic viscosity and d_{eq} the equivalent diameter of bubbles:

$$d_{eq} = \left(\frac{6 \cdot V_b}{\pi} \right)^{\frac{1}{3}}$$

4.4.9

The description of a bubble on the basis of just one diameter, as has been considered by many researchers, is rather incomplete.

The wake angle is a function of Re_b and can be estimated from the diagram given in Fig 4.4.4.

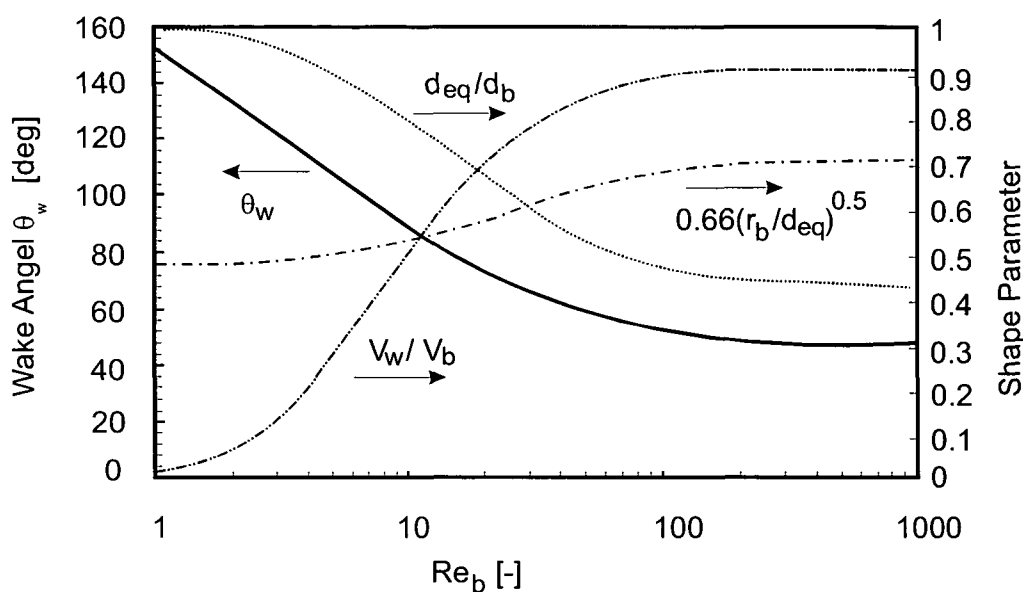


Fig.4.4.4 Bubble parameters as a function of Re_b .

4.5 Estimation of the bubble velocity

Some fluidized systems show bubbling as soon as the point of minimum fluidization is reached, others show bubbling only at superficial velocities higher than u_{mf} , at some others bubbles do not appear at any superficial velocity of the fluid.

The minimum superficial gas velocity, at which the bubble starts to form (u_{mb}), is calculated with an empirical correlation proposed from Geldart & Abrahamson [17] or Hetsroni [1], see chapter 2, formula 2.12.2.

This correlation is applicable only for $u_{mb} \geq u_{mf}$. If u_{mb} is less than u_{mf} it must be assumed that $u_{mb} = u_{mf}$.

The rise velocity of the single bubble in fluidized beds is calculated with the following equation:

$$u_{h\infty} = K \cdot \sqrt{g \cdot d_b} \quad 4.5.1$$

where d_b is the bubble diameter, calculated with Equation 4.5.1, K is a parameter $K=0.66$ for a gas bubble in a liquid and, from empirical measurements $K=0.711$ in a fluidized bed according to Gilbertson *et al.*, [22]. Wallis, [24], proposed to consider the reduced rise velocity due to wall effects by the following correlation valid for $0.125D < d_{eq} < 0.6D$:

$$u_b = 1.13 \cdot u_{h\infty} \exp\left(\frac{-d_b}{D}\right) \quad 4.5.2$$

Nevertheless, equation given in 4.5.1 gives a good agreement to many experimental results. Some authors incorporated a dependence on the reactor diameter see Kunii and Levenspiel [15]. Gera *et al.* [55] and Tsuchiya *et al.* [56] have investigated the single bubble rise velocity. The bubble rise velocity depends strongly on the wake angle.

In the current version of the simulation program the model of Johnsson was used, see Chap. 2, section 2.24. The minimum bubbling velocity is calculated according to formula 2.12.2 (model of Hetsroni [1]).

5 Test calculations with the flow program for three plants

5.1 Geometrical data and input parameters:

In this section three plants are tested with the simulation flow program and the results are compared. Below in table 5.1.1 are given the geometrical data for the boilers:

	Boiler A	Boiler B	Boiler C
Total height of furnace [m]	19.925	37.2	29.95
Length of air distributor plate [m]	4.2	5.0	Diameter of distributor plate [m] 3.9
Width of air distributor plate [m]	2.3	5.5	
Length of furnace at the upper part [m]	4.2	7.48	Diameter of furnace at the upper part [m] 7.3
Width of furnace at the upper part [m]	4.2	7.48	
Height of cone in furnace [m]	3.7	4.8	9.2
Height of refractory in furnace [m]	3.7	7.25	9.4
Height of return leg (standpipe) [m]	8.4	16.5	11.4
Level of siphon above the inlet of the return leg [m]	2.4	6.0	4.93
Horizontal length of return leg [m]	4.946	7.0	6.824
Height of cover in furnace [m]	1.28	0.80	2.48
Diameter of return leg and valve [m]	0.71	1.40	2.080

Table 5.1.1 Geometrical data of the plants

Boilers A and B have a rectangular form and the boiler C has a circular cross section. For the simulation of boiler A the solids inventory material was subdivided into 11 size fractions; for boiler B and C the number of size fraction was 16. Each

boiler is subdivided in to 8 balance cells along the riser's height. Below a table is given which shows the size distribution of the inventory material.

The particle distribution of inventory material is determined with the sieve analysis and is specified in table 5.1.2 for boilers.

Boiler A

Particle diameter [m]	Inventory Material [kg/kg]
70.E-6	0.16E-2
80.E-6	1.03E-2
100.E-6	2.73E-2
125.E-6	12.13E-2
160.E-6	65.33E-2
250.E-6	15.83E-2
315.E-6	2.255E-2
400.E-6	0.305E-2
500.E-6	0.180E-2
630.E-6	0.050E-2
800.E-6	0.000E-2

Boiler C

Particle diameter [m]	Inventory Material [kg/kg]
20.E-6	0.00E-2
38.E-6	0.50E-2
54.E-6	1.50E-2
70.E-6	4.00E-2
90.E-6	7.00E-2
116.E-6	5.00E-2
156.E-6	22.00E-2
180.E-6	19.00E-2
300.E-6	29.00E-2
500.E-6	7.000E-2
1000.E-6	3.000E-2
2500.E-6	2.000E-2
5000.E-6	0.000E-2
8000.E-6	0.000E-2
12000.E-6	0.000E-2
20000.E-6	0.000E-2

Boiler B

Particle diameter [m]	Inventory Material [kg/kg]
20.E-6	0.00E-2
38.E-6	0.10E-2
54.E-6	0.10E-2
70.E-6	0.20E-2
90.E-6	0.40E-2
116.E-6	3.20E-2
156.E-6	8.000E-2
180.E-6	23.00E-2
300.E-6	61.00E-2
500.E-6	3.800E-2
1000.E-6	0.200E-2
2500.E-6	0.000E-2
5000.E-6	0.000E-2
8000.E-6	0.000E-2
12000.E-6	0.000E-2
20000.E-6	0.000E-2

Table 5.1.2 Grain size distribution of inventory material for the three boilers.

In Fig. 5.1.1 is given the particle size distribution of inventory material for plant A and in the Fig. 5.1.2 for the plants B and C.

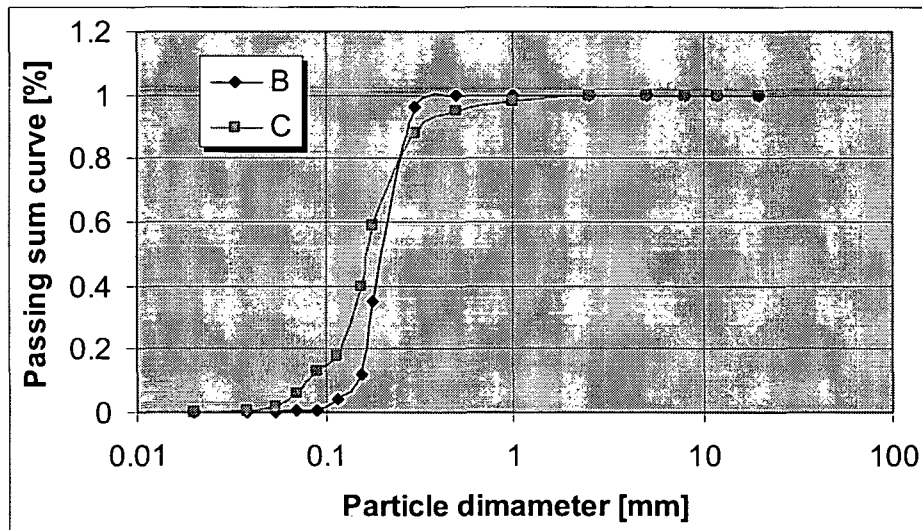


Fig. 5.1.1 Particle distribution of inventory material for plant B and C

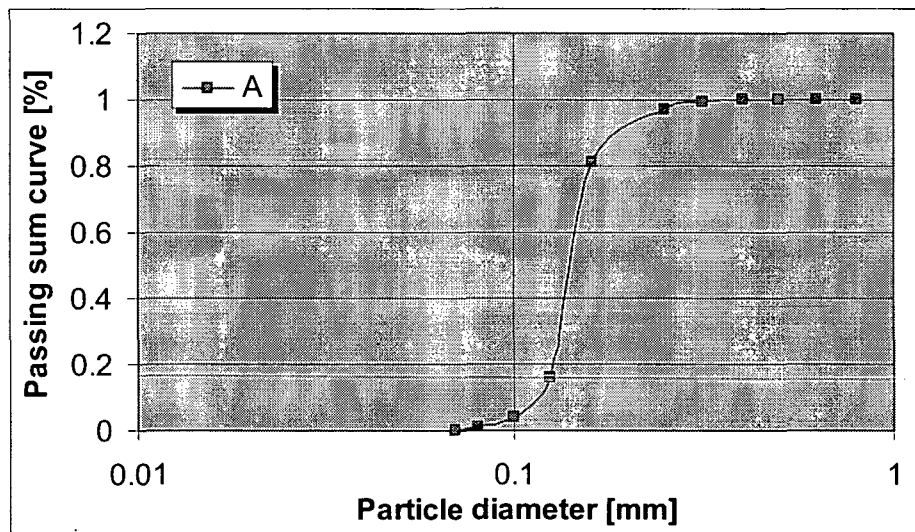


Fig. 5.1.2 Particle distribution of inventory material for plant A

Table 5.1.3 shows where primary and secondary air is injected. It is important to denote that in the first case about 60% of the air is used as primary air, in the second case about 56% and in the third case about 42%. The rest of the gas is added as secondary and tertiary air or gas.

	A	B	C
Primary air [kg/s]	15.287	50.66400	46.570
Secondary air [kg/s]	7.6430	21.36473	36.591
Tertiary air [kg/s]	2.5478	16.10970	27.720

Table 5.1.3 Distribution of air

The fluidization air is added to the system at different heights (primary, secondary and tertiary air).

Heights of the secondary and tertiary air injection are denoted in table 5.1.4.

	A	B	C
Height of secondary air injection [m]	2.2	1.5	2.282
Height of tertiary air injection [m]	3.2	3.8	7.5

Table 5.1.4 Height of secondary and tertiary air injection

The rest of used input parameters for these calculations are tabled and announced below in Table 5.1.5.

	A	B	C
Separation efficiency at furnace outlet [-]	0.15	0.12	0.15
Porosity at minimum fluidization velocity [-]	0.44	0.44	0.44
Sphericity of solids [-]	0.86	0.80	0.86
Density of solid material [kg/m ³]	2600	2500	2600
Kinematic viscosity of flue gas at furnace temperature [m ² /s]	1512.E-7	1512.E-7	1512.E-7
Density of flue gas at furnace temperature [kg/m ³]	0.3099	0.3099	0.3099

Table 5.1.5 Input parameters

5.2 Simulation Results

The calculation for the three plants is based on the input parameters denoted in section 5.1 of this chapter. The results returned by our simulation program will be discussed in this section. In Figures 5.2.1 and 5.2.2 are presented the upwards (E) and downwards mass fluxes (W) over furnace height for the performed calculations. In Figures 5.2.3 and 5.2.4 are presented the diagrams for average porosity and porosity in annulus over furnace height, and in Figure 5.2.5 is shown the ratio of core to total area α .

For the calculation of the upwards mass flux the following assumptions are taken into account:

- In the core zone the core porosity is constant over the cross section,
- all particles in the core flow upwards,
- the injected gas mass flux all enters in the core zone.

As can be seen, the upwards mass flux is a function of the gas velocity in the core of the riser, the terminal velocity, the core porosity, the density of solids and the ratio of core area to total area of the riser:

$$E = \rho_s \cdot (1 - \varepsilon_c) \cdot \alpha^2 \cdot (u_{g,c} - v_t \cdot \varepsilon_c^{n_s-1}) \quad 5.2.1$$

Assumptions for the downwards mass flux:

- the particles are moving downwards as agglomerates with uniform velocity in the annulus
- the annulus porosity depends like the average porosity on height.

Similar the solids downwards flux, W , can be expressed as:

$$W = (1 - \alpha^2) \cdot \rho_s \cdot (1 - \varepsilon_a) \cdot v_a \quad 5.2.2$$

The external solid circulation rate G_s follows from a mass balance for a local cross section:

$$G_s = E - W \quad 5.2.3$$

Detailed explanation is given from Glatzer [5].

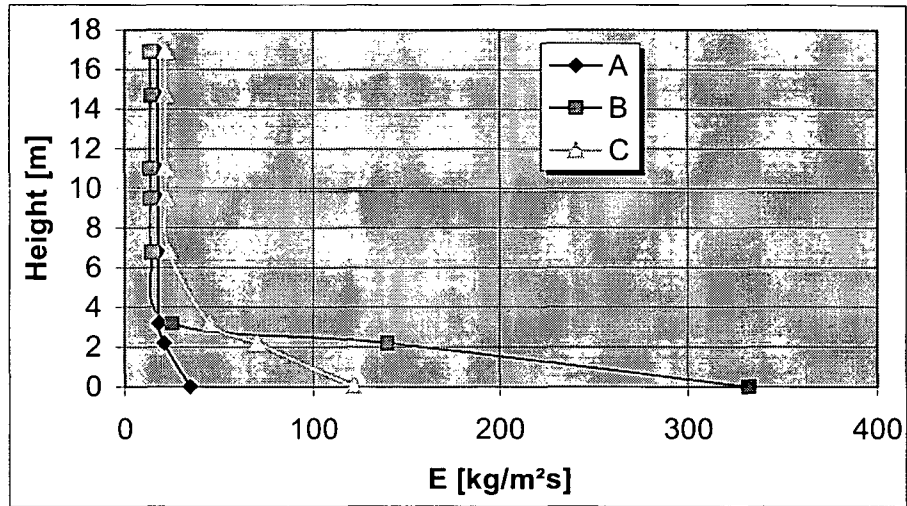


Figure 5.2.1 Upwards mass flux E [kg/m²s] for plant A, B and C

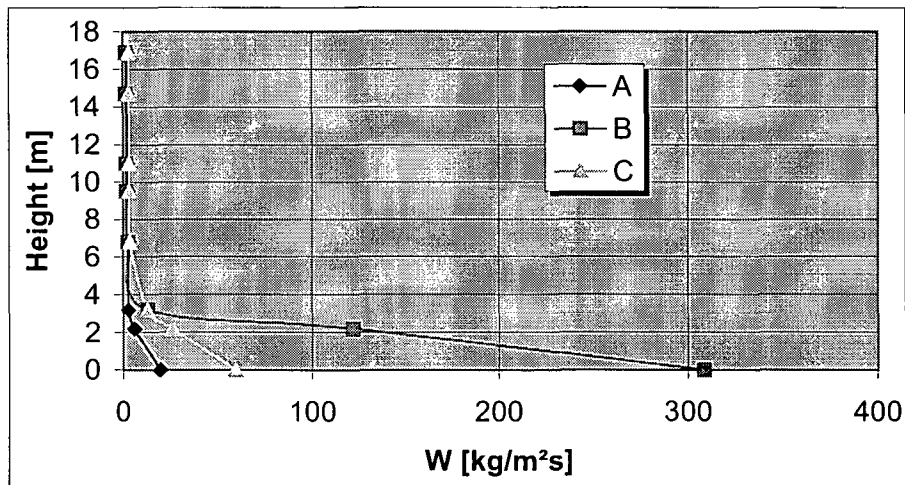


Figure 5.2.2 Downwards mass flux W [kg/m²s] for plant A, B and C

The ratio α is independent of the geometry of the cross section of the boiler and is defined as the ratio between local core cross section to the boiler cross section at the same height of the chamber.

$$\alpha^2 = \frac{A_c}{A_{lckal}} = \frac{\varepsilon - \varepsilon_a}{\varepsilon_c - \varepsilon_a} \quad 5.2.4$$

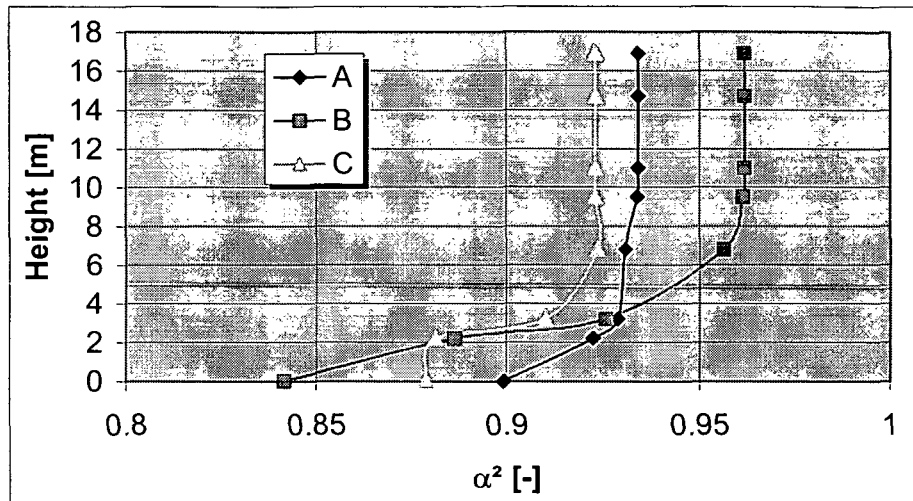


Figure 5.2.3 Ratio of core to total area for plant A, B and C

The annulus porosity is expressed as:

$$\varepsilon_a = k_1 + k_2 \varepsilon(h) + 15 \cdot (\varepsilon(h) - \varepsilon_{mf})^7 \quad 5.2.5$$

where

$$k_1 = 15 \cdot \varepsilon_{mf} \cdot (1 - \varepsilon_{mf})^6 \quad 5.2.6$$

and

$$k_2 = 1 - 15 \cdot (1 - \varepsilon_{mf})^6 \quad 5.2.7$$

are coefficients which determinate ε_a .

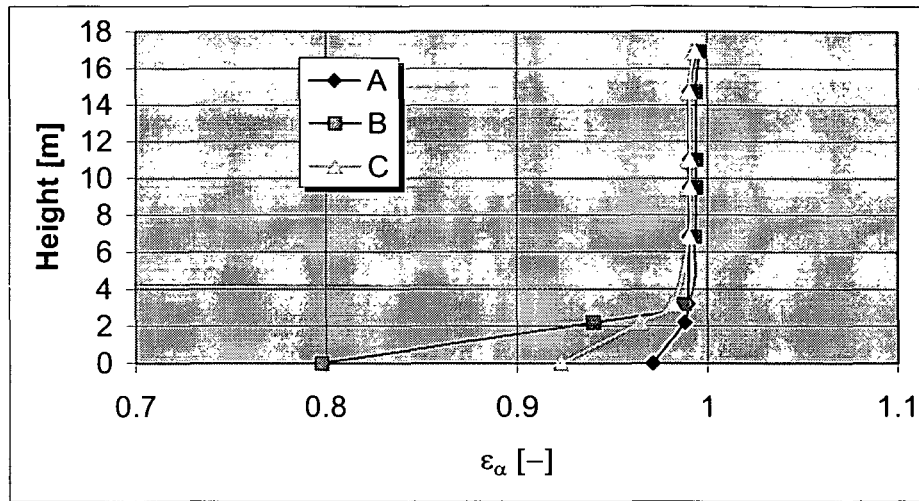


Figure 5.2.4 Porosity in annulus for plant A, B and C

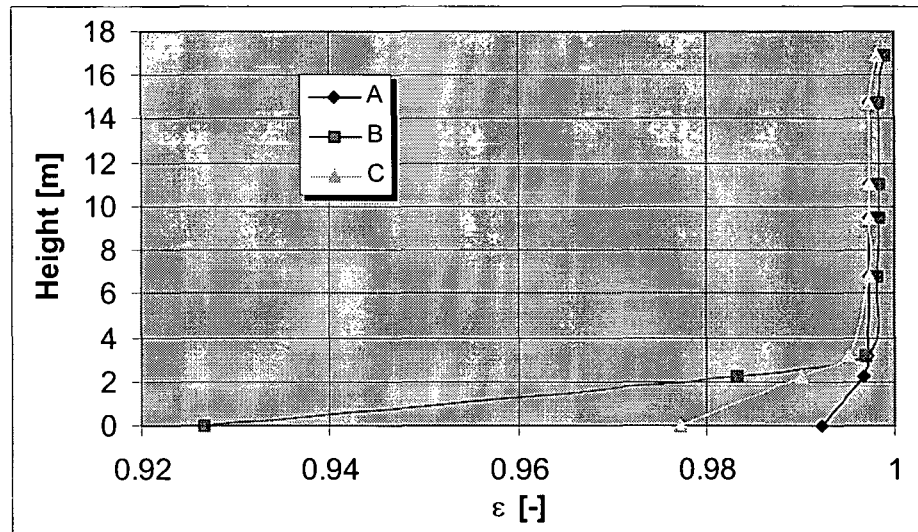


Figure 5.2.5 Average porosity for plant A, B and C

The average porosity is mean value of the respective cell for the assigned height element. The mean profile of porosity over furnace height is determined according to Kunii and Levenspiel, [6].

$$\varepsilon(h) = \varepsilon_{\infty} - (\varepsilon_{\infty} - \varepsilon_0) \cdot e^{-a(h-h_0)} \quad 5.2.8$$

The parameters ε_0 and h_0 specify the initial value for porosity and the height at the upper end of the dense zone of the boiler.

To calculate the average porosity at a certain height $(h-h_0)$ inside (within) the transition zone the coefficient a and the porosity ε_∞ at (theoretical) infinite height of the riser must be known.

The coefficient a describes the decay of the solids concentration with increasing height of the riser. Higher values of a cause a rapid approximation of actual porosity $\varepsilon(h)$ towards its limit ε_∞ . For certain dimensions of riser and particle size Kunii and Levenspiel, [6] the decay constant is expressed according to the following equation:

$$a = \frac{k_a}{u_0} \quad 5.2.9$$

In literature the values for k_a are given in the range 2-4 [1/s]. To take into consideration the influence of gas properties the product was tried to be correlated using Ar . According to the upper explanation the parameter k_a is estimated with Equation 2.4.2 from chapter 2. Kunii and Levenspiel [36] give more explanation about the coefficient k_a .

The figures 5.2.1 and 5.2.2 show the up- and downward mass fluxes (mean values). The differences of the up- and downward mass flux correspond to the circulating solid mass flux at each cross section of the transition zone. From the diagrams, it can be recognized that the dependence of up- and downward mass fluxes from the height in plant A and C is relatively low compared with plant B. In case of plant A and C the size distribution of fine particles of inventory material is more recirculated (lead buck).

Figure 5.2.3 shows the ratio of core to total cross section area of the plant. According to the conclusions for figures 5.2.1 and 5.2.2 the ratio of cross section of the plant B changes strongest (most strongly).

The figures 5.2.4 and 5.2.5 show the porosity in annulus and the average porosity of the plant. As can be seen from the figures the porosity in annulus and the average porosity of the plant B changes more than that of plants A and C. This differences are based on conclusions for Fig. 5.2.1 and 5.2.2.

6 Calculation with the overall simulation program and comparison to experimental data

In the following chapter the results calculated with the simulation program and experimental data for plant B will be discussed and compared. Experiments and calculations are made for full load conditions. Geometrical data are given in chapter 5 in table 5.1.1. The performance test was done for a CFBB with a steam rate of 250 t/h, 540°C and 125 bar pressure of life steam.

The CFBB-part of the plant consists of a riser, a cyclone and a return leg including a siphon for the reintroduction of solids into the furnace. Air is injected to the furnace as primary, secondary and tertiary air. Pressures are measured at eight positions in the riser.

The temperatures are measured at seven positions along the riser height. In the lower part of the furnace temperatures are measured at five positions, in the upper part at a height of 26.5 m even 5 measuring positions for temperature were available.

6.1 Estimation of pressure profiles over the furnace height

By measuring the pressure drop along the riser a pressure profile is determined. A total pressure drop along the riser Δp_{FR} is calculated:

$$\Delta p_{FR} = \Delta p_{acc} + \Delta p_{TRAN} + (1 - \varepsilon_{DEN}) \cdot g \cdot \rho_s \cdot (H_{GES1} - H_{DEN}) + (H_{GES} - H_{GES1}) \cdot \rho_s \cdot (1 - \varepsilon_{ex}) \cdot g \quad 6.1.1$$

where Δp_{acc} is the pressure loss due to acceleration and friction, Δp_{TRAN} is the pressure loss in the transition zone, ε_{DEN} is the porosity at the dense zone, ε_{ex} is the porosity at the level of the outlet, g is the acceleration of gravity, H_{GES} is the total height of the furnace, H_{GES1} is the height of the furnace up to the center line of the cyclone's outlet, and H_{DEN} is the height of the dense bed.

The measured results for the pressure drop along the riser and the calculated results are given in Table 6.1.1 and 6.1.2.

	Pa
Pressure loss at air distributor left	8500
Pressure loss at air distributor right	8200
Pressure loss in furnace (0.8 m) left	1500
Pressure loss in furnace (0.8 m) right	1800
Pressure loss in furnace (4.5 m) left	3200
Pressure loss in furnace (4.5 m) right	3500
Pressure loss in furnace (29 m) left	1600
Pressure loss in furnace (29 m) right	1600

Table 6.1.1 Experimental results measured along riser's height

Pressure drop [Pa]	Height [m]
7973.47	0.0 (at air distributor)
2266.51	1.480
1136.62	5.790
872.59	10.490
694.81	15.490
532.45	20.490
372.74	25.490
213.44	30.490

Table 6.1.2 Calculated results for pressure drop over furnace height

In the Tables 6.1.1 and 6.1.2 are given the results for measured and calculated values of the pressure drop.

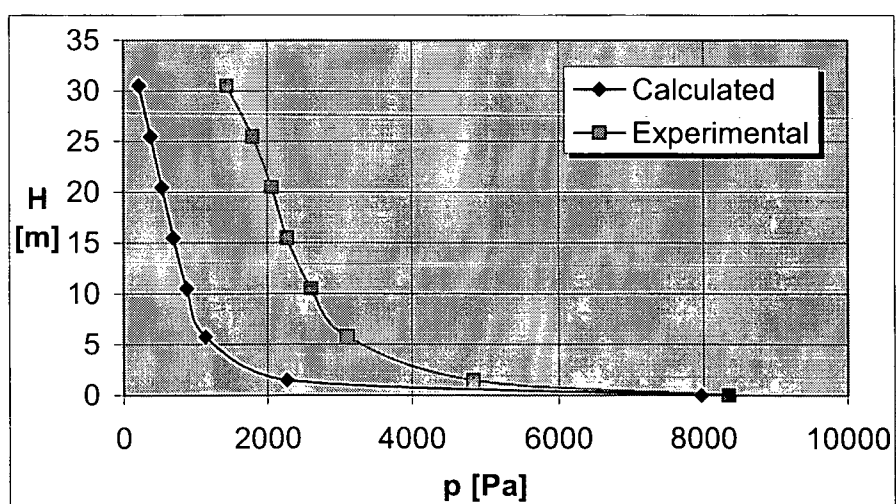


Figure 6.1.1 Pressure profile over furnace height

As can be seen from Figure 6.1.1 the calculated values with the simulation program are not in good agreement with the experimental values. The values measured over riser's height are clearly higher, than the values calculated with simulation program except at lower positions.

The shape of the experimental and calculated pressure drop curves is similar, but an absolute (more or less) constant difference exists. The reason for that difference could be an underestimated starting value for solids concentration $(1-\epsilon)$ at the upper end of the riser, because the geometry-dependent influence of the separation efficiency of the exit can't be taken into consideration.

The figure below shows a scheme of the furnace where the black points signify the pressure measuring positions.

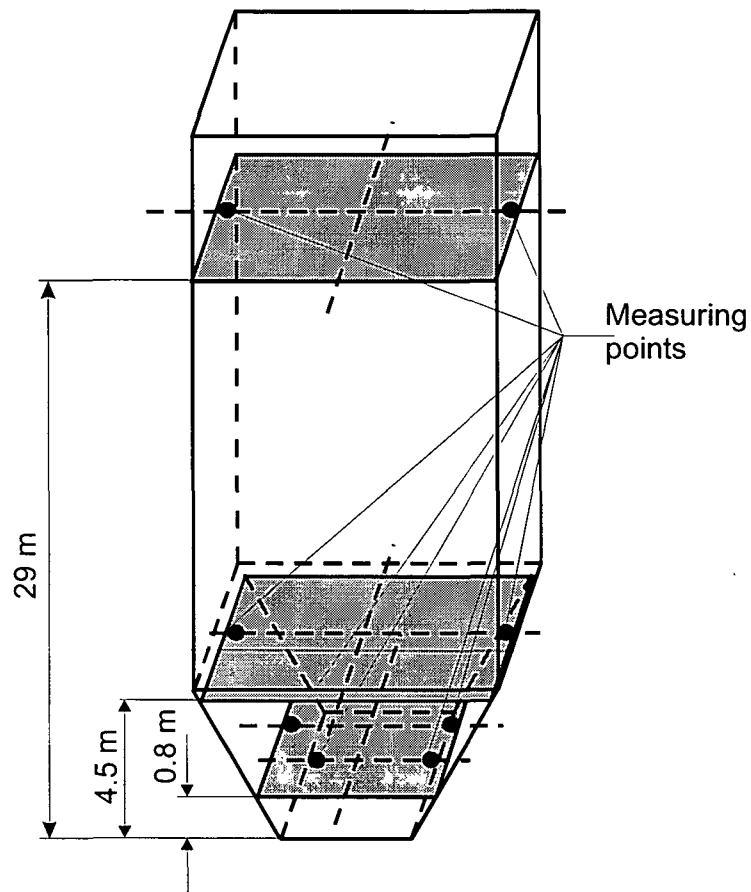


Fig. 6.1.2 Pressure measuring points

6.2 Determination of temperature profile over furnace height:

To calculate the temperature profile along the furnace height of the CFBC, the boiler is divided into cells and each cell is assumed to be a well stirred tank. The formulation of the energy balance for each cell supplies a set of equations for the calculation of the temperature distribution and the transferred heat flows. By modeling the balance cells as well stirred tanks the following simplifications are necessary:

- Each balance cell is considered to be ideally mixed. There is a homogeneous two-phase mixture in which no temperature gradient occurs. The calculation is done with concentrated parameters for density, porosity and temperature,
- All mass flows that leave the balance cell have the same temperature,
- All mass flows that enter the balance cell are ideally dispersed.

In the present form the boiler is divided into eight cells. The first cell reaches from the air distributor to a height closely below secondary air injection. The second cell ends at the height of refractory and the remaining six cells subdivide the rest of the boiler.

In the tables below are given the calculated and experimental values for the temperature profile.

	°C
Temperature in furnace (26.5m) 1 left	900
Temperature in furnace (26.5m) 2 right	895
Temperature in furnace (0.4m) 1 left	919
Temperature in furnace (0.4m) 2 right	926
Temperature in furnace (0.4m) 3 right	928
Temperature in furnace (0.4m) 4 middle	918
Temperature in furnace (0.4m) 5 left	895

Table 6.2.1 Measured temperature distribution in furnace

Cell height	Average temperature [°C]	Core temperature [°C]	Annulus temperature [°C]
1.49	1004.57	1005	1003.33
5.8	998.95	1001.93	997.42
10.5	981.56	1006.89	947.94
15.5	975.56	997.22	911.7
20.5	961.35	982.71	880.22
25.5	939.05	959.5	857.29
30.5	919.44	938.61	842.23
37.2	900.39	916.06	837.3

Table 6.2.2 Calculated Temperature Profile

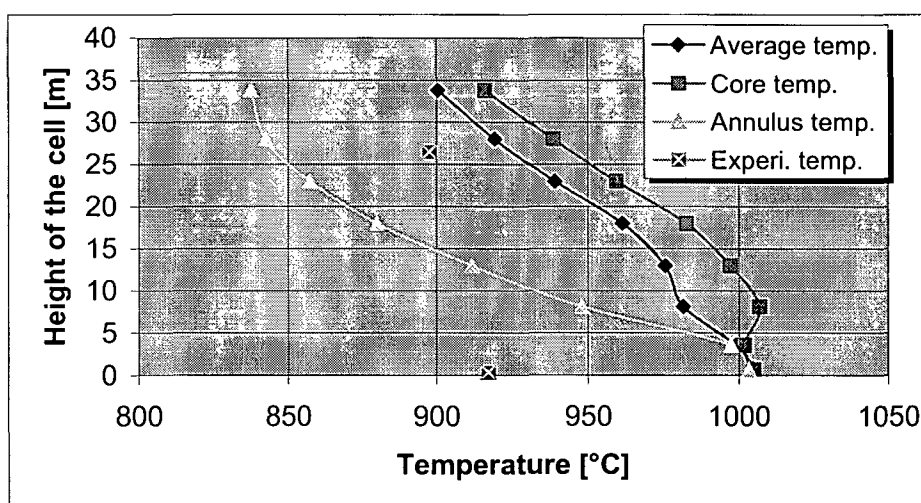


Figure 6.2.1 Comparison of calculated and measured temperature values along the furnace height

At the upper figure the curves are depicted for the average, core and annulus temperature and the experimental average temperatures at two measuring points of the furnace. The difference between calculated and measured temperature in furnace is higher in the bottom section of the reactor than in the upper zone, where the value of difference is only about 90°C. In the bottom section the reason for the difference could be the higher measured solids concentration in the bottom of the riser which enhances the heat transfer coefficient in that zone.

The figure below shows a scheme of the furnace where the black points signify the temperature measuring positions.

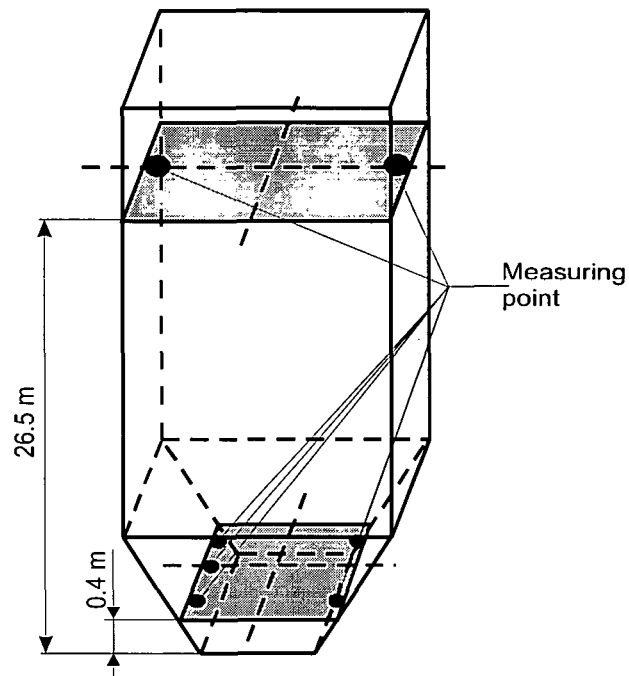


Fig. 6.2.2 Temperature measuring points

6.3 Boiler efficiency

The boiler efficiency is calculated in accordance to DIN 1942, [32]. The determination of the boiler efficiency is done following the "indirect method" by determining the different heat losses. The efficiency of boiler 1 was calculated for coal with high ash-content (25.23%).

$$\eta_{DE} = 1 - V_{FRV} - V_{ABGV} - V_{STRV} - V_{WAV} \quad 6.3.1$$

In equation 6.3.1 V_{FRV} is the combustion loss, V_{ABGV} is the waste gas loss, V_{STRV} is the radiation loss and V_{WAV} are the losses due to the sensible heat of ash.

The calculated value of the boiler efficiency (0.925) is in good agreement with the result of the operating plant (0.9189).

Determination of the combustion loss in accordance to DIN 1942, [32]:

$$V_{FRV} = V_{GA} + V_{FA} + V_{CO} \quad 6.3.2$$

where V_{GA} is the loss due to unburned carbon in bottom ash, V_{FA} is the loss due to unburned carbon in fly ash and V_{CO} is the loss due to CO in waste gas.

Calculation of the loss due to the unburned in bottom ash, see Haider, [53]:

$$V_{GA} = \frac{\dot{m}_{GA,K} \cdot H_{uK}}{\dot{m}_{BR} \cdot H_u \cdot (1 + k_{BV} + k_{LV} + k_{S/K})} \quad 6.3.3$$

where $\dot{m}_{GA,K}$ is the C_{fix} mass flow at coarse ash, \dot{m}_{BR} is the fuel mass flow, H_{uK} is the calorific value of unburned carbon, H_u is the calorific value of fuel, k_{BV} is the correction factor for external fuel preheating, k_{LV} is the correction factor for the external air preheating and $k_{S/K}$ is a correction factor for calcination and sulfation of added limestone.

Calculation of the loss due to the unburned carbon in fly ash, see Haider, [53]:

$$V_{FA} = \frac{\dot{m}_{FA,K} \cdot H_{uK}}{\dot{m}_{BR} \cdot H_u \cdot (1 + k_{BV} + k_{LV} + k_{S/K})} \quad 6.3.4$$

where $\dot{m}_{FA,K}$ is the C_{fix} mass flow at fly ash.

Calculation of the loss due to CO in waste gas, according to Haider, [53]:

$$V_{CO} = \frac{k_{GDS} \cdot (1 - V_{GA} - V_{FA}) \cdot x_{CO,Abg} \cdot \Delta \tilde{H}_{CO,CO}}{H_u \cdot (1 + k_{BV} + k_{KL} + k_{S/K}) \cdot M_{CO}} \quad 6.3.5$$

where k_{GDS} is the specific mass of flue gas, taking into account desulfurization, $x_{CO,Abg}$ is the CO concentration in the flue gas, $\Delta \tilde{H}_{CO,CO}$ is the formation enthalpy of CO_2 at CO oxidation, M_{CO} is the molar mass of the carbon monoxide.

The flue gas loss is calculated according to the following equation, see Haider, [53]:

$$V_{ABGV} = \frac{[(k_{GDS} \cdot c_{pf,Abg} \cdot t_{Abg}) - (k_L \cdot c_{p,a} \cdot t_{at})] \cdot (1 - V_{GA} - V_{FA})}{H_u \cdot (1 - k_{BV} + k_{LV} + k_{S/K})} \quad 6.3.6$$

where $c_{pf,Abg}$ is the specific heat capacity of flue gas, $c_{p,a}$ is the specific heat capacity of ash, k_L is the specific air request at air excess, t_{Abg} is the temperature of the flue gas and t_{a1} is the air temperature before the air preheater.

Calculation of radiation loss, according to DIN 1942:

$$V_{STRV} = \frac{a_{STRV} \cdot 10^6 (\dot{Q}_{ND} \cdot 10^{-6})^{b_{STRV}}}{\dot{m}_{BR0} \cdot H_u (1 + k_{BV} + k_{LV})} \quad 6.3.7$$

where a_{STRV} and b_{STRV} are parameters for the calculation of radiation loss in accordance to DIN 1942 [32], \dot{Q}_{ND} is the net enthalpy flow of life steam and \dot{m}_{BR0} is the feed mass flow of fuel.

Calculation of the losses due to the sensible heat of ash, see Haider [53]:

$$V_{WA} = \frac{\dot{m}_S \cdot (1 - \eta_{Z,s}) \cdot (1 - \eta_{F,s}) \cdot c_{p,s} \cdot t_{S,FA} + \dot{m}_{GA} \cdot c_{p,s} \cdot t_{S,GA}}{\dot{m}_{BR} \cdot H_u \cdot (1 + k_{BV} + k_{LA} + k_{S/K})} \quad 6.3.8$$

where \dot{m}_S is the mass flow of circulating material, \dot{m}_{GA} is the mass flow of bottom ash, $c_{p,s}$ is the specific heat capacity of total solid matter, $t_{S,FA}$ is the temperature of fly ash, $t_{S,GA}$ is the temperature of bottom ash, $\eta_{Z,s}$ is the separation efficiency of solids in cyclone and $\eta_{F,s}$ is the separation efficiency of solids in filter.

6.4 Size distribution of bed and circulating material:

In addition the Sauter diameters of the circulating and the bed material are calculated. The influence of the ash on the size distribution is tested for different particle distribution of the combustion ash.

Sauter's diameter of circulating material:

$$d_{psCirc} = \frac{1}{\sum_i \frac{k_{sCirc}(i)}{d_{Av}(i)}} \quad 6.4.1$$

Sauter's diameter of bed material:

$$d_{psBed} = \frac{1}{\sum_i \frac{k_{sBed}(i)}{d_{Av}(i)}} \quad 6.4.2$$

where k_{sCirc} is the particle size distribution of circulating material (mass fraction of size fraction), k_{sBed} is the particle size distribution of bed material (mass fraction of size fraction), and d_{Av} is the average particle diameter of size fraction (i).

In the following the influence of the size distribution of coal ash on the size distribution of bed and circulating material is investigated:

Case 1 assumes a size distribution of coal ash as obtained from an ordinary combustion process without mechanical impact.

Case 2 uses the size distribution of coal ash after an additional grinding procedure to approximate the size reduction mechanisms which could occur in a CFB-reactor. Results are given in Figures 6.4.1 and 6.4.2.

Figure 6.4.1 shows the shift of the size distribution of bed material (in the bottom region of the riser) to smaller size fractions, according to the additional (mechanical) size reduction of coal ash, due to grinding. In the same way even at the circulating material a shift towards finer size distribution is observed.

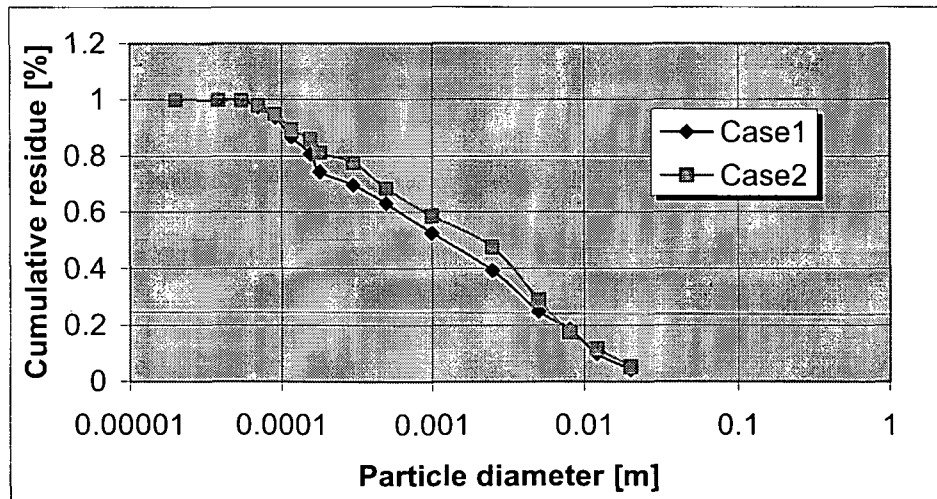


Figure 6.4.1 Particle size distribution of bed material

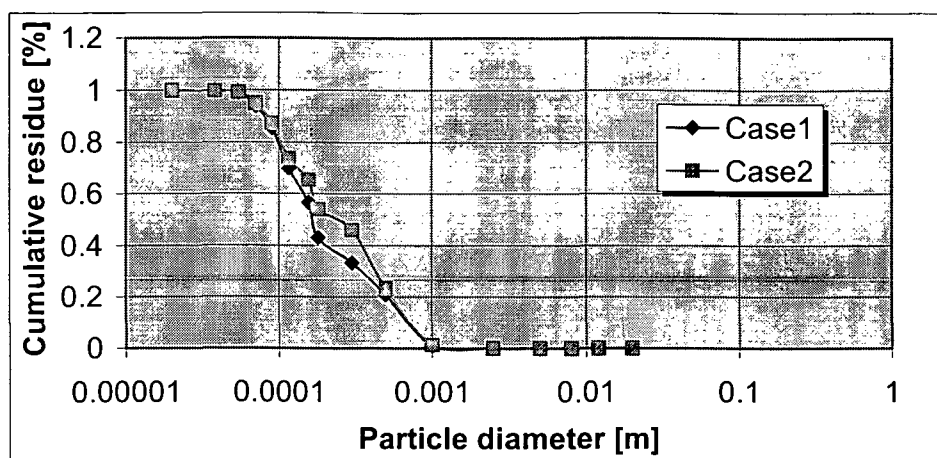


Figure 6.4.2 Particle size distribution of circulating material

6.5 Solids mass flow through ash classifier and filter

Another important parameter checked with the simulation program and compared to experimental results is the ash split to bottom and fly ash. Experiments showed a value of 60:40 % between bottom and fly ash.

From the total mass balance of solids the mass flow of bottom ash is calculated as below:

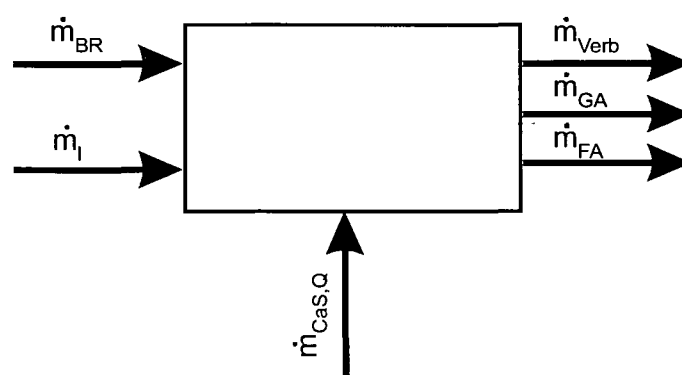


Figure 6.5.1 Overall mass balance for solid matter

$$\dot{m}_{GA} = \dot{m}_{BR} + \dot{m}_{CaS,Q} + \dot{m}_I - \dot{m}_{FA} - \dot{m}_{Verh} \quad 6.5.1$$

where \dot{m}_{BR} is the mass flow of fuel, $\dot{m}_{CaS,Q}$ is the mass flow of sorbent, \dot{m}_I is the mass flow of inert material, \dot{m}_{FA} is the mass flow of fine ash, and \dot{m}_{Verh} is the mass flow of gasified fuel.

The mass flow of fly ash is calculated as follows:

$$\dot{m}_{FA} = \dot{m}_{K_FA} + \dot{m}_{L_FA} + \dot{m}_{I_FA} \quad 6.5.2$$

where \dot{m}_{K_FA} is the mass flow of char, \dot{m}_{L_FA} is the mass flow of sorbent and \dot{m}_{I_FA} is the mass flow of inert material through the filter.

In the following the mass flows of bottom and fly ash are investigated. More explanation is given under point 6.4. Figures 6.5.1 and 6.5.2 show the assumption for the size distribution of combustion ash used for the simulation program as input values.

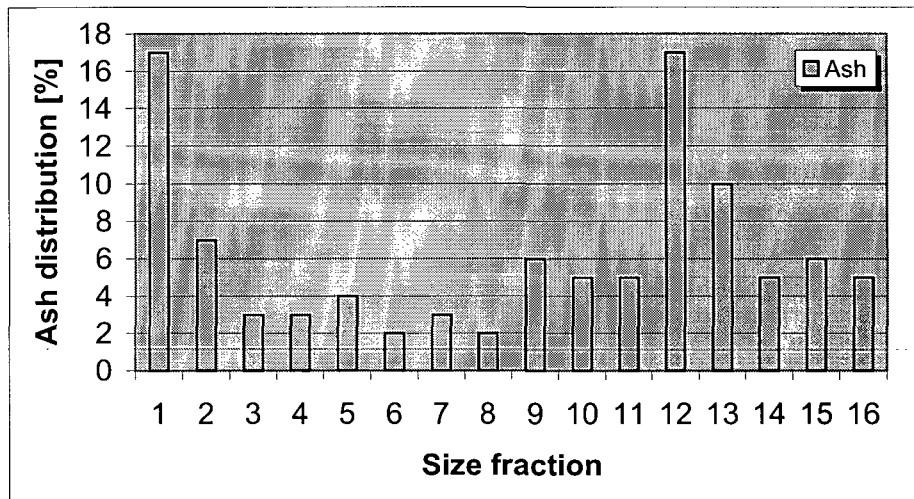


Figure 6.5.2 Particle size of combustion ash before grinding

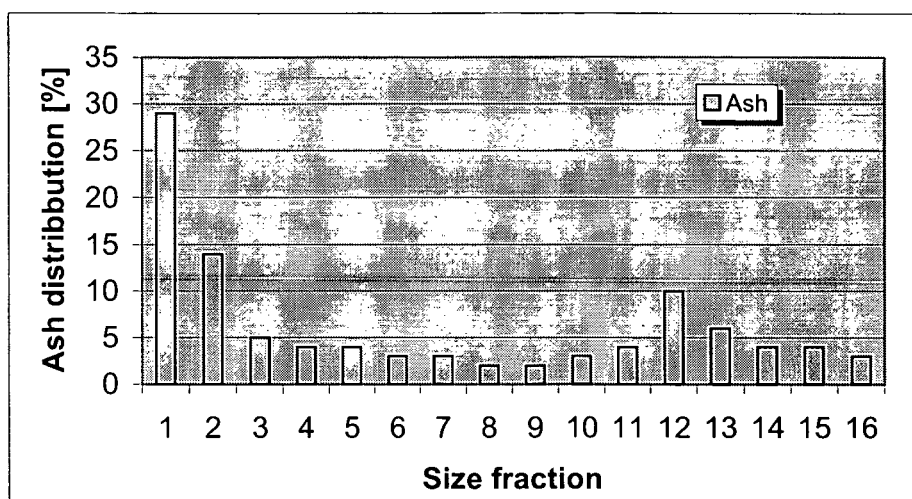


Figure 6.5.3 Particle size of combustion ash after grinding

The calculated values for the CASE1 are:

Solid mass flow through ash classifier: 2.26394 [kg/s]

Solid mass flow through filter: 0.72201 [kg/s]

As can be seen the proportion for the first case is about 75/25%.

The calculated values for CASE2 are:

Solid mass flow through ash classifier: 1.68859 [kg/s]

Solid mass flow through filter: 1.29321 [kg/s]

The proportion for the second case is about 58/42%.

The upper results show that changes of the source term of ash have a significant influence on the ash split to bottom and fly ash. For fine particles of combustion ash the compared upper results (CASE2) are in good agreement to the experimental results.

7 Overview about grain size reduction mechanisms in fluidized bed boilers

7.1 General remarks about attrition and fragmentation

In this chapter the size reduction mechanisms in fluidized bed boilers are discussed. Attrition of particulate materials is widespread in many different areas and happens at many different types of particles. Attrition may arise from mechanical forces, thermal stress, chemical stress, or pressure changes from the inside and outside of particles, Vaux, [44]. In the case of fluidized bed combustion, the attrition of char and limestone particles can have a negative effect on combustion efficiency and on sulfur retention.

7.1.1 Fragmentation

Fragmentation is the breakage of the particles during the drying, devolatilisation and char combustion process into smaller pieces. In many cases fragmented particles are large enough to burn in the bed, whereas attrited particles are generally elutriated as combustible solids in fluidized bed combustors.

7.1.1.1 Fuel Fragmentation

Primary fragmentation is defined as the breakage of fuel particles during their devolatilization period and has been attributed to the build-up of internal pressure due to the delayed mass transfer of released volatiles through the pore structure of the fuel particles (Chirone and Massimilla [40], Chen *et al.* [49], Stubington *et al.* [48], Sundback, Beér and Sarofim [54]). Usually, the fragmentation of particles is considered to end when the devolatilization step is completed, because no volatiles remain inside the particles.

Chirone *et al.* [40] developed a model e. g. to investigate the primary fragmentation, occurring during the devolatilization of the South African coal in a laboratory fluidized bed combustor. Measurements were made at room temperature and at temperatures between 200°C and 600°C. The fuel particle size used for these experiments was 1 to 16 mm (Chirone and Massimilla, [40]). The model assumptions which they have used for these experiments are:

- Spherical coal particles.

- During the devolatilisation process the coal spheres are both exposed to thermal stresses and to stresses due to pressure increase inside the porous structure because of volatile release.
- The coal temperature, voidage and pressure are known during devolatilisation.

7.1.1.2 Sorbent Fragmentation

Hu and Scaroni [37] have used a laser heating technique to study the fragmentation behavior of sorbents. They have used 8 different types of sorbents with particle size between 37-105 μm and particle temperatures in the range of 600-1600°C. There are several mechanisms, which can cause the fragmentation:

- When a particle is heated up at a high heating rate, thermal shock may cause fragmentation even before calcination begins.
- A sorbent particle may contain a small amount of organic matter and/or water. When the particle is heated up to temperatures below the onset of calcination, the organic matter decomposes.
- When a particle is heated up to higher temperatures and the decomposition of the carbonate starts, CO_2 is released.

Hu *et al.* [37] concluded that the fragmentation behavior was influenced by the sorbent type, particle size, and particle temperature. The sorbent type had the major influence on the fragmentation.

7.1.2 Attrition

Attrition produces fines when particle collide each other, combustor walls and internals. Abrasive attrition, fragmentation and fragmentation by percolation are series-parallel phenomena that together with gas-solid reactions determine (fuel) comminution. Arena *et al.* [33] investigated the comminution phenomena occurring during the fluidized bed combustion of a refuse derived fuel. A South African bituminous coal is used as reference. The experiments carried out show that both waste fuels present a probability of breakage, higher than that of the South African coal.

Attrition is affected by several factors, which can be properties of the parameters as indicated in fig. 7.1.2.1 and in both cases larger particles are broken down into smaller ones either by fragmentation or by generation of fines [45].

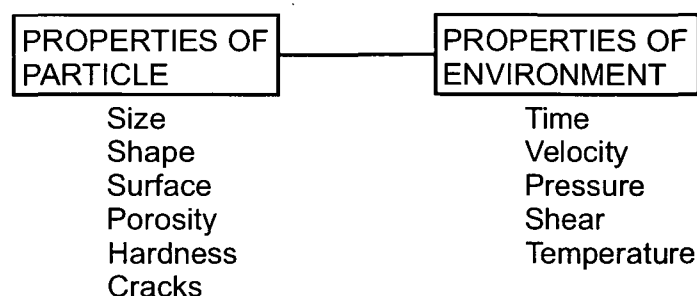


Fig. 7.1.2.1 Some parameters affecting attrition

Bemrose *et al.* [45] and Kokkoris *et al.* [46] give a "Blinichev-scheme" for attrition processes occurring in a fluidized bed fig. 7.1.2.2.

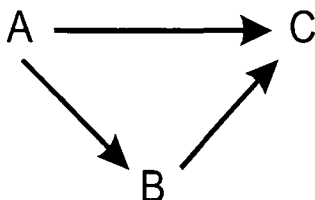


Fig. 7.1.2.2 Paths for the size reduction of particles

where A represents the initial particle, B the smaller fragment, and C the fines product. The first path ($A \rightarrow C$) represents the surface abrasion of initial particles and results in a slightly smaller particle and many fine particles. The second path

$(A \rightarrow B \rightarrow C)$ represents an initial fragmentation of the mother particle, followed by surface abrasion of the resulting fragments. This path produces a small number of intermediate size particles, as well as, many fine particles.

Takeuchi *et al.*, [39], has investigated the influence of fuel attrition on combustion efficiency. They have used four different types of fuels. The attrition rate is different according to coal types and weight loss by attrition is small enough to be ignored in comparison to that caused by reaction.

Vaux, [44], modeled low-velocity impact attrition in the bubbling zone of a fluidized bed. He confirmed experimentally that the attrition rate was proportional to $(u_0 - u_{mf})$, where u_0 is the superficial velocity, and u_{mf} the minimum fluidization velocity, and that the attrition rate decreases with time to a steady-state value. Impacts between particles gave rise to abrasion and occurred throughout the bed, whereas grid jets caused high-velocity impacts and particle fracture only in the lower (~ 0.5 m) part of the bed.

Different types of tests are performed in order to determine the attrition tendency of particulate materials. Bemrose *et al.*, [45], describes different test equipments and procedures. These types for attrition tests are given in Fig. 7.1.2.3.

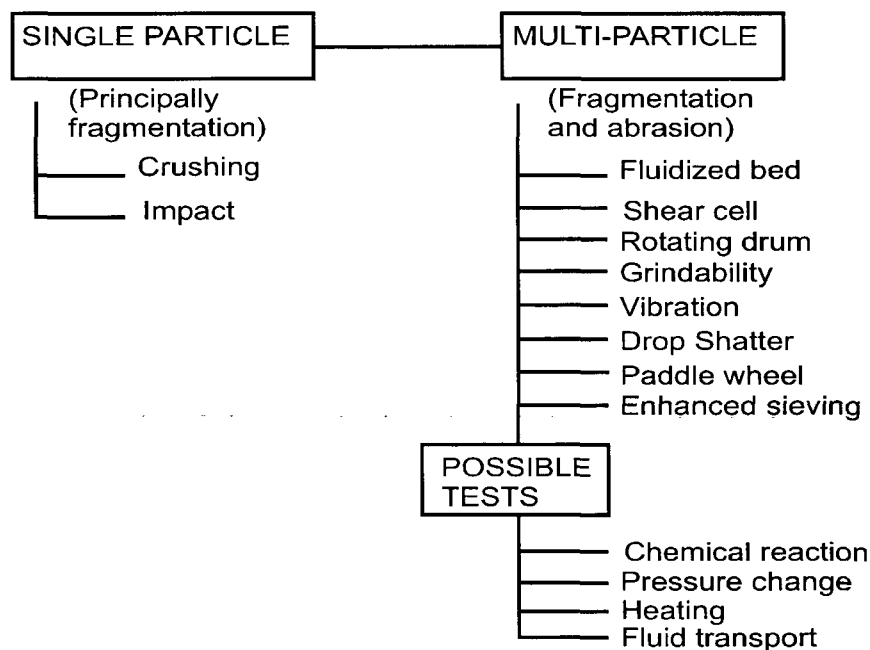


Fig. 7.1.2.3 Types for attrition tests

7.1.2.1 Char Attrition

According to the experimental results the following empirical correlation was obtained from Takeuchi *et al.*, [39]:

$$\frac{W}{W_0} = \exp(-k_a \cdot t) \quad 7.1.2.1.1$$

where k_a is the constant of attrition rate and is different according to char type, t time, W weight of char, W_0 initial weight of char. Upper correlation denotes the weight loss of char by attrition and is very small compared to the weight loss due to reaction. The weight loss due to reaction is given below:

$$\frac{dW}{dt} = -k_s \cdot S \cdot p_{O_2} \quad 7.1.2.1.2$$

where k_s is the surface reaction rate coefficient, S is the surface area of char, p_{O_2} is the partial pressure of oxygen. k_s is expressed as follows:

$$k_s = 0.86 \exp\left(\frac{149000}{R \cdot T_s}\right) \quad 7.1.2.1.3$$

where R is the gas constant, and T_s is the temperature of the char surface.

7.1.2.2 Catalyst Attrition

Forsythe and Hertwig (see Bemrose *et al.*, [45]) were concerned with the attrition of catalysts and were the first who defined a simple high-velocity air-jet attrition apparatus, which became the basis of many subsequent procedures. The typical apparatus is shown in the figure below.

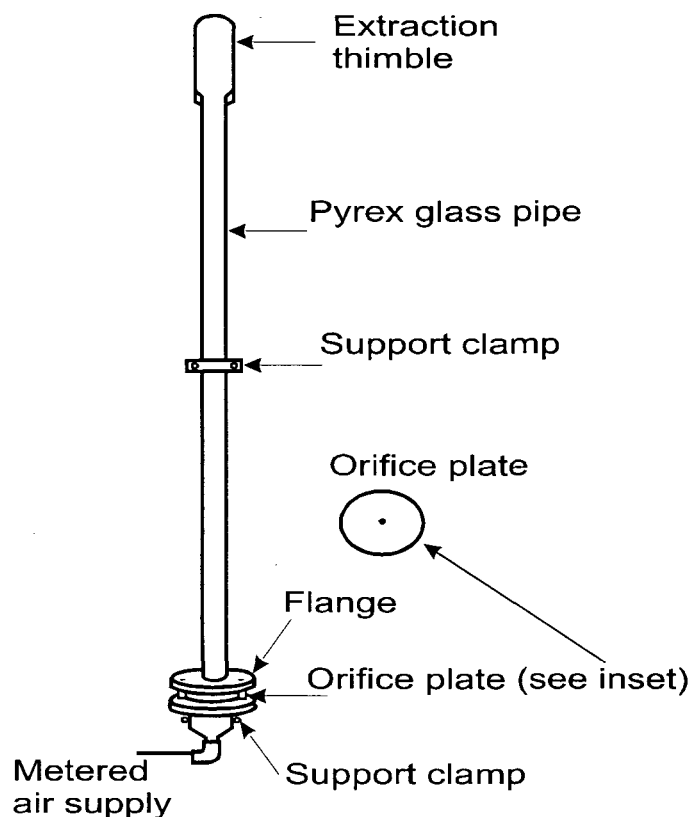


Fig. 7.1.2.2.1 Apparatus for the determination of attrition (from Forsythe and Hartwig, see Bemrose *et al.*, [45])

The attrition rate is proposed by Gwyn (see Bemrose *et al.*, [45]):

$$\frac{dW}{dt} = k \cdot m \cdot t^{m-1}$$

7.1.2.2.1

where W is the weight fraction attrited, t is the time, k is the constant which is a function of the initial particle size and m is the exponent (approximately independent of initial particle size). Gwyn found that the parameter m is about 0.46 for the catalyst particles.

Gwyn assumed that all elutriated material has been produced due to attrition processes because all his primary material had a diameter above 40 μm . Gwyn's correlation does not incorporate explicitly the effects of gas velocity, minimum fluidization velocity, and gas density, [45].

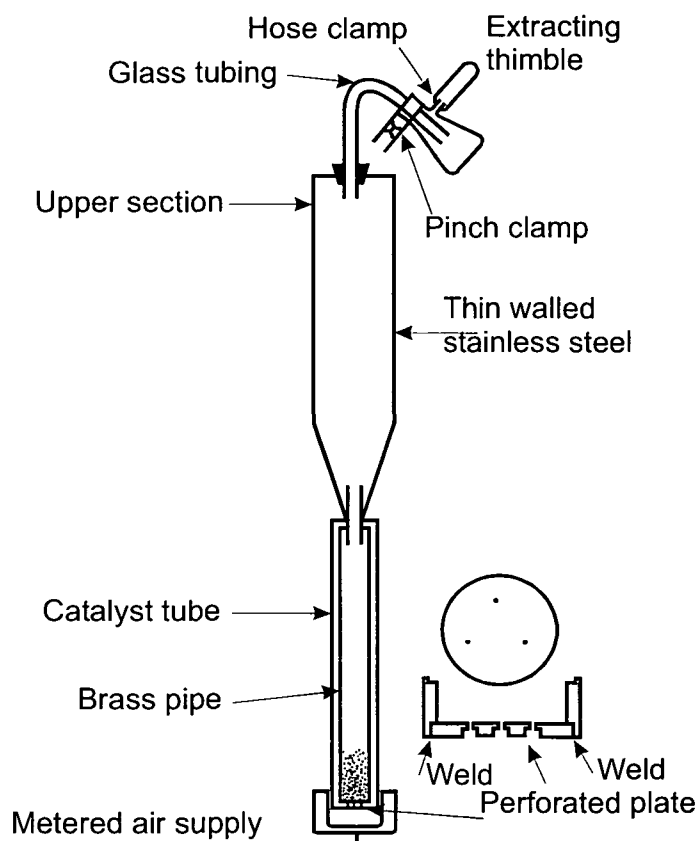


Fig. 7.1.2.2.2 Modification of attrition apparatus by Gwyn (see Bemrose *et al.*, [45])

Werther and Xi, [43], have investigated the mechanism of jet attrition of catalyst particles in gas-fluidized beds both theoretically and experimentally for two different catalysts. The aim of attrition measurements was to establish the amount of attrited fines. Jet attrition of the catalyst particles in gas fluidized beds suggested from [43] gives a good description of the effect of orifice diameter, jet velocity and gas density, on the attrition rate.

7.2 Coal ash attrition

The size distribution of produced fines is independent from the original particle size. Pis *et al.* [34] made an attrition study using a fluidized bed of coal ash. They have studied the effect on attrition of the following parameters:

- bed particle size,
- static bed depth,
- time of attrition and
- fluidization velocity

In general two types of mechanisms were observed:

- 1) Abrasion: particles of a much smaller size break away from the original particle. The resulting bed particles are slightly smaller than the original one.
- 2) Fragmentation: The breaking-away process gives rise to a number of particles of a smaller size than that of the original mother particle.

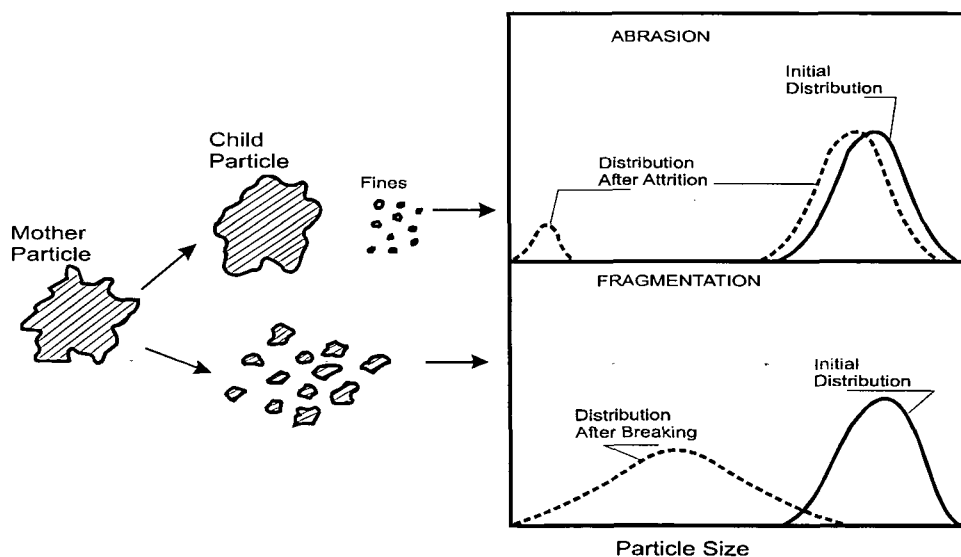


Figure 7.2.1 Size reduction mechanisms

They conclude that the attrition rate is independent of the bed depth and the attrition rate varies linearly with the parameter $(u_0 - u_{mf})$.

The attrition rate is defined (Pis *et al.* [34] and Vaux [44]) as follows:

$$R = -\frac{1}{W} \frac{dW}{dt} \quad 7.2.1$$

where W represents the mass of coarse particle.

The extent of attrition is defined as:

$$A = 100 \cdot \int_0^t R \cdot dt = 100 \cdot \ln \left(\frac{W_0}{W} \right) \quad 7.2.2$$

where W_0 represents the initial mass of coarse particles.

According to [34, 44] an empirical equation to express the variation of the attrition rate with time is proposed:

$$R = R_{\infty} \cdot (1 + a \cdot e^{-b \cdot t}) \quad 7.2.3$$

where a and b are coefficients whose values depend on the characteristics of the material as well as on the operation condition. R_{∞} is the attrition rate under steady-state conditions. The coefficients a , b are in [34] determined.

The attrition rate in steady-state condition is expressed as:

$$R_{\infty} = K \cdot (u_0 - u_{mf}) \quad 7.2.4$$

where $K=1.6 \times 10^{-7} \text{ m}^{-1}$ is the attrition rate constant which has to be determined experimentally.

In the fluidized bed combustors the attrition rate of solids (ash, sand, limestone) depends on the residence time. The attrition rate can be determined only if parameters such as: ash content, sulfur content (Ca/S), bed depth, excess air, fluidization velocity, are taken in the account.

To describe the grain size reduction mechanisms in fluidized beds (especially in CFB's) only a few models are available. Therefore, the aim of the further work must be the development of a standard test method. By using this method it should be possible to determine the necessary model parameters for different solids used in CFB's.

8. Summary

In the present work here, the solid flow program (SOLDIST) and the main simulation program for circulating fluidized bed boilers (CFBB) developed at the Institute of Thermal Engineering (ITW) are extended, partially reprogrammed and tested. The program SOLDIST is reorganized and documented. Each subroutine and function was written to an own file and each formula is described in details.

New test calculations are preformed (to check the functionality of the simulation program) using the new version of the simulation program. The multi-air injection model allows to inject the additional air in each balance cell of the riser. In Chapter 3, test results are discussed and compared for six test cases, whereby the first case is used as reference case. Test results have shown that up- and downward mass fluxes have no significant differences to each other (from case to case). The influence of the additional air injected at certain heights, at each cell of the riser, can be seen from the ratio of core to total cross section area, compare Fig.3.3.1. For this calculations is analyzed only the solid flow program (SODIST).

Calculations for three plants with different geometry and particle size distribution are performed. The inventory material of plant A has 8 size fractions and the inventory material for the plants B and C was subdivided into 16 size fractions. From the figures presented in chapter 5 can be seen that the main influence comes from the recirculated fine particles of the inventory material.

Furthermore, the test results obtained from the main simulation program and experimental data for plant B are discussed and compared. Experiments and calculations are made for full load conditions and the performance test was done for a CFBB with a steam rate of 250 t/h, 540°C and 125 bar pressure of live steam. The following parameters are analyzed: pressure drop over furnace height, temperature profile over furnace height, boiler efficiency, size distribution of bed and circulating material and solids mass flow through ash classifier and filter.

The shape of the experimental and calculated pressure drop curves is similar, but an absolute constant difference exists. As can be seen from Fig. 6.1.2 the cause for these differences between the experimental and calculated results could be an underestimated starting value for solids concentration $(1-\epsilon)$. Fig. 6.2.1 shows the temperature profile between the calculated and measured temperature over furnace height. The difference between the calculated and measured temperature in furnace is higher in the bottom zone of the reactor than in the upper zone. The value of temperature difference is only about 90°C and the reason for this

difference could be the higher measured solids concentration in the bottom zone of the riser.

The boiler efficiency was calculated using the "indirect method". The calculated value of the boiler efficiency (0.925) is in good agreement with the results of the operating plant (0.9189). The ash split to bottom and fly ash is also calculated with the simulation program and compared to the experimental results.

The ratio between bottom and fly ash estimated experimentally is about 60:40%. Calculations are made for two cases: case 1 assumes a size distribution of coal ash as obtained from an ordinary combustion process without mechanical impact and case 2 uses the size distribution of coal ash after an additional grinding procedure. Results show that case 1 is almost identical to the experimental results.

REFERENCES

- [1] **Hetsroni, G.:** Handbook of Multiphase Systems. McGraw Hill, 1982.
- [2] **Johnsson, F.:** Fluid Dynamics and Heat Transfer in Fluidized Beds – with application to boiler. PhD-thesis. Dept. Of Energy Conversion, Chalmers University of Technology, Sweden, 1991.
- [3] **Wirth, K.:** Zirkulierende Wirbelschichten, Springer-Verlag Berlin, 1990
- [4] **Wein, J.:** Das Expansionsverhalten von Gas/Feststoff-Wirbelschichten bei höheren Gasgeschwindigkeiten. Disertation, TU Hamburg-Hamburg, 1992.
- [5] **Glatzer, A.:** Feststoffverteilung und Wärmeübergang durch Strahlung in Zirkulierenden Wirbelschichten, Dissertation, TU Wien, 1994.
- [6] **Kunii, D.; Levenspiel, O.:** Entrainment of Solids from Fluidized Beds, I. Hold-Up of Solids in the Freebord, II. Operation of Fast Fluidized Beds. Powder Technology 61, pp. 193-206, 1990.
- [7] **Haider, A.; Levenspiel, O.:** Drag Coefficient and Terminal Velocity of Spherical and Nonspherical Particles. Powder Technology 58, pp.63-70, 1989.
- [8] **Cheremisinoff, N. and Cheremisinoff, P.:** Hydrodynamics of gas-solid fluidization. 1984.
- [9] **Goedicke, F.:** Strömungsmechanik und Wärmeübergang in zirkulierenden Wirbelschichten. Dissertation, ETH Zürich, 1992.
- [10] **Ellenberger, J.; Krishna, R.:** A unified approach to the scale-up of gas-solid fluidized bed and gas-liquid bubble column reactors. Chemical Engineering Science, Vol. 49, pp 5391-5411, 1994.
- [11] **Darton, R. C., LaNauze, R. D., Davidson, J. F. and Harrison, D.:** Bubble growth due to coalescence in fluidized beds. Trans. Inst. Chem. Engrs. 55, pp 274-280, 1977.

- [12] **Wether, J.:** Hydrodynamics and mass transfer between the bubble and emulsion phase in fluidized beds of sand and cracking catalyst, in *Fluidization IV* (Edited by D. Kunii and R. Toei), pp. 93-102. Engineering Foundation, New York. 1984.
- [13] **Yang, W. Ch.:** A Model for the Dynamics of a Circulating Fluidized Bed Loop. *Circulating Fluidized Bed Technology II* (Basu, P.; Large, J. F.), Pergamon Press, 1988.
- [14] **Geldart, D.:** Types of Gas Fluidization. *Powder Technology* 7, pp. 285-292, 1973.
- [15] **Kunii, D., Levenspiel, O.:** *Fluidization Engineering*. 1991.
- [16] **Kuipers, J. A. M., Prins, W., Van Swaaij, W. P. M.:** Theoretical and Experimental bubble Formation at a Single Orifice in a Two-Dimensional Gas-Fluidized Bed. *Chemical Engineering Science*, Vol. 46, No. 11, pp. 2881-2894. 1991.
- [17] **Geldart, D., Abrahamsen, A. R.:** Homogeneous Fluidization of fine Powders Using Various Gases and Pressures, *Powder Technology* 19, pp. 133-136, 1978.
- [18] **Clift, R., Grace, J. R., Weber, M. E.:** *Drops and Particles*, Academic, New York. 1978
- [19] **Miwa, K., Mori, S., Kato, T., & Muchi, I.:** Behaviour of Bubbles in Gaseous Fluidized Beds, *Int. Chem. Eng.* 12, pp. 187-194, 1972
- [20] **Nicklin, D., J.:** Two-phase Bubble flow, *Chemical Engineering Science*, vol. 17, pp. 693-702, 1962
- [21] **Yang, W. C., Revay, D., Anderson, R. G., Chelen, E. J., Keaorns, D. L. and Cicero, D. C.:** Fluidization Phenomena in a Large-Scale, Cold-Flow Model, in *Fluidization IV* (Edited by D. Kunii and R. Toei), pp. 77-84. Engineering Foundation, New York. 1984.
- [22] **Gilbetson, A. M., Cheesman, J. D. and Yates, G. J.:** Observation and Measurements of Isolated Bubbles in a Pressurized Gas-Fluidized Bed, in

Fluidization IX (Edited by Liang-Shih Fan and Ted M. Knowelton), pp. 63-68. Engineering Foundation, New York. 1998.

[23] **Hartge, E-U., Werther, J.:** Gas Distributors for circulating Fluidized Bed Combustion, in *Fluidization IX* (Edited by Liang-Shih Fan and Ted M. Knowelton), pp. 213-220. Engineering Foundation, New York. 1998.

[24] **Wallis, G. B.:** One Dimensional Two-Phase Flow, McGraw-Hill, New York, 1969

[25] **Geldart, D.:** Gas Fluidization Technology, 1986.

[26] **Hyppänen, T., Lee, Y. Y. and Raino, A.:** A Three-dimensional Model for Circulating Fluidized Bed Boilers. Proceedings 11th Int. FBC-Conf., Montreal (Can.), ASME-Book (Antony, E. J.), 1991.

[27] **Leithner, R., Schulz, A. and Wang, J., Vockrodt, S. and Müller, J.:** Simulation Zirkulierender Wirbelschichtfeuerungen. VGB-Konferenz 'Forschung in der Kraftwerkstechnik 1993', VGB-TB 231, D 15, 1993.

[28] **Ishii, H., Nakajima, T. and Horio, M.:** The Clustering Annular Flow Model of Circulating Fluidized Beds. Journal of Chemical Engineering of Japan, Vol. 22, No. 5, pp. 484-490, 1989.

[29] **Manno, V. P. and Reitsma, S. H.:** A Fluid Dynamic Model of a Circulating Fluidized Bed. Proceedings 11th Int. FBC-Conf., Montreal (Can.), ASME-Book (Antony, E. J.), 1991.

[30] **Eder, N.:** Neugestaltung eines FORTRAN-Programmes zur Berechnung der Wärmeströme und des Temperaturprofiles in einer Zirkulierenden Wirbelschichtfeuerung. Diplomarbeit 2000, TU-Wien.

[31] **Wong, R., Pugsley, T. and Berruti, F.:** Modeling the Axial Voidage Profile and Flow Structure in Risers of Circulating Fluidized Beds. Chemical Engineering Science, Vol. 47, No. 9-11, pp. 2301-2306, 1992

[32] **DIN** Deutsches Institut Für Normung E.V. DIN 1942, Abnahmeversuche an Dampferzeugern. (VDI-Dampferzeugerregeln) Berlin, Köln

[33] **Arena, U., Cammarota, A. and Chirone, Riccardo.**: Fragmentation and Attrition During the Fluidized Bed Combustion of Two Waste-Derived Fuels. Fluidization VIII. (Edited by: Jean-Francois Large and Claude Laguérie) Tours, pp. 437-444 France 1995.

[34] **Pis, J. J., Fuertes, B., Artos, V., Suárez, A. and Rubiera, F.**: Attrition of Coal Ash Particles in a Fluidized Bed. Powder Technology 66. Pp. 1225-1239 1991

[35] **Senior, R. C., Brereton, C.**: Modeling of Circulating Fluidized Beds Solids Flow and Distribution. Chemical Engineering Science, Vol. 47, No.2, pp. 281-296, 1992.

[36] **Kunii, D., and Levenspiele, O.**: The Vertical Distribution of Solids in Circulating Fluidized Beds, CFB. . Fluidization VIII. (Edited by: Jean-Francois Large and Claude Laguérie) Tours, pp. 229-236. France 1995.

[37] **Hu, N. and Scaroni, W. A.**: Fragmentation of calcium-based sorber under high heating rate, short residence time conditions. Fuel Volume 74. No.3. pp. 374-382. 1995.

[38] **Berruti, F. and Kalogerakis, N.**: Modeling the Internal Flow Structure of Circulating Fluidized Beds. The Canadian Journal of Chemical Engineering, Vol. 67. pp. 1010-1014, 1989

[39] **Takeuchi, H., Deguchi, A., Hosoda, H. and Hirama, T.**: Influence of Coal Attrition on Combustion Efficiency in a Fluidized Bed. Hokkaido 061-01, Japan.

[40] **Chirone, R. and Massimilla, L.**: The Application of Weibull Theory to Primary Fragmentation of a Coal During Devolatilization. Powder Technology . 57 pp. 197-212. 1989.

[41] **Hirayama, O. and Takaki, R.**: Numerical Analysis of Nonlinear Stability of two-dimensional Uniform Fluidized Bed: Part 1. Numerical check of Linear Stability. Fluid Dynamics Research 17 pp. 275-291. 1996.

[42] **Knoebig, T., Luecke, J. and Werther, J.**: Mixing and Reaction in the Circulating Fluidized Bed – A three-dimensional combustor model. Chemical Engineering Science, 54 pp. 2151-2160, 1999.

- [43] **Werther, J. and Xi, W.:** Jet Attrition of Catalyst Particles in Gas Fluidized Beds. Powder Technology, 76 pp. 39-46. 1993.
- [44] **Vaux, G. W.:** Attrition of Particles in the Bubbling Zone of a Fluidized Bed. Vol. 40, Proceeding of the American Power Conference, pp. 792-802 1978.
- [45] **Bemrose, C. R. and Bridgwater, J.:** A Review of Attrition and Attrition Test Methods. Powder Technology, 49 pp. 97-126 1987.
- [46] **Kokkoris, A. and Turton, R.:** The Reduction of Attrition in Fluidized Beds by the Addition of Solid Lubricants. AIChE SYMPOSIUM SERIES No. 281, Vol 87. pp.20-31.
- [47] **Kawaguchi, T., Tnaka, T. and Tsuji, Y.:** Numerical Simulation of two-dimensional Fluidized Beds Using the Discrete Element Method (Comparison Between the two- and three-dimensional Models). Powder Technology, 96 pp. 129-138. 1998.
- [48] **Stubington, F. J. and Moss, B.:** On the Timing of Primary Fragmentation During Bituminous Coal Particle Devolatilization in a Fluidized bed Combustor. The Canadian Journal of Chemical Engineering, Vol. 73. Pp. 505-509. 1995.
- [49] **Chen, W. Y., Nagarajan, G. and Zhang, Z. P.:** Stochastic Modeling of Devolatilization-Induced Coal Fragmentation during Fluidized bed Combustion. Ind. Eng. Chem. 33 pp. 137-145. 1994.
- [50] **Glatzer, A.:** Ein Vergleich Mathematischer Modelle zur Strömungsmodellierung Zirkulierender Wirbelschichten. Diplomarbeit. TU Wien, 1991.
- [51] **Krause, H.:** Erweiterung und Umstrukturierung eines Strömungsprogrammes zur Bestimmung in Dampferzeugern mit Zirkulierender Wirbelschichtfeuerung. Studienarbeit. TU Wien, 1996.
- [52] **Rosza, M.:** Entwicklung Zweier Rechenprogramme zur Wärmetechnische Simulation von Dampferzeugern mit Zirkulierender Wirbelschichtfeuerung. Diplomarbeit. TU Wien, 1992.

- [53] **Haider, M.:** Ein Stationäres Simulationsmodell für Dampferzeuger mit Zirkulierender Wirbelschichtfeuerung. Dissertation, TU Wien, 1993.
- [54] **Sundback, A. C., Beér, M. J. and Sarofim, F. A.:** Fragmentation Behavior of Single Coal Particles in a Fluidized Bed. Twentieth Symposium on Combustion. pp. 1495-1503 1984.
- [55] **Gera, D. and Gautam, M.:** Bubble Rise Velocity in Two-Dimensional Fluidized Beds. Powder Technology 84. pp. 283-285. 1995
- [56] **Tsuchiya, K., Furumoto, A., Fan, L-Sh. and Zhang, J.:** Suspension Viscosity and Bubble Rise Velocity in Liquid-Solid Fluidized Beds. Chem. Engineering Science, Vol. 52. No. 18. pp. 3053-3066. 1997.
- [57] **O'Brien, T. and Syamlal, M.:** Particle Cluster Effects in the Numerical Simulation of a Circulating Fluidized Bed. Proceedings CFB IV Conf., Somerset (USA), 1993.
- [58] **Fischer, C. K.:** Dreidimensionale Simulation der Gas-Feststoff-Strömung in Kohlegefeuerten Dampferzeugern. Fortschritt-Berichte VDI, Nr.: 415.Düsseldorf 1999.
- [59] **Werner, A.:** Ein Beitrag zur Modellierung der Kohlenverbrennung in zirkulierenden Wirbelschichtfeuerungen. Dissertation, TU Wien, 1996.

Lebenslauf

Geboren am **01.03.1968**, in Bernica e Eperme, Prishtinë, KOSOVO.

- | | |
|-----------|--|
| 1975-1983 | Besuch der Grundschule in Bernicë e Eperme. |
| 1983-1987 | Besuch der Mittelschule in Prishtinë. |
| 1988-1996 | Studium (Fachrichtung Maschinenbau) an der Universität Prishtina. |
| 1997-1998 | Besuch des Deutschkurses am Vorstudienlehrgang in Wien. |
| 1998- | Beginn des Doktoratsstudiums am ITW (Institut für technische Wärmelehre) an der TU-Wien. |
| 2001- | April- September: Arbeit an einem von der Universität Wien und dem Unternehmen Babcock Borsig Power Austrian Energy gemeinsam durchgeführten Projekt über die numerische Simulation zirkulierender Wirbelschichten |

Dipl.-Ing. Bedri M. Dragusha